Dynamic Testing and Numerical Modeling of Residential Building Modules

Dynamisk testing og numerisk modellering
av byggmoduler

Anders Jørstad

Abstract

This thesis was initiated by a project planing the world's tallest timber building in Bergen, Norway, (the VHT project). The concept of the building is based on a load baring glulam frame with building modules stacked inside to create the residential area of the building. Calculation done by Sweco showed that more damping was needed to lower the accelerations in the top floor of the building. Since little was known about the dynamic properties of building modules and whether these could be used to increase the damping of the building, a survey was wanted.

In this master thesis the dynamic properties of the building modules have been evaluated. This has been done by preforming dynamic test on building modules similar to those planed for the VHT project. Two test protocols were used to test the modules, an experimental modal analysis method using a modal hammer and a system identification method. The goal of the tests was to identify the modal frequencies, damping ratios and mode shapes of the building modules.

The tested modules were modeled in a finite element (FE) method program and scaled to fit the size of the VHT modules. This way the dynamic properties of the VHT modules could be estimated. Simple shear frame models of the VHT modules were made to be implemented in a larger model of the VHT building to evaluate the effect of the modules on the entire structure. Several detailed FE models were made to evaluate how the separate parts of the modules influenced the dynamic response of the modules. An evaluation of the dynamic properties of the sound reducing material Stepisol was also done by dynamic testing in the lab and FE modeling.

It was found that the tested modules had two translational modes and one torsional mode. The overall damping ratio of the modules was found to be roughly 3%. From the numerical tests the stiffness of the module walls were found to be more or less constant per meter wall. The walls can therefor easily be scaled for similar modules with different dimensions to predict the dynamic properties of the new modules.

The Stepisol was found to influence the dynamic properties of the stacked building modules severely. The lab tests showed that Stepisol has a high material damping that helps increasing the damping in the modules. The FE models showed that layers of Stepisol makes the stacked modules a lot less stiff and it is a key feature that can be used to alter the dynamic behavior of stacked modules.

Sammendrag

Denne masteroppgaven ble startet på bakgrunn av et prosjekt der det planlegges å bygge verdens høyeste trehus i Bergen, Norge (VHT prosjektet). Byggekonseptet er basert på en lastbærende ramme av limtre med byggmoduler som vil bli stablet inni for å skape boarealet i bygget. Beregninger gjort av Sweco viste at akselerasjonene i toppen av bygget ville bli for store hvis man ikke kunne innføre mer demping i bygget. Ettersom de dynamiske egenskapene til byggmodulene var ukjente kunne man kanskje finne mer demping i disse, som igjen kunne øke den totale dempningen i bygget og senke akselerasjonene i toppen. For å finne ut av dette måtte de dynamiske egenskapene til byggmodulene kartlegges.

I denne masteroppgaven har de dynamiske egenskapene til byggmoduler blitt kartlagt. Dette har blitt gjort ved å utføre dynamiske tester på byggmoduler som ligner på de som skal brukes i VHT prosjektet. Det ble brukt to ulike metoder for å teste modulene, en eksperimentell modal analyse ved bruk av en modalhammer og en system identifikasjonsmetode. Målet med testene var å finne egenfrekvensene, dempningen og svingemodene til modulene.

Etterpå ble modulene modelert i et elementmetodeprogram for å skalere de testede modulene til samme størrelse som modulene som er planlagt til VHT prosjektet. Ved å gjøre dette kunne man anslå de dynamiske egenskapene til VHT modulene. Forenklede skjærrammemodeller av VHT modulene ble laget for å bli satt inn i en større modell av hele bygget for å kunne se på effekten av disse. Det ble også laget flere detaljerte elementmetodemodeller for å kunne se hvilken effekt hver enkelt komponent i en modul hadde på de dynamiske egenskapene til modulene. De dynamiske egenkapene til lydisoleringsmaterialet Stepisol ble også testet, både i lab og ved elementmetodemodelering.

Testene viste at modulene hadde to moder som gikk på tvers av modulene og en torsjonsmode. Dempningen i modulene ble funnet å være ca. 3%. Fra de numeriske modellene ble det funnet at stivheten i modulveggene var mer eller mindre konstant per løpemeter. Dette gjør at modulene lett kan skaleres og de dynamiske egenskapene til den nye modulen anslått.

Stepisolen viste seg å ha stor innvirkning på de dynamiske egenskapene til modulene. Labtestene viste at Stepisol har høy materialdempning hvilket bidrar til å øke dempningen i modulen. Elementmetodemodellene viste at Stepisolen gjør modulstablene langt mindre stivere enn hva de ville vært uten, og at dette er en nøkkelegenskap som kan utnyttes til å endre modulenes dynamiske respons.

Preface

This master thesis is the end of the 5-year study programme Master of Science in Civil Engineering. It is carried out at the Department of Structural Engineering, under the Faculty of Engineering, Science and Technology at the Norwegian University of Science and Technology in Trondheim. The work presented in this thesis is a result of 20 weeks work, starting fall 2012, finishing early winter 2013 , corresponding to 30 credits.

The topic of this master thesis was chosen due to the exciting challenges of bringing timber engineering to new heights. Sweco had contacted NTNU for help in researching the dynamic properties of building modules. These were to be used in the planing of the world's tallest timber building and I was asked if I was interested. The work has involved a lot of dynamic testing and FE modeling. It has been challenging, and I have learned a lot about dynamics, dynamic test methods and the FEM program Abacus. I have even learned some basics in instrumentation along the way. However, it would be wrong to say that frustration has not been a part of the process as well. During the module testing in Tartu, Estonia, there were times when I doubted that we would ever succeed, but with much good help and guidance, some useful information was brought back home.

I hope my work has contributing to making the VHT project a reality and I am looking forward to seeing the project being finished.

I would first of all like to thank my supervisor professor Kjell Arne Malo for great help and guidance trough the whole process and to associate professor Ole Øyseth for helping with test setups and system identification, both at the Department for Structural Engineering, NTNU.

I would also like to thank Magne Bjertnær and Rune Abrahamsen, at Sweco for good hospitality, help and support when ever it was needed, Senior Engineer Paal Brokka Rike, for helping with instruments, electronics and dynamic testing of the building modules, the management of Kodumaja, for providing the modules that were tested and great hospitality, Nathalie Labonnote, for help with modal hammer testing and finally fellow student Ingunn Utne, for problem solving and discussions threw the hole precess.

<div align="center">

Trondheim, January 25th 2013

Anders Jørstad

Anders Jørstad

</div>

Contents

List of Figures

List of Tables

Chapter 1

Introduction

The demand for tall buildings is increasing due to limited space in cities and both architects and engineers are eager to take on the challenge to create taller and more spectacular buildings than those built before. At the same time, the requirement for environmentally friendly solutions has become of capital importance. Out of this, the development of tall timber buildings has risen as an environmentally friendly alternative to the traditional steel and concrete constructions. New methods and concepts are being developed for building taller timber buildings, and with new methods comes the need for for more research on related subjects.

1.1 Scope of the Thesis

The scope of this thesis is to identify the dynamic properties of building modules used in tall timber buildings and find a way to make representative numerical *finite element (FE)* models of these. The dynamic properties of the numerical model should be as similar as possible to the real modules and should be general enough so that the models can be scaled to predict the dynamic properties of different sized modules. The driving force behind this paper is the *VHT project* (Verdens Høyeste Trehus - the Worlds Tallest Timber Building) which is a 14 storey timber building that is planed in Bergen, Norway. If built, this will be the tallest timber building in the wold, for the time being.

This thesis has two main parts. In the first part, dynamic tests will be carried out on modules similar to those that are planed for the VHT project. In the second part, numerical FE models will be developed to replicate the results of the tests made the first part and to predict the dynamic properties of scaled models. The scaled models will be implemented in a numerical FE model of the entire case building (VHT building) to see how they effect the total response of the building. This last part was a topic in Ingunn Utne's masters theses [48], and is therefor not part of this thesis.

One of the problems related to tall timer buildings is high accelerations in the top floors of the buildings, when exposed to strong winds. Increasing the damping in the building reduces the accelerations and can therefor help solving this problem. It is however hard to increase the damping of a building without installing some sort of dampers. It is therefor of interest to find the damping properties of the modules and see if this can be utilized to increase the damping of entire building. The aim of the tests was therefor to estimate the eifenfrequencies, damping ratios and eigenmodes of the modules, to see if these could contribute to the total damping of the building.

Several numerical models will be made in the FE program Abaqus. The goal of the

numerical modeling is to make a model with the same dynamic properties as the tested modules, and scale this to estimate the properties of the VHT modules. Further detailed numerical modeling will be done to see how the different parts of the module contribute to the dynamic response. The focus of the detailed modeling will be to create a model that is as similar as possible to the tested modules, without tuning the model by altering the input properties to get the "right" results. The reason for this approach is that the models should represent a general module, to enable prediction of other models with different dimensions.

Chapter 2

Background

The demographic development in Norway over the last twenty years show that more and more people are moving in to the larger cities[8]. This creates a demand for both residential and commercial building space and since the area of the cities are often limited due to geographical reasons the need for taller buildings is increasing. At the same time, the demand for more environmentally friendly alternatives to steel and concrete buildings has increased. This has created a challenge which both engineers and architects are eager to take on. The motivation for this is for sure not blotted for the prestige involved in building tall buildings with new technology and extravagant designs.

Since timber is a natural product that stores CO_2 rather than emitting it in the production process, timber buildings are considered an environmentally friendly alternative to steel and concrete buildings. With the development of new materials and technologies in timber engineering, the possibility of building tall timber structures has become a reality. The interest for and willingness to invest in the development of tall timber buildings has increased much due to these reasons over the last years.

At the present time, all existing tall buildings in Norway are made of concrete and/or steel. This is due to a law from 1904 which stated that no timber buildings were to be built taller than four sotreys within defined city limits, due fire hazards[21]. This law was relived by new building regulations in 1997 which stated that timber buildings could be built taller that four storeys if they fulfilled the requirements of TEK97[38]. The development of tall timber buildings in Norway has therefor only barely started.

There are of course other reasons why there are few tall timber buildings in the world. Much of it is due to the convenience of the materials and available technology in steel and concrete engineering. New and exciting technologies in timber engineering are however being developed, and can soon compete with steel and concrete buildings in both price and performance.

The development engineering wood like glue laminated timber (glulam) is one of the major reasons why tall timber buildings are now possible. The manufacturing proses of glulam elements and other forms of engineering wood allows high precision and detailed cross sections to be made in almost any dimensions. The elements can be joined together with steel connectors which allows large structures of high strength to be built.

2.1 Timber as construction Material

Timber has been used as construction material since humans moved out of caves in the early stone age, and has since been been used in all kinds of constructions, from

medieval war machines and boats to bridges and tall buildings. Timber technology has come a long way since humans first started using it.

Timber constructions are no longer limited by the height and diameter of trees much due to the development of weather resistant glues. Adhesive materials like glue has removed the limitations of the size of trees, which means timber can now be engineered into almost unlimited dimensions and shapes. Typical examples of engineered wood is oriented standard boards (OSB plates), glulam beams, plywood and finger joined lumber. The upshot of this is that timber can be tailor made for specific purposes in different constructions[1].

2.1.1   Structural Properties

Timber is a high strength, low weight, composite material that consists of cellulose fibers held together by lignin. The fibers have high tensile strength and runs along the length of the tree. Due to the orientation of the fibers the tensile strength and stiffness is very high parallel to the fibers, while the stiffness normal to the fibers is much lower, since the fibers are not engaged the same way. This makes timber an orthotropic material which is a important to take into account when designing timber structures [37].

Since wood is a natural material, there are variations in the properties of the material that are influenced by how the tree has grown. The fibers are not always growing in the same direction due to wind loading, loading from branches, etc. Branches also creates knots that are fibers growing normal to the fibers of the trunk, creating weak points in the wood. The growth rate of the tree also influences the strength of the material. Softwood trees become stronger when grow slowly, while hardwood trees becomes stronger when growing quickly. Different types of wood also have vastly different material properties [28]. The Young's modulus for different kinds of wood goes from very low up to roughly 20.6 GPa (Iron wood). Normal construction timber has a Young's modulus in the vicinity of 11 GPa [4].

This creates big variation in the material properties of timber. All timber products are therefor tested and classified according to Eurocodes. This enables more accurate calculations for timber structures and better utilization of the products. Engineering woods like finger joined and glulam timber elements are made of several smaller pieces of wood that are glued together. This reduces the effect of imperfections since there is very little chance for all the imperfections to ends up in the same cross section. The timber can also be used more effectively since stronger wood can be used where the largest stresses/strains occur in the cross section.

Compared to steel and concrete, timber is a lot less stiff, but is on the other hand much lighter. When comparing the stiffness to weight ration of normal construction timber to steel and concrete, timber has more or less the same stiffness to weight ratio as steel [10].

2.1.2   Environmental Aspects

Wood is a natural, sustainable and recyclable resource that can help reduce CO_2 emissions related to the building industry. Trees grows through the process of photosynthesis which means that they absorb CO_2 from the air, and with the help of sun light is able to store the carbon and grow larger. The use of timber as a construction material therefor stores carbon instead of emitting CO_2 in the production process as is the case for concrete and steel[6].

The processing of the timber after the trees are cut produces little waste. The parts that are to small to be used as studs or planks can for instance be used as plate materials.

The processing also allows high precision, which means there is very little waste at the building site. The waste that is produced is however highly recyclable[6].

Forrest industry is a sustainable industry as long as the production do not exceed growth of forests. At the moment the growth of forests in Norway is larger than the production which means that the production can be increased without hurting the sustainability. It is important that only certified timber is used so that for instance hardwood from rainforests is not used, since this is not a sustainable resource.

Wood has low heat conductivity compared to steel and concrete, which means less trouble with cold-bridges and water condensation in walls. Studies also show that wood creates a good indoor environment for humans[19].

2.2 Building Tall with Timber

When comparing what is considered a tall timber building to tall steel and concrete buildings the word *tall* may be an exaggeration. The tallest building in the world is the 829.8 meter *Burj Khalifa* in Dubai, United Arab Emirates. The tallest timber building in the world is the *Forté* building in Melbourne, Australia, that is 10 storeys (32.17 meters) tall [12]. Tall timber buildings are therefor not very tall when compared to other buildings, but the design problems are the same, they only come into effect at lower heights for timber structures.

One of the major problems with tall timber buildings is that they have high stiffness to mass ratio. From a static point of view, this is a good thing, but when considering the dynamic effects this can be problematic. The low mass causes high accelerations in the top of the building when exposed to large wind loads. This is due to the lack of inertia forces. This is a mainly serviceability limit state problem since the accelerations are not in the range of causing the structure to collapse. The problem is that people occupying the top floors of the building will feel discomfort due to the accelerations. The accelerations can cause structural fatigue, which can make the building collapse. This is however unlikely[47]. Due to the high strength of timber, there are few problems in the ultimate limit state for timber structures.

A positive effect from the low mass of timber structures is that the load on the foundation is smaller, which makes the foundation work easier. The cost of ground works is very high, and includes much concrete and steel. With lighter buildings the cost of ground work is lowered and the environment is spared form excess use of polluting materials. Low weight buildings can also be built where the soil condition are sensitive to large loads.

2.2.1 Examples of Large Timber Structures

There are many large timber structures worth mentioning in the world, some of them are shown here.

2.2.1.1 Forté, Melbourne, Australia

Forté was finished late 2012 and is the tallest timber building in the world, with 32.17 meters over 10 storeys. The load bearing system is made of cross laminated timber plates (CLT)[12]. The building is shown in Figure 2.1 (b).

2.2.1.2 Stadthaus, London, UK

Stadthaus was the tallest timber building in the world from when it was finished in 2009, with 9 storeys, until the Forté was finished late in 2012. The load bearing system

a - Stadthaus [9]   b - Forté[12]

Figure 2.1: Tall Timber Buildings

a - Barentshus [17]   b - Kjøllsæter bur [5]

Figure 2.2: Barentshus and Kjøllsæter bru

is made of CLT[9]. The building is shown in Figure 2.1 (a).

2.2.1.3   Barentshus, Kirkenes, Norway

Barentshus is a planed 20 storey tall building in the north of Norway. The project started in 2009 and the planning is still not finished. Unfortunately there is now little chance of the project being realized. The planed load bearing system was based on a glulam frame [41]. The building is shown in Figure 2.2 (a).

a   b
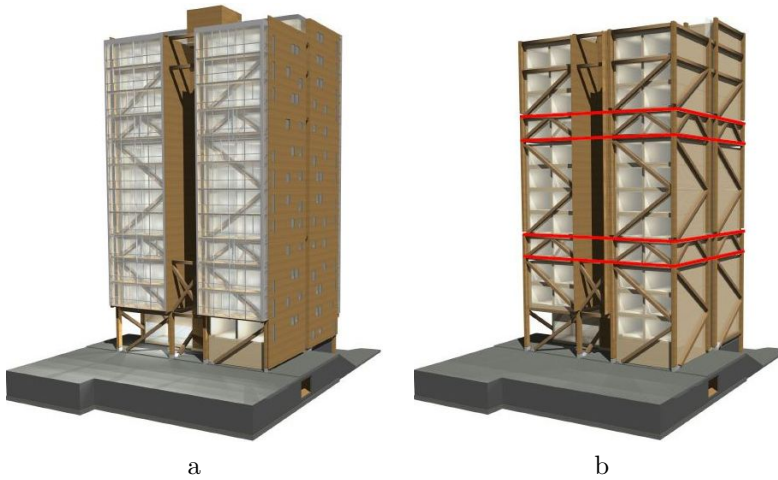
Figure 2.3: VHT building[46]

2.2.1.4   Kjøllsæter bru, Rena, Norway

Kjøllsæter bru, is a bridge crossing the river *Rena* in Norway. It can take a load of 109 tons, which makes it one of the strongest timber bridges in the world. It has a total length of 158 meters with the longest span of 45 meters [5]. The bridge is shown in Figure 2.2 (b).

2.3   The VHT Project

VHT project is a collaboration between *Bergen og Omegn Bolibyggerlag (BOB)*, *Sweco* and *Artec*[1] to plan a 14 storey timber apartment building in Bergen, Norway. With a planed height of 44 meters this will be the tallest timber building in the world[2]. The load bearing substructure of the construction will be made of glulam beams, forming a truss frame. Building modules will be placed inside the frame to serve as the residential are of the building. The cladding will be attached to the glulam frame on the sides of the building and glassed balconies to the front and back. Figure 2.3 (a) shows the complete building, and (b) shows the glulam frame with the modules placed inside.

There will be two *power floors*, located at floor five and ten from the ground (marked as red in Figure 2.3 b). The power floors are reinforced floors that strengthens the frame, and serve as foundation for the building modules. Concrete slabs will be placed on top of the power floors, to give the modules sufficient support and to add mass to the building.

Stacks of four modules in the height will be placed on top of the concrete slabs, making them act as individual buildings within the glulam frame. The modules forming the first four storeys will be supported on the ground and will not effect the rest of the building. The modules located in the power floors will be supported by the horizontal timber beams, making them independent of the module stacks. Each floor is made up by nine modules connected in two 2 x 1 connections and one 5 x 1 connection, as shown in Figure 2.4 where the connected modules are marked by the red rectangles.

---

[1]BOB - Housing cooperation operating in and around Bergen
Sweco - Consulting engineering company
Artec - Architect
[2]VHT - Verdens Høueste Trehus - The World's Largest Timber Building
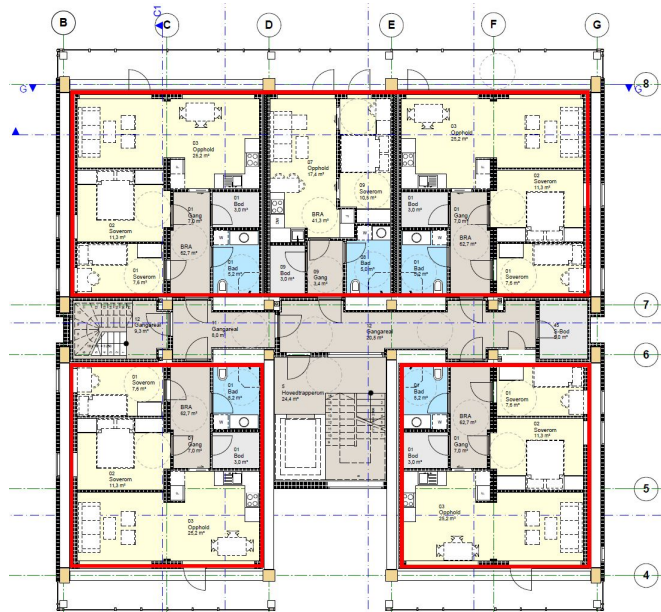
Figure 2.4: Cross Section of the VHT Building [46]

The modules will be produced by *Kosumaja* and the timber frame by *Moelven limtre*[3]. Sweco also engaged NTNU[4] in the project to evaluate the dynamic properties of the building modules and to see if they could be used to increase the damping in the building.

---

[3]Kodumaja - Estonian module building company

Moelven limtre - Norwegian glulam manufacturing company

[4]Norwegian University of Science and Technology

Chapter 3

Theoretical Background

3.1 Basic Dynamics

3.1.1 Single Degree of Freedom System (SDOF)

A fundamental understanding of structural dynamics is needed to understand the test methods used in this thesis. These fundamentals are not only important to obtaining the end results, but to be able to interpret the output of the tests during testing. To go from a frequency response measurement to obtaining the frequency response function (FRF) and the dynamic parameters of the function, a simplified case is presented. The theory presented in this section can be found in sources [37, 25, 44, 24].
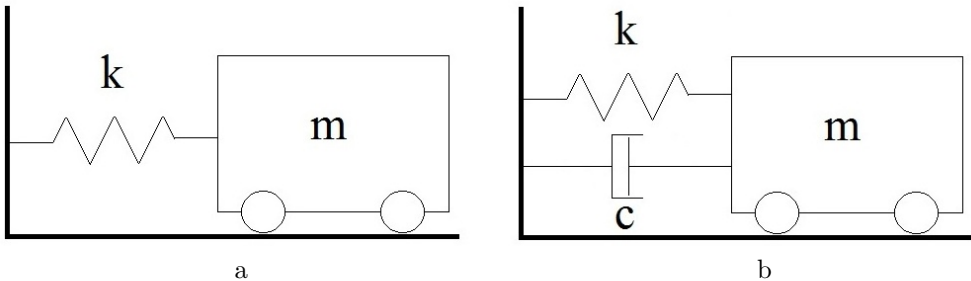
Figure 3.1: Single Degree of Freedom System

For a single degree of freedom system (SDOF) in free vibration, as shown in Figure 3.1 (a), consisting of a spring and a mass, the fundamentals are the same as for a more complex undamped system. For this SDOF case the equation of motion is given by Newton's law:

$$F_r = ma \qquad (3.1)$$

Here F_r =restoring force, m =mass of the system, and a =acceleration of the mass at time t. a is usually expressed as $\ddot{x}(t)$, as in the second derivative of the displacement at time t. In this case the restoring force is given by the spring stiffness k and its displacement x. The equation of motion may now be written as:

$$m\ddot{x}(t) + kx(t) = 0 \qquad (3.2)$$

The general solution of the undamped case is given by:

$$x(t) = C_1 \cos(\omega_n t) + C_2 \sin(\omega_n t) \tag{3.3}$$

By introducing the initial conditions, the response is given by[1]:

$$x(t) = x_0 \cos(\omega_n t) + \frac{\dot{x}_0}{\omega_n} \sin \omega_n t \tag{3.4}$$

$$x(t) = Re[x_0 e^{(i\omega_n t)} - i\dot{x}_0 \omega_n e^{(i\omega_n t)}] \tag{3.5}$$

Where:

$$\omega_n = \sqrt{\frac{k}{m}} \tag{3.6}$$

ω_n is the *circular eigen frequency*, or the *circular natural frequency* of the system and represents the frequency of resonance. To make the model more realistic a viscous damper is introduced to the system, as shown in Figure 3.1 (b). This means that an energy dissipating term must be included in the equation of motion. The damping constant is c is introduced, and the equation of motion is expanded to:

$$m\ddot{x}(t) + c\dot{x}(t) + kx(t) = 0 \tag{3.7}$$

c can be defined by $c = 2\zeta m\omega_n$ where ζ is the damping ratio. The equation of motion can therefor be expressed by the damping ratio and the natural frequency as:

$$\ddot{x} + 2\zeta\omega_n\dot{x} + \omega_n^2 x = 0 \tag{3.8}$$

If $\zeta < 1$ the system is *underdamped* and the soulution will be given by:

$$u(t) = e^{(-\zeta\omega_n t)} \left[u_0 \cos(\omega_D t) + \frac{\dot{u}_0 + u_0\zeta\omega_n}{\omega_D} \sin \omega_D t \right] \tag{3.9}$$

The damped circular eigen frequency ω_D included in the solution is defined as $\omega_D = \omega_n\sqrt{1 - \zeta^2}$, but as the damping is small in most structures[2] ζ^2 becomes very small and it is assumed that $\omega_D = \omega_n$. The solution can also be written as a single harmonic:

$$x(t) = \rho \cos(\omega_D t - \phi)e^{(-\zeta\omega_n t)} \tag{3.10}$$

$$\rho = \sqrt{(x_0)^2 + \left(\frac{\dot{x}_0 + x_0\zeta\omega_n}{\omega_D} \right)^2} \tag{3.11}$$

$$\phi = \arctan \frac{\dot{x}_0 + x_0\zeta\omega_n}{x_0\omega_D} \tag{3.12}$$

Here, ρ is the amplitude, and ϕ is the phase angle.

3.1.1.1   Forced vibration
If the system is subject to an external harmonic load, the equation of motion is expanded to include the force. A harmonic force may be given by $F(t) = \sin(\omega t)$ where

---

[1]The response is represented in two ways, where the only difference is that
$$\cos(\omega_n t) = Re\left[e^{(i\omega_n t)}\right]$$
$$\sin(\omega_n t) = Re\left[-ie^{(i\omega_n t)}\right]$$
[2]Typically buildings, bridges and towers
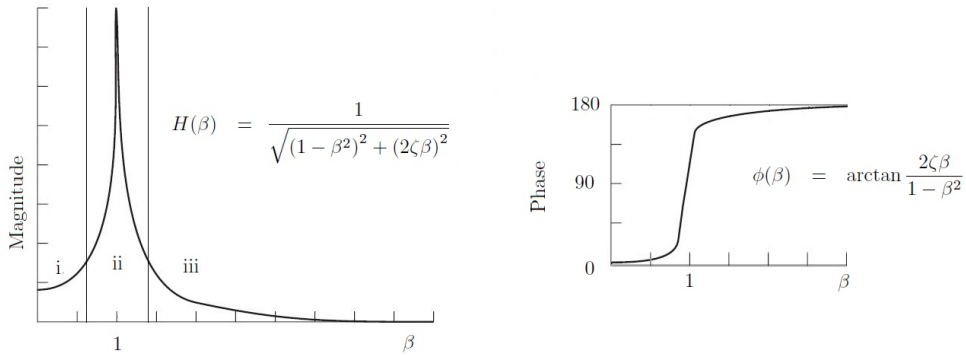
Figure 3.2: Frequency Response $H(\beta)$ and $\phi(\beta)$

p_0 is the maximum load amplitude and ω is the circular frequency of the harmonic loading. The equation of motion is written:

$$m\ddot{x}(t) + c\dot{x}(t) + kx(t) = p_0 \sin(\omega t) \tag{3.13}$$

The particular solution of the system is given by:

$$x_p(t) = \frac{p_0}{k}\left(\frac{2\zeta\beta}{(1-\beta^2)^2 + (2\zeta\beta)^2} - i\frac{1-\beta^2}{(1-\beta^2)^2 + (2\zeta\beta)^2}\right)e^{i\omega t} \tag{3.14}$$

$$\beta = \frac{\omega}{\omega_n} \tag{3.15}$$

The steady-state solution is than given by:

$$x(t) = \frac{p_0}{k}\frac{1}{\sqrt{(1-\beta^2)^2 + (2\zeta\beta)^2}}\sin(\omega t - \phi) \tag{3.16}$$

$$H(\beta) = \frac{1}{\sqrt{(1-\beta^2)^2 + (2\zeta\beta)^2}} \tag{3.17}$$

$$\phi(\beta) = \arctan\frac{2\zeta\beta}{1-\beta^2} \tag{3.18}$$

Here $H(\beta)$ represents the amplitude and $\phi(\beta)$ represents the phase lag of the response. In Figure 3.2 $H(\beta)$ is plotted against β, and the areas numbered i, ii and iii are defined as stiffness, damping and inertia controlled areas respectively. The maximum amplitude is found when $\beta = 1$ and the response is only limited by the damping ratio. The phase angle ϕ is 90° out of phase when $\beta = 1$. The frequency response function (FRF) is a complex dimensionless function which provides a relationship between the input and output of the system. It can be described in several different plot styles, and in terms of displacement, velocity and acceleration often referred to as compliance, mobility and accelerance, respectively [25].

3.1.2 Multiple Degree of Freedom System (MDOF)

Single degree of freedom systems are rarely found out side of laboratories. Most civil engineering structures have multiple degrees of freedom which presents more complex

Definition	Response	Variable	Function
Compliance	$\frac{X}{F}$	$\frac{Displacement}{Force}$	$G = \frac{1}{k}H(\beta)e^{-i(\phi(\beta))}$
Mobility	$\frac{V}{F}$	$\frac{Velocity}{Force}$	$G = \frac{\omega}{k}H(\beta)e^{-i(\phi(\beta)-\frac{\pi}{2})}$
Acceleration	$\frac{A}{F}$	$\frac{Acceleration}{Force}$	$G = \frac{\omega^2}{k}H(\beta)e^{-i(\phi(\beta)-\pi)}$

Table 3.1: Frequency Responce Functions

dynamic systems [24]. To handle the expanded systems the equation of motion is written in matrix form. The MDOF equation of motion is given by:

$$\mathbf{M}\{\ddot{\mathbf{x}}(t)\} + \mathbf{K}\{\mathbf{x}(t)\} = \mathbf{0} \tag{3.19}$$

Here $\mathbf{M}$= mass matrix and $\mathbf{K}$ = stiffness matrix both of size N x N. $\{\ddot{\mathbf{x}}(t)\}$ and $\{\mathbf{x}(t)\}$ represents accelerations and displacements respectively and are N x 1 sized vectors. The solution to the equation leads to the modal parameter. By assuming that a solution exists on the form:

$$\{\mathbf{x}(t)\} = \mathbf{x}e^{i\omega t} \tag{3.20}$$

$\mathbf{x}$ is an N x 1 vector that is not dependent on time. This suggests that $\{\ddot{\mathbf{x}}(t)\}=-\omega^2\mathbf{x}e^{i\omega t}$ and the equation of motion is given by:

$$(\mathbf{K} - \omega^2\mathbf{M})\mathbf{x}e^{i\omega t} = \mathbf{0} \tag{3.21}$$

to which the only non-trivial solution is given by:

$$\det\left|(K - \omega^2 M)\right| = 0 \tag{3.22}$$

This gives N different values of ω^2which is the undamped systems eigen frequencies. By substituting each eigen frequencies back in to 3.21 a relative value for $\mathbf{x}$ is calculated, corresponding to each of the eigen frequencies. These values are describes as mode shapes. The mode shapes does not have unique values, but can be multiplied by a scale factor to increase or reduce the influence of a given frequency response. The relation between the values within each mode shape is however fixed [24]. By forming two matrices of sizes N x N, $\begin{bmatrix} \ddots\, \omega_r^2\, \ddots \end{bmatrix}$ and $[\Psi]$, the modal model is defined. ω_r is eigen frequency number r, which corresponds to the mode shape vector $\psi_{\mathbf{r}}$.

   The orthogonal properties of the modal model provides a great tool for further response analysis. By generalizing the mass and stiffens matrices the system is uncoupled.

$$[\Psi]^T \mathbf{K} [\Psi] = [\ddots\, k_r\, \ddots] \tag{3.23}$$

$$[\Psi]^T \mathbf{M} [\Psi] = [\ddots\, m_r\, \ddots] \tag{3.24}$$

From this it can be seen that:

$$\omega_r^2 = \frac{k_r}{m_r}$$

By scaling the mode shape vectors the mass-normalized eigenvector $[\Phi]$ may be obtained. When this is applied to $\mathbf{M}$ and $\mathbf{K}$ as in the previous equations, the generalized entities become:

$$[\Phi]^T \mathbf{M} [\Phi] = [\mathrm{I}] \tag{3.25}$$

$$[\Phi]^T \mathbf{K} [\Phi] = \begin{bmatrix} \ddots\, \omega_r^2\, \ddots \end{bmatrix} \tag{3.26}$$

By applying a cyclical excitation force $\mathbf{f}e^{i\omega t}$ of dimensions N x 1 and assuming the same solution as in 3.20 the equation of motion is given by:

$$(\mathbf{K} - \omega^2\mathbf{M})\mathbf{x}\mathrm{e}^{\mathrm{i}\omega\mathrm{t}} = \mathbf{f}\mathrm{e}^{\mathrm{i}\omega\mathrm{t}} \tag{3.27}$$

The response is now given by:

$$\mathbf{x} = (\mathbf{K} - \omega^2\mathbf{M})^{-1}\mathbf{f} \tag{3.28}$$

By rearranging this equation, it can be found that:

$$[\alpha(\omega)] = \mathbf{f^{-1}x} \tag{3.29}$$

$[\alpha(\omega)]$ is now the response model for the system, where $\alpha_{jk}(\omega) = \frac{x_j}{f_k}$ which is equivalent to the compliance term in Table 3.1. However, this is an inefficient way to present the FRFs, especially in a modal analysis perspective where only a few FRF may be required [25]. Nor does it provide any information about properties of each FRF. Thus, an alternative way of presenting this is derived by starting with:

$$(\mathbf{K} - \omega^2\mathbf{M}) = [\alpha(\omega)]^{-1} \tag{3.30}$$

By premultiplying and postmultiplying both sides with $[\Phi]^T$ and $[\Phi]$ respectively, the equation is given by:

$$[\ddots(\omega_\mathrm{r}^2 - \omega^2)\ddots] = [\Phi]^\mathrm{T}[\alpha(\omega)]^{-1}[\Phi] \tag{3.31}$$

By reorganizing this to:

$$[\alpha(\omega)] = [\Phi][\ddots(\omega_\mathrm{r}^2 - \omega^2)\ddots]^{-1}[\Phi]^\mathrm{T} \tag{3.32}$$

One can easily see that $[\alpha(\omega)]$is symmetrical, and that each FRF parameter can be calculated from:

$$\alpha_{jk}(\omega) = \sum_{r=1}^{N}\frac{(\phi_j\phi_k)_r}{\omega_\mathrm{r}^2 - \omega^2} = \sum_{r=1}^{N}\frac{(\psi_j\psi_k)_r}{m_r(\omega_\mathrm{r}^2 - \omega^2)} \tag{3.33}$$

3.1.3 Damping

Damping has been mentioned in the previous sections, but not explained properly. Damping is an energy dissipating process, which lowers the energy of an oscillating system. The effect of damping on system in free vibration is that the amplitude will decay over time, according to the amount of damping. The amount of damping in a system is divided in to three categories. Under critical, critical and over critical damping, where the amount of damping is often expressed as fraction of critical damping. There is only oscillation in a free vibrating system if it is underdamped. This is shown in Figure 3.3. Damping in structural dynamics is usually very low [24].
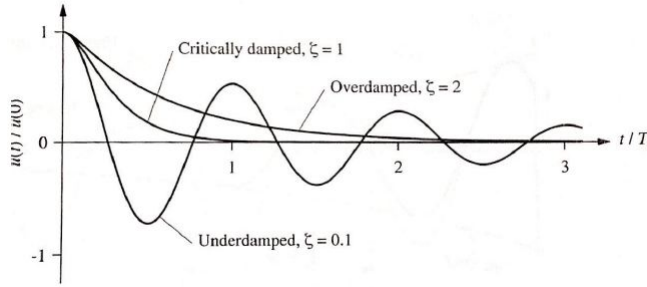
Figure 3.3: Damping of System in Free Vibration [24]

Four kinds of damping is usually recognized. These are defined by [44] as:

Radiation damping is energy dissipated to surrounding medium, such as to the soil that supports the structure.

Coulomb damping is related to dry friction, such as the friction in joints when they slip.

Hysteresis damping also known as *solid* or *material* damping and is related to energy dissipation within materials such as plastic action on a very low scale.

Viscous damping is a velocity related damping. The damping is equivalent to the energy needed to move threw a gas or fluid at a given velocity.

Since most structures are subjected to several of these at all times, it is hard to create a mathematical model for damping in structures that take in to account all these effects. The damping that is easiest to represent in a mathematical dynamic model is viscous damping. Since the damping in structures is usually very low this can be used to represent the damping, regardless of actual source. This viscous damping represents the damped response of structures well enough fro most cases.

Two approaches to viscous damping in structures are usually used. These are called *proportional damping* and *modal damping[44]*. The proportional damping relates the damping to a weighted combination of the mass and stiffness of the system defined as:

$$[\mathbf{C}] = \alpha\,[\mathbf{M}] + \beta\,[\mathbf{K}] \tag{3.34}$$

Modal damping is used when the dynamic equations are uncoupled by the modal method described in Section 3.1.2. With modal damping one individual damping ration is assigns each modal frequency. This allows modes to be individually damped according to mode shapes and how the they engages the damping elements in the structure [44]. This is the method used in the tests in this thesis.

3.1.3.1   Multiple Degree of Freedom System with Modal Viscous Damping

By introducing viscous damping to a MDOF system, the equation of motion is given by:

$$\mathbf{M}\,\{\ddot{\mathbf{x}}(t)\} + \mathbf{C}\,\{\dot{\mathbf{x}}(t)\} + \mathbf{K}\,\{\mathbf{x}(t)\} = \mathbf{0} \tag{3.35}$$

This is equivalent to the SDOF system. Due to the orthogonal nature of the mode shapes the equation of motion can be written as:

$$\{\ddot{\mathbf{x}}(t)\} + \left[\begin{matrix} \ddots & & \\ & 2\zeta_r\omega_r & \\ & & \ddots \end{matrix} \right] \{\dot{\mathbf{x}}(t)\} + \left[\begin{matrix} \ddots & & \\ & \omega_r^2 & \\ & & \ddots \end{matrix} \right] \{\mathbf{x}(t)\} = 0 \tag{3.36}$$

The same general solution as for the SDOF system is assumed on the form:

$$\{\mathbf{x}(t)\} = \{\mathbf{X}\}\, e^{st} \tag{3.37}$$

By using the *state-space* formulation, the complex eigenvalue problem in Equation 3.35 can be solved. The complex state vector is defined by:

$$\{\mathbf{u}(t)\} = \begin{matrix} \{\mathbf{x}(t)\} \\ \{\dot{\mathbf{x}}(t)\} \end{matrix} \tag{3.38}$$

Equation 3.35 can now be solved by:

$$\left[\begin{matrix} C & M \\ M & 0 \end{matrix} \right] \{\dot{\mathbf{u}}(t)\} + \left[\begin{matrix} K & 0 \\ 0 & -M \end{matrix} \right] \{\mathbf{u}(t)\} = 0 \tag{3.39}$$

The response model for an MDOF system with equivalent viscous modal damping can be expressed be:

$$\alpha_{jk}(\omega) = \sum_{r=1}^{n} \frac{(\psi_j\psi_k)_r}{(\omega_r^2 - \omega^2 + 2i\zeta_r\omega_r\omega)} \tag{3.40}$$

3.2 Experimental Modal Analysis

Experimental modal analysis can generally be described as the study of dynamic properties of vibrating structures. It is used fore measuring and analyzing dynamic responses of structures when excited by a known input. In short, a structure is excited by a measurable input force and the response is registered. By combining these, a frequency response function (FRF) can be generated by using a fast Fourier transform (FFT) and the modal parameters identified by using a curve fitting technique. It is used to determine modal parameters as frequencies, damping rations and modal vectors. The method was originally developed by air plane manufacturers in the 1940's to solve the fluttering problem, in the wings of airplanes. The method has been developed a lot since then, and with the development of computers and use of the FFT the method is now a lot simpler to use and can be applied to a large variety of structures, from bridges to car components. It can be used for both structural and acoustic testing [15].

To days typical modal testing equipment involves accelerometers and load cells to measure output and input of the structure, a signal conditioner and an analog-digital converter, to transform the analog signal to binary code and feed this in to a host computer. The computer records the signals, and analyzes the data so that the operator can view the results. The method is now a mixed collaboration of signal conditioning, computer interaction of electrical engineering, theory of mechanics and applied mathematics[15].

Generally two types of experimental modal analysis are recognized, a single input multiple output (SIMO) method and a multiple input single output (MISO) method[3]. The difference between the methods lies in how the structure is excited and how the response is measured. For the SIMO method, a shaker is used to excite the structure at one point and an accelerometers measure the response in different locations on the structure. For the MISO method a hammer, or different sort of impact device, is used to

---

[3]Excitation = input, acceleration = output

excite the structure in several locations, while an accelerometer fixed to a single location on the structure measure the response form each excitation. The later is commonly known as the roving hammer method[7].

Mathematically the two methods are treated equally, due to some basic assumptions regarding the structure. First it is assumed that the structure behave linearly, implying that the response of the structure form any combined forces applied simultaneously, is the same as the sum of the response form each of the force applied alone. The second assumption is that the structure is time invariant, which means that the properties of the structure does not wary in time or with different conditions e.g. variation in temperature or humidity. The third assumption is that the structure obeys Maxwell's reciprocity theorem. This states that a force applied at location a and response measured at location b is the same as response measured at location a with the same force applied at location b ($H_{ab} = H_{ba}$). The upshot of this is that the SIMO method and MISO method can be treated the equally mathematically. The fourth assumption is that the structure is observable, meaning that the input and output measurements contain enough information to generate a model with the adequate dynamic properties [**15**].

3.2.1   Modal Hammer Testing

Since only the modal hammer method has been used in this thesis, the following part will focus only on this.

The most common modal hammer technique is a MISO method, also known as the *roving hammer* method, which means that the structure is excited in several different locations by the hammer, and the response measured by a fixed accelerometer somewhere on the structure.

The location of the accelerometer should not be sett at random, as it may be placed in a location of zero response for some of the modes. The location of the accelerometer should be chosen by considering the anticipated modes of the structure. The accelerometer must be properly attached to the structure, and should have an eigenfrequency as far apart form the structural frequencies of interest as possible. The size and weight of the accelerometer should not affect the properties of the structure.

In modal hammer testing there are two different test protocols that can be used. These are called the *driving point* test and the *roving hammer* test. The rowing hammer test is described above as a MISO test. The test identifies the modal frequencies, modal damping and mode shapes of the structure. For the driving point test the accelerometer is fixed to a specific location, and the hammer excites the structure in the same location as the accelerometer[4]. This gives the modal frequencies and modal damping of the structure, but not the mode shapes. The reason for this is described in Section 3.2.2.2.

Since the impact force is applied by a hammer, force is a function of the velocity and weight of the hammer. The weight of the hammer should be chosen according to the desired impact force, since it is hard to control the velocity. A load cell is built in to the hammer to measure the applied force and pulse duration. When the hammer excites the structure several modes are excited simultaneously. This can be a source of frustration if only a band of the frequencies are of interest. However, the amplitude of the different modes can be controlled to some extent, by varying the stiffness of the hammer tip. A short impulse duration will excite high frequencies and a long impulse duration will excite the lower frequencies. I.e., if the lower frequencies are of grater interest, a soft tip should be chosen to give a longer pulse duration [37].

---

[4]The accelerometer is usually placed on the opposite side of the walls or floor form the impact location, but in the same location in the test plane or line etc.

3.2.2 Recording and Processing the Experimental Data

3.2.2.1 Recording

When the impact and accelerations are recorded, only one impact is recorded in each time series. The length of the recording should be sett so the response goes to zero before the recording is ended. This means that the recording time vary with different structures. E.g. the recording time for a lightly damped structure should be longer than for a highly damped structure. However, the damping is usually not known before the tests begin, so the recording time will have to be sett to an assumed appropriate length. This presents two potential signal processing problems for impact testing. If the recording time is long, noise may disturb both the force signal and the response signal. If the recording time is short, leakage may a occur, which means that the response is not allowed to die out before the recording ends.

Both problems may be compensated for by applying a windowing technique. By multiplying the force pulse by a *force window*, only the first part of the recording has an actual value. This does usually not affect the results since the pulse duration is a lot shorter then the recording time, and only the noise is removed. The same can be done for the response, by multiplying it with a *response window*. The response is an exponentially decaying function, which may or may not die out during the recording time. If the tested structure is highly damped, the response will probably have died out, and the applied response window will mainly reduce the noise. If the response does not die out, the window will reduce the leakage by forcing the response to die out. This affects the FRF since the response window adds artificial damping to the system. This is mainly a problem for lightly damped structures where the artificial damping may be higher than the structural damping. Figure 3.4 (a) shows a typical impulse and a force window. Figure 3.4 (b) shows a response of a free vibrating structure, an exponential window and the response multiplied by the window. The use of response windows should be avoided if possible, but the effects form using windows are far more acceptable than the effect of leakage[7].

Usually the recording is initiated by a trigger in the recording software related to the hammer. The recording starts when the load cell in the hammer exscids a force higher than a given trigger value. To avoid missing the first part of the time series, the software starts recoding before the trigger value is registered and cuts down the time series, so that it starts saving the recording just before the trigger value is reached and no information is lost. This also minimizes the amount of noise recorded before the impact.

In some situations, it can be hard to get perfect impacts, which can lead to bad FRFs. The validity of the output FRF is assessed by a coherence function, based on the cross spectral density (G_{XF}), load signal spectral density (G_{FF}) and the response signal spectral density (G_{XX}), defined as:

$$\gamma^2 = \frac{\mid G_{XF}(\omega)^2 \mid}{G_{FF}(f)G_{XX}(f)} \tag{3.41}$$

To enhance the chance of getting a good coherence factor ($\gamma \geq 0.75$), several measurements form the same location of impact can be averaged in one FRF. This reduces the influence of a bad impact on the FRF [37].

3.2.2.2 Establishing the Frequency Response Function

To be able to identify the modal parameters of the tested structure, the FRF must be established. The frequency response of a structure is in full described by the frequency
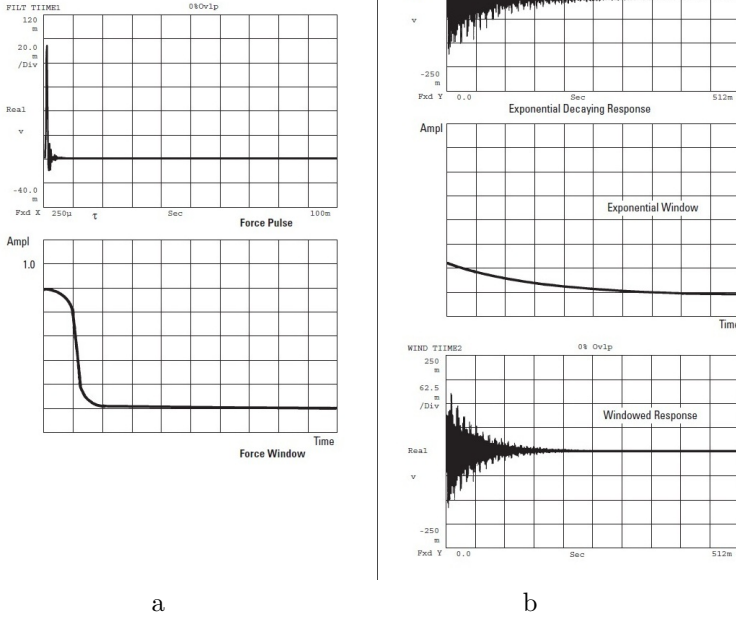
Figure 3.4: Window Functions[7]

response matrix which is represented by $\mathbf{H}$ in Equation 3.42

$$\mathbf{X}(\omega) \quad = \quad \mathbf{H}(\omega)\mathbf{F}(\omega) \tag{3.42}$$

$$\left\{ \begin{array}{c} X_1 \\ X_2 \\ \vdots \\ X_n \end{array} \right\} = \left[\begin{array}{cccc} H_{11} & H_{12} & \cdots & H_{1n} \\ H_{21} & H_{22} & \cdots & H_{2n} \\ \vdots & \vdots & \ddots & \vdots \\ H_{n1} & H_{n2} & \cdots & H_{nn} \end{array} \right] \left\{ \begin{array}{c} F_1 \\ F_2 \\ \vdots \\ F_n \end{array} \right\} \tag{3.43}$$

Each element in $\mathbf{H}$ is can be described by:

$$H_{ij}(\omega) = \frac{X_i(\omega)}{F_j(\omega)} = \frac{Responce(i)}{Excitation(j)} \tag{3.44}$$

Where $X_i(\omega)$ = Fourier transform of the response $x(t)$ measured at location i and $F_j(\omega)$ = Fourier transform of the excitation $f(t)$ applied at location j.

Remembering that for the roving hammer test, the accelerometer was kept in one place during the entire test and that the hammer excited the structure at different locations. The rowing hammer test describes one row of the the frequency response matrix (i = constant, j = 1, 2, ... n). This only describes the structural response sufficiently if no modes have the same modal frequency. If this requirement is not satisfied, the tests should be repeated with the accelerometer in a different location.

For the driving point test, $i = j$, which means that only one diagonal element of **H** is described, and no mode shape can be found.

For SIMO testing, using a shaker, the accelerometer would be moved around and the shaker kept in one place, describing a column instead of a row. Thus can the tests be treated equally form a mathematical point of view[25].

3.2.2.3   Curve Fitting

Curve fitting is also referred to as *modal parameter extraction* when used in experimental modal analysis. This is the proses where the three modal parameters modal frequency, modal damping and mode shapes are estimated. This is done by minimizing the squared difference between an assumed analytical functions and the FRF obtained form the tests. The FRF contain the parameters of all modes excited and measured during the tests. Usually, only a certain range of frequencies are of interest and by only looking the this part of the FRF, the response of the structure can be reduced to a discrete set of modes. The FRF of the structure can thus be described as a discrete sum of analytical modal parameters. By using equivalent viscous modal damping (ζ), the FRF is described by:

$$H_{ij}(\omega) = \sum_{r=1}^{n} \frac{(\psi_i \psi_j)_r}{(\omega_r^2 - \omega^2 + 2i\zeta_r \omega_r \omega)} \tag{3.45}$$

Here r is the mode number, n is the total number of modes, $(\psi_i \psi_j)_r$ is the residuals and ω_r is the undamped natural frequency[25]. The damping ratio and the undamped natural frequency can be extracted directly form the equation, whilst the mode shape vectors are a bit more cumbersome. The mode shape vector is described by:

$$[\Psi]_r = \{\psi_i\}_r \{\psi_j\}_r^T \tag{3.46}$$

And by looking at a single row, the mode shape vector can be extracted as:

$$[\Psi]_r = \left[\ \{\psi_1^2\}_r \quad \{\psi_1 \psi_2\}_r \quad \cdots \quad \{\psi_1 \psi_n\}_r \ \right] \tag{3.47}$$

There are several different methods available for doing this, and it is a subjects which can be studied in great extent. This is however not the main subject of this thesis, so only a short overview will be given.

There is a large amount literature and algorithms available for curve fitting, and it can not be said that one method is better than the others for all cases. The different methods have different advantages and disadvantages, where some work best on lightly damped systems and others on heavily damped systems. Some methods are quick and some are slow and with varying accuracy. It is however important to remember that all solutions obtained form curve fitting are approximations, regardless of method. The applied method should be chosen according to the nature of the FRF and requirements for accuracy and analysis time[18].

Curve fitting methods can generally be categorized as SDOF methods and MDOF methods. The SDOF methods identify the modal parameters of one mode at a time. This is done by limiting the analyzed part of the FRF to include only one mode. The MDOF methods estimate the parameters of several modes at the same time, and are often used with heavily coupled systems, where single modes can not be separated [7]. Figure 3.5 (a) illustrates a SDOF curve fitting and (b) illustrates a MDOF curve fitting of the same FRF. The method that has been used in this thesis is called the *Frequency-domain Direct Parameter Identification* (FDPI). The method estimates the modal properties by using

a   b
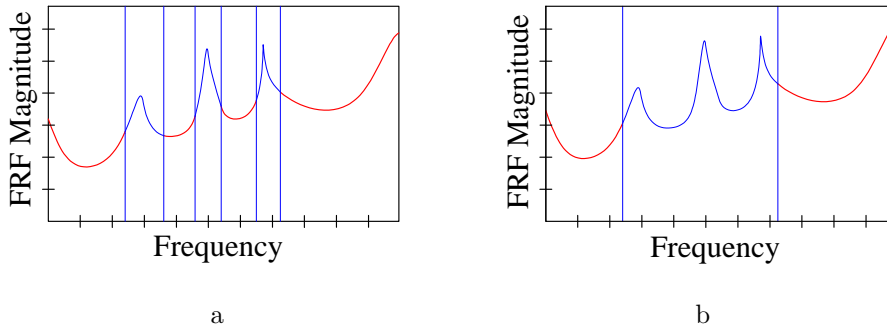
Figure 3.5: Curve Fitting

a *state model*[5], and can be used for both SDOF and MDOF identification. It is ideal for heavily damped modes in a narrow frequency band.[49] For further reading about curve fitting see, Ewins [25].

3.3   System Identification

System identification has been used to estimate the modal parameters of the tested structure, described in this thesis. However, system identification theory is not the main focus of this thesis, so only a short explanation is given. For a thorough review of this subject, see [**39, 43, 32, 42, 16**].

System identification, in structural engineering, is a method for estimating dynamic properties of structures. It can be described as an advanced form of curve fitting based on mathematical algorithms that can be hard to follow for people with a background in classical structural dynamics. Besides experimental evaluations of dynamic properties of structures, system identification is used as a monitoring system of ready built structures to get a better understanding of their dynamic properties. The information gained form such monitoring can be used to update and build better numerical models for similar structures in the future[39].

There are several available algorithms for system identifications. Some are the *Least square method,* the *Extended Kalman filter* and the *Maximum likelihood method.* The method that was used in this thesis is called the *Numerical Subspace State Space System Identification method (N4SID).* This is a least square method, which is part of the *System Identification Toolbox* in MATLAB. It is therefor easy to use and is considered robust due to its well-understood algorithms based no numerical linear algebra. The method estimates a state sequence directly from the given input data trough the use of certain block Hankel matrices. Then comes a singular value decomposition, followed by the least square method to obtain the solution. The method can handle both input - output measurements and output-only measurements[32].

3.3.1   Dynamic Model

The response of a dynamic system can not be determined unless the *state* of the system is known at a certain time. This means that the dynamic response of a structure depends on its previous load history. Thus is a state space model required to describe the

---

[5]State space models are described in Section **3.3,** (however, the SID and MA don't use the not the same algorithm).

system, together with previous inputs. The equation of motion of a structure subjected to stochastic loading can be described by:

$$\mathbf{M}\ddot{\mathbf{y}}(t) + \mathbf{C}_{eff}\dot{\mathbf{y}}(t) + \mathbf{K}_{eff}\mathbf{y}(t) = \mathbf{p}(t) \tag{3.48}$$

This represents a damped system of n degrees of freedom, where $\mathbf{M}$= mass matrix, $\mathbf{C}_{eff}$= damping matrix, $\mathbf{K}_{eff}$= stiffness matrix, $\mathbf{p}(t)$= load vector and $\mathbf{y}(t)$= stochastic response[43].

3.3.2   State Space Model

The n second order differential equations for the dynamic system may be re written as $2n$ first order differential equations as:

$$\begin{bmatrix} \dot{\mathbf{y}}(t) \\ \ddot{\mathbf{y}}(t) \end{bmatrix} = \begin{bmatrix} 0 & \mathbf{I} \\ -\mathbf{M}^{-1}\mathbf{K}_{eff} & -\mathbf{M}^{-1}\mathbf{C}_{eff} \end{bmatrix} \begin{bmatrix} y(t) \\ \dot{y}(t) \end{bmatrix} + \begin{bmatrix} 0 \\ \mathbf{M}^{-1} \end{bmatrix} \mathbf{p}(t) \tag{3.49}$$

This is a more convenient form, for the use in system identification. A state space model for continuous time is given by [39]:

$$\dot{x}(t) \quad = \quad \mathbf{A}_c\mathbf{x}(t) + \mathbf{B}_c\mathbf{u}(t) + \mathbf{w}_c(t) \tag{3.50a}$$
$$\mathbf{y}(t) \quad = \quad \mathbf{C}\mathbf{x}(t) + \mathbf{D}\mathbf{u}(t) + \mathbf{v}(t) \tag{3.50b}$$

Where subscript c stands for continuous time $\mathbf{x}(t)$ = the state vector, $\mathbf{u}(t)$ = input vector[6], $\mathbf{y}(t)$ = output vector, $\mathbf{A}$ = system matrix, $\mathbf{B}$ = load matrix, $\mathbf{C}$ = output matrix $\mathbf{D}$ = direct freedthrough matrix, $\mathbf{w}$ = input noise and $\mathbf{v}$ = output noise. The equivalent equation for discrete time is given by:

$$\mathbf{x}_{k+1} = \mathbf{A}_d\mathbf{x}_k + \mathbf{B}_d\mathbf{u}_k + \mathbf{w}_k \tag{3.51a}$$
$$\mathbf{y}_k = \mathbf{C}\mathbf{x}_k + \mathbf{D}\mathbf{u}_k + \mathbf{v}_k \tag{3.51b}$$

Where subscript d stands for discrete time, and subscript k stands for discrete time instant $t_k = k\Delta t$. For systems where the input vector is not measured ($\mathbf{u}_k = 0$), the equations are reduced to:

$$\mathbf{x}_{k+1} \quad = \quad \mathbf{A}_d\mathbf{x}_k + \mathbf{w}_k \tag{3.52a}$$
$$\mathbf{y}_k \quad = \quad \mathbf{C}\mathbf{x}_k + \mathbf{v}_k \tag{3.52b}$$

The expected values of noise is given by:

$$\mathbf{E}\left[\begin{bmatrix} \mathbf{w}_p \\ \mathbf{v}_p \end{bmatrix} \begin{bmatrix} \mathbf{w}_q^T & \mathbf{v}_q^T \end{bmatrix} \right] = \begin{bmatrix} \mathbf{Q} & \mathbf{S} \\ \mathbf{S}^T & \mathbf{R} \end{bmatrix} \delta_{pq} \geq 0 \tag{3.53}$$

Where $\mathbf{E}$ = expectation value operator, δ_{pq} = Kronecker delta, $\mathbf{Q}$, $\mathbf{S}$ and $\mathbf{R}$ = covariance matrices of the noise sequences $\mathbf{w}_k$ and $\mathbf{v}_k$.

---

[6]Also translates to the load vector

3.3.3   N4SID Algorithm

Since only the algorithm for the output-only method was used in this thesis, this is the one explained here. This means that the system matrix $\mathbf{A}$ and the output matrix $\mathbf{C}$ will be calculated and the covariance matrices $\mathbf{Q}$, $\mathbf{S}$ and $\mathbf{R}$ estimated from the output matrix $\mathbf{y}$. The first step of the algorithm is to establish the block Hankel matrix[42].

3.3.3.1   Block Hankel matrix

The block Hankel matrix play an important role in the algorithm, and is constructed from the output data obtained from measurements. The matrix is defined as[16]:

$$
\mathbf{Y}_{0|2i-1} = \left[\begin{array}{ccccc}
y_0 & y_1 & y_2 & \cdots & y_{j-1} \\
y_1 & y_2 & y_3 & \cdots & y_j \\
\vdots & \vdots & \vdots & \cdots & \vdots \\
y_{i-1} & y_i & y_{i+1} & \cdots & y_{i+j-2} \\
\hline
y_i & y_{i+1} & y_{i+2} & \cdots & y_{i+j-1} \\
y_{i+1} & y_{i+21} & y_{i+3} & \cdots & y_{i+j} \\
\vdots & \vdots & \vdots & \cdots & \vdots \\
y_{2i-1} & y_{2i} & y_{2i+1} & \cdots & y_{2i+j-2}
\end{array} \right] = \left(\frac{\mathbf{Y}_{0|i-1}}{\mathbf{Y}_{i|2i-1}} \right) = \frac{\mathbf{Y}_p}{\mathbf{Y}_f} \qquad (3.54)
$$

Where i is defined by the user as a number larger than the maximum order of the system. j is the number of output samples to be used in the analysis[7]. Subscript p stands for past and subscript f stands for future.

3.3.3.2   Orthogonal Projection

The projection of the block Hankel matrix is done by LQ decomposition.

$$
\left[\begin{array}{c}
\mathbf{Y}_{0|i-1} \\
\mathbf{Y}_{i|i} \\
\mathbf{Y}_{i+1|2i-1}
\end{array} \right] = \left[\begin{array}{ccc}
\mathbf{L}_{11} & 0 & 0 \\
\mathbf{L}_{21} & \mathbf{L}_{22} & 0 \\
\mathbf{L}_{31} & \mathbf{L}_{32} & \mathbf{L}_{33}
\end{array} \right] \left[\begin{array}{c}
\mathbf{Q}_1^T \\
\mathbf{Q}_2^T \\
\mathbf{Q}_3^T
\end{array} \right] \qquad (3.55)
$$

Where $\mathbf{L}=$ lower triangular matrix and $\mathbf{Q}$ = orthogonal matrix.

Two projections are needed, $\mathbf{O}_i$ and $\mathbf{O}_{i-1}$ where the future is projected on to the row space of the past. These are defined as:

$$
\mathbf{O}_i = \frac{\mathbf{Y}_f}{\mathbf{Y}_p} = \left[\begin{array}{c} \mathbf{L}_{21} \\ \mathbf{L}_{31} \end{array} \right] \mathbf{Q}_1^T \qquad (3.56a)
$$

$$
\mathbf{O}_{i-1} = \frac{\mathbf{Y}_f^-}{\mathbf{Y}_p^+} = \left[\begin{array}{cc} \mathbf{L}_{31} & \mathbf{L}_{32} \end{array} \right] \left[\begin{array}{c} \mathbf{Q}_1^T \\ \mathbf{Q}_2^T \end{array} \right] \qquad (3.56b)
$$

Where $\mathbf{O}_{i-1}$ is found by simply shifting the line down one row form $\mathbf{O}_i$. It can also be shown that:

$$
\mathbf{O}_i = \mathbf{\Gamma}_i \hat{\mathbf{X}}_i \qquad (3.57a)
$$

$$
\mathbf{O}_{i-1} = \mathbf{\Gamma}_{i-1} \hat{\mathbf{X}}_{i+1} \qquad (3.57b)
$$

Where $\mathbf{\Gamma}_i$ = observability matrix and $\hat{\mathbf{X}}_i$ = state sequence. The order of the model is defined as the rank of $\mathbf{O}_i$.

---

[7]Usually $j = s - 2i + 1$ which means that all available samples are used

3.3.3.3   Singular Value Decomposition

By singular value decomposition of $\mathbf{O}_i$, the order of the model can be found, together with the matrices $\mathbf{\Gamma}_i$ and $\hat{\mathbf{X}}_i$. This is done by:

$$\left[\begin{array}{c} \mathbf{L}_{21} \\ \mathbf{L}_{31} \end{array}\right] = \left[\begin{array}{cc} \mathbf{U}_1 & \mathbf{U}_2 \end{array}\right] \left[\begin{array}{cc} \mathbf{S}_1 & \mathbf{0} \\ \mathbf{0} & \mathbf{0} \end{array}\right] \left[\begin{array}{c} \mathbf{V}_1^T \\ \mathbf{V}_2^T \end{array}\right] = \mathbf{U}_1 \mathbf{S}_1 \mathbf{V}_1^T \qquad (3.58)$$

Which gives the observability matrix and the state sequence[8]:

$$\begin{align} \mathbf{\Gamma}_i &= \mathbf{U}_1 \mathbf{S}_1^{1/2} & (3.59\mathrm{a}) \\ \hat{\mathbf{X}}_i &= \mathbf{S}_1^{1/2} \mathbf{V}_1^T \mathbf{Q}_1^T & (3.59\mathrm{b}) \\ \hat{\mathbf{X}}_{i+1} &= \left(\underline{\mathbf{U}_1 \mathbf{S}_1^{1/2}}\right)^\dagger \left[\begin{array}{cc} \mathbf{L}_{31} & \mathbf{L}_{32} \end{array}\right] \left[\begin{array}{c} \mathbf{Q}_1^T \\ \mathbf{Q}_2^T \end{array}\right] & (3.59\mathrm{c}) \end{align}$$

3.3.3.4   System Matrices

The system matrix and the output matrix can now be calculated using the least square method on the equation below. The equation is based on $\mathbf{Y}_{i|i}$ from Equation 3.55 and $\hat{\mathbf{X}}_i$ and $\hat{\mathbf{X}}_{i+1}$ from Equations 3.59b and c:

$$\left[\begin{array}{c} \hat{\mathbf{X}}_{i+1} \\ \mathbf{Y}_{i|i} \end{array}\right] = \left[\begin{array}{c} \mathbf{A} \\ \mathbf{C} \end{array}\right] \hat{\mathbf{X}}_i + \left[\begin{array}{c} \rho_w \\ \rho_v \end{array}\right] \qquad (3.60)$$

This equation corresponds to Equation 3.52a, and thus the dynamic properties can be found. The noise covariance matrices can be estimated from the residuals ρ_w and ρ_v.

$$\left[\begin{array}{cc} \mathbf{Q} & \mathbf{S} \\ \mathbf{S}^T & \mathbf{R} \end{array}\right]_i = \frac{1}{j} \left(\left[\begin{array}{c} \rho_w \\ \rho_v \end{array}\right] \left[\begin{array}{cc} \rho_w^T & \rho_v^T \end{array}\right]\right) \qquad (3.61)$$

3.3.4   Matlab Script

As mentioned previously, the N4SID method is implemented in Matlab, which makes it available for users without much programing. Two Matlab scripts were used in this thesis, both made by Ole Øyset, NTNU, consisting of a *preprocessing* script and an *analysis* script.

3.3.4.1   Preprocessing Script

The preprocessing script was used to "prep" the raw data form the accelerometers to make it easier to identify the dynamic properties in the analysis script. The preprocessing "cleans" up the raw data by filtering out higher frequencies and detrending the measurement to ensure zero mean value. After the filtering is done, the operator chooses what part of the time series to use in the identification part. When the excitation is a single impact, the first part of the time series is chaotic, before it settles in to an exponentially decaying oscillation governed by the various eigenfrequencies. The vibrations eventually die out, and the last part of the time series is only noise. By only using the middle part of the time series (the exponentially decaying part), the system identification has a better chance of identifying the appropriate modes. Figure 3.6 illustrates what is done in the preprocessing script. The red lines represent the filtered data and the blue lines represent the original data. It is obvious form the applied frequency response function that the frequency cutof is quite large. The FFT shows how the frequencies are filtered out.

---

[8]† denotes the Moore-Penrose pseudo-inverse of the matrix
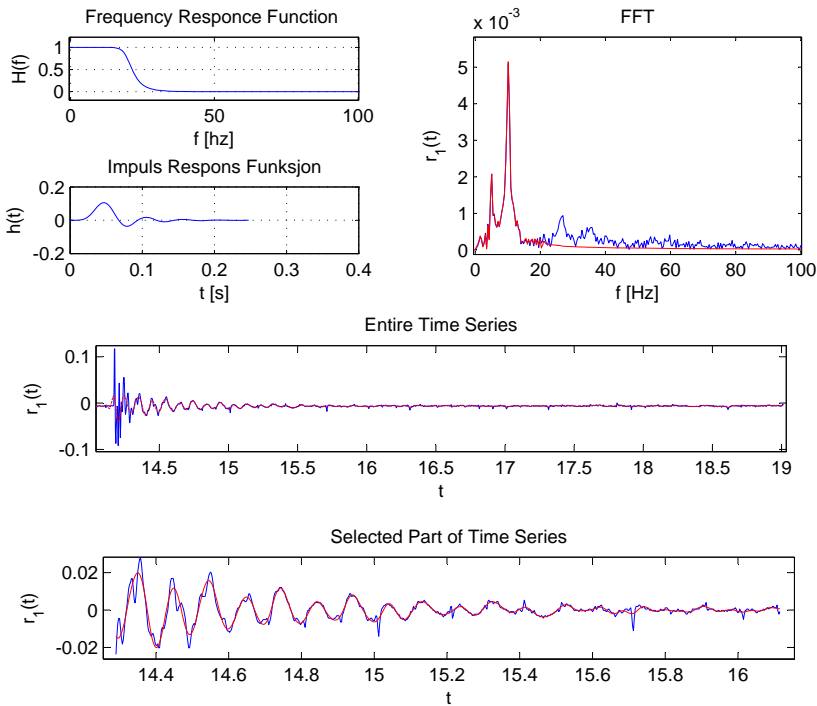
Figure 3.6: Preprocessing

3.3.4.2   Analysis Script

The analysis script is where the system identification tools are used. But before the analysis is carried out, the data needs to be down sampled. The recording rate of a test is chosen by the operator, and is usually a lot higher than what is needed for the system identification. If the sampling rate is to high, the estimation of low frequencies may be distorted due to numerical problems. The sampling rate is therefor reduced before the analysis is carried out. The recommended sampling rate is roughly double the expected eigenfrequencies. By varying the sampling rate, an optimal sampling rate may be found for the time series in question.

The next step is to specify the model order for the analysis. This is usually done by looking at the singular values of the block Hankel matrix, which provides information about the effective rank of the system. The model order that gives the best results is usually the order where the largest drop in singular value is found[9]. The model order of the system should be close to double the number eigenfrequencies since the state vector contains both displacement and velocity. If the chosen model order is to low, the model will not be able to identify the system properly[32]. Figure 3.7 (a) shows a plot of the singular values for a typical analysis, where the largest drop is between order 4 and 5. Figure 3.7 (b) show a plot of estimated natural frequencies and damping ratios against model order of from the same analysis. The red lines indicate the chosen model order, and the blue circles indicate the estimated natural frequencies and damping ratios. From

---

[9]The model order can also be set to +1 of the largest drop in singular values.
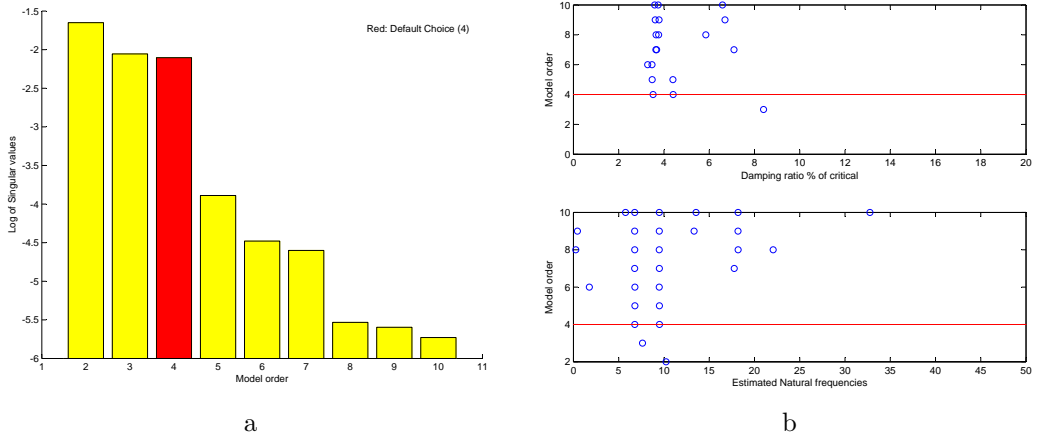
Figure 3.7: System Identification, Model Order and Dynamic Properties

this figure it is clear that a model order lower than 4 would not identify the dynamic properties properly. The figure also shows that both frequencies and damping ratios remain sable for higher model orders. This increases the confidence of the estimated values. If the dynamic properties have different values for increasing model order, the values are not to be trusted. If this is the case, the sampling rate can be changed to see if a more stable estimation can be made.

The operator can also chose which time series to include in the analysis. This way, bad preforming accelerometers can be discarded so that they do not disturb the analysis.

Chapter 4

Dynamic Testing of Building Modules

4.1 Module Testing Background

In the VHT project modules will be placed on top of each other to create the residential area of the building. These stacks will have a height of four modules and a width of two and five modules. The stacked modules will only be connected to the load-baring frame threw the concrete slab on top the power floors". This means that the module stacks will be supported at a height of roughly 16 and 32 meters above ground level. Since the modules are placed this high up in the building, their dynamic properties may influence the dynamics of the entire building.

Early calculations preformed by *SWEVO* showed that the accelerations in the top of the building exceeded the the requirement of building code ISO 10137, and that something has to be done to reduce the accelerations. By increasing the damping in the building, the accelerations may be reduced, but that involves either a a damper, finding elements in the building with more damping that can be utilized. In Eurucode (EC) 1-1-4 Table F.2 it is stated that the largest allowed value of damping in timber bridges is 1.91% and EC 5-1 states that the unless other values are documented the damping in a timber floor should be sett to 1% . These values are generally regarded to be conservative and further surveys in this field is needed to establish a better building code. Several studies has done no the subject of damping in timber structures, with a special attention to timber floors, with a general consensus that the *in situ* damping ratio is considerably higher than the prescribed value of EC 5 [30, 33, 37, 34]. However, little has been been done on the subjects of dynamic properties of building modules and since these properties, if determined and utilized, could contribute to lowering the accelerations in the VHT building, further surveys are warranted.

To test the dynamic properties of building-modules a test method was required. In a preceding project to this survey, laboratory testing of a model module was carried out to determine weather a modal analysis test using a hammer to excite the building would be suitable for testing building modules. This study showed consistent results for frequency, damping and mode shapes. The results had a good correspondence with the mode shapes of a FE model of the same module. Based on this project, modal hammer analysis was chosen as test method for the modules. In addition to the modal hammer tests, a system identification setup was made. The system identification method was

tested in the lab, and gave the same properties as the modal hammer tests in [31].

Another factor that was considered when the test methods were chosen was the portability of the required equipment. Since both methods require relatively small amounts of equipment, the setup could easily be transported to different test locations. This was an important factor since the modules that were to be tested were located in Tartu, Estonia. Further explanation of the test methods can be found in Sections 3.2 and 3.3.

There are several different ways of looking at the dynamic properties of a building-module. One can look at the acoustics of the modules, floor vibrations or comfort perspectives, and so on. There are a lot of different challenges regarding dynamics of timber structures, but here, the main focus has been the global modes of the modules. This means that local modes like internal floor vibrations and acoustics has been neglected. The goal was to determine the lowest fundamental modes with corresponding frequencies and damping ratios. The results would be used to build a representative FE model with the same dynamic properties, and re scale this to fit the modules of the VHT project.

To be able to create a FE model of the stacked modules, it wold be useful to know what happens to the dynamic properties when the modules are connected together. This knowledge could be acquired by testing both connected and unconnected modules. Two different test setups were chosen. The first with four modules stacked two by two and connected together, and the second with a single unconnected module.

4.2   Modules

The tests were preformed on modules produced by Kodumaja[1], an Estonian module building company located in Tartu, Estonia. The modules are produced indoors on a big factory floor and are built from the ground up along the production line. The people working at each station have specific tasks to preform, which means that the work is always preformed by professional and qualified personnel. Kodumaja mainly produces modules for multistorey residential buildings and smaller private houses. They have built domestic buildings with more than four stories in previous projects, which means that the VHT project will not be the tallest in terms of modules stacked on top of each other. The challenge in this project is therefor not how to build the modules in terms statical loading, but rather how to build the load bearing gluelam frame around the modules and how the modules will effect the dynamics of the load bearing frame.

The test modules were built for a project in Bjørnåsen, Oslo. They are longer than the once planed for the VHT project, but height and width is almost the same. The layout of doors and windows matches what the VHT modules will probably look like, but as the details for the VHT modules are not yet finished this is as close as it gets. The modules were taken out of the production line before the exterior cladding was attached and covered in plastic to keep them weather tight in case of rain during the testing. The exterior dimensions of the modules are given in Table 4.1.

Modules	Length	Width	Height
Tested	12.5m	4.005m	3.01m
VHT	8.7m	4m and 5.3m	3.m

Table 4.1: Module Dimensions

---

[1]Kodumaja will also build the modules for the VHT project
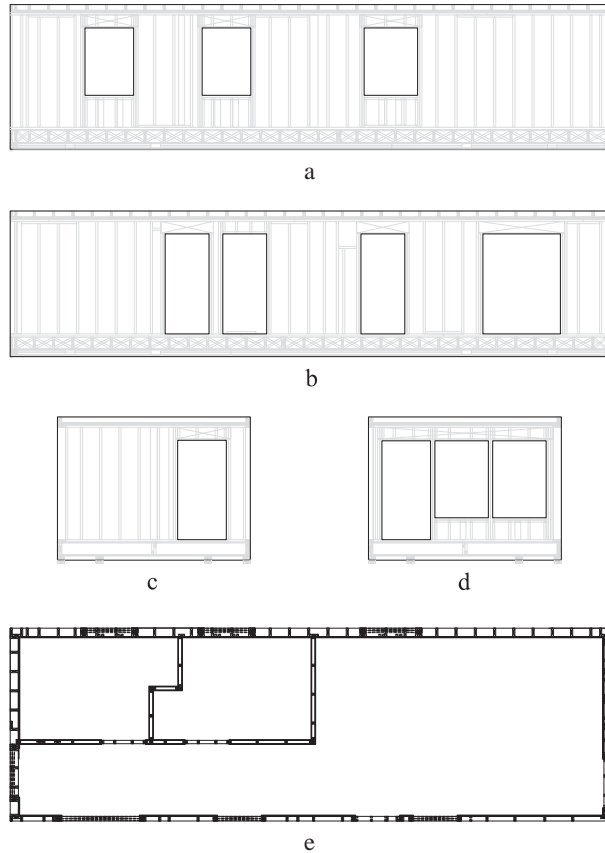
Figure 4.1: Single Module

All test modules, had the same layout, with three load bearing exterior walls (Figure 4.1 (a), (c) and (d)), one load bearing interior wall (Figure 4.1 (b)) and interior light walls (Figure 4.1 (e)). They were built with stud frames as the load bearing components, as shown in Figure 4.1, and apart from the thickness of the studs and the vapor barrier in the exterior walls, the construction of load baring interior and exterior walls are the same. (see Figure 4.2). The short walls were very different from each other. One was built with windows and a glass door, and the other with a normal exterior door.

The stud frames are filled with mineralwool, covered with two layers of plasterboard on the inside and 8mm OSB plates on the outside. When finished the modules will be covered with more insulation, and exterior cladding. However, the VHT modules will have no exterior cladding as this will fitted to the load bearing gluelam frame instead of the modules. The slightly unfinished state of the test modules therefor made them ideal for comparison with the VHT-modules.

Four modules were tested, two first floor modules and two second floor modules. There were only a few design details separating the first and second floor modules. The internal load bearing wall in the first floor modules are reinforced by reducing the center distance between the studs from 600 mm to 400 mm. The floors and ceilings are the same at both levels, except from some wind barrier plates on the underside of the

modules at ground level. Se Figure 4.2. When the modules were lifted to the test sight, a rough weight measurement was made by the instrumented crane lifting the modules. This showed that the first floor modules weighed roughly 9500 kg and the second floor modules 9100kg. The weight difference has been assumed to be due to the extra plates on the underside of first floor modules.
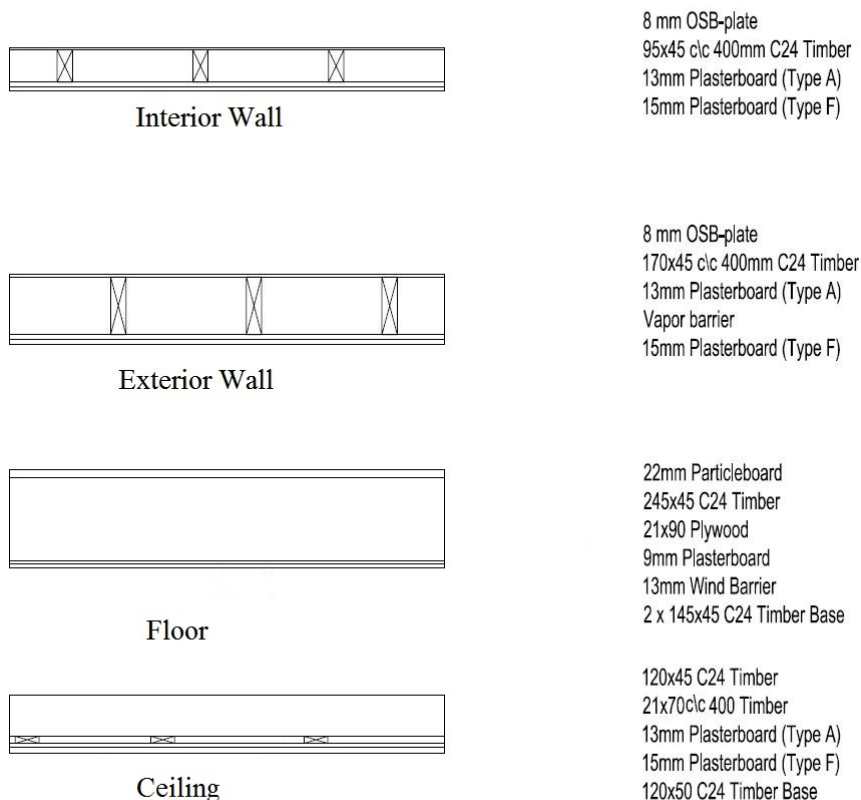
Figure 4.2: Cross Sections of Module Elements

4.2.1   Module Setups

Two different test setups were made, a two by two setup and a single module setup. The first setup involved four modules stacked two by two and connected together. When connected, the long internal wall of the first module would line up with the internal wall of the second, mirroring the first. This was the same at both floors, and since there were two left oriented and two right oriented modules, only exterior walls were exposed to the weather. Figure 4.3 shows the two by two stacked modules close to the Kodumaja factory.

Windows   Doors

Long Side

Figure 4.3: Staked Modules

The second test setup only involved one second floor module, that had been part of the previous two by two setup. By comparing the results from the two setups, the effect of connecting and stacking modules might be found. Figure 4.4 shows the single module setup.

Long Exterior Wall

Long Interior Wall

Short Exterior Wall

Figure 4.4: Single Module

4.2.2   Connections and Foundations

For the two by two setup a foundation was made as shown in Figure 4.5. The foundation consisted of a timber frame propped up by blocks of wood to make the foundation horizontal. This was covered by continuous layers of 8mm of OSB plates, 15mm of Stepisol[2] and 3mm timber fiber boards. The two first floor modules were placed on top of the frame and connected to the frame by a continuous vertical strip of 8mm OSB plates nailed to the module and the foundation. The frame was locally secured to the ground by steel brackets anchored to the asphalt. Figure 4.6 (a) shows a vertical cross section of the foundation with a module mounted on top.

On top of the first floor modules there was a low timber frame, covered the same way as the foundation, with OSB plates, Stepisol and timber fiber boards. The second floor modules were placed on top of this and connected horizontally with a continuous vertical strip of 8mm OSB plate in the same way as to the foundation. Figure 4.6 (c) shows a vertical cross section of the connection between the first and second floor modules. The exterior vertical connections were also made with 8mm OSB plates nailed to both

---

[2]Stepisol is a product designed for sound reducing purposes. This is further described in **Chapter X**

Figure 4.5: Two by Two Foundation

modules, while the internal connections in the doorways were made with plaster board, as they would have been in their finished state. The horizontal plate cowering the low frame on top of the first floor modules was nailed to both modules to create a horizontal connection along the seem between the aligned modules. A similar connection was made on top of the second floor modules. A vertical cross section of this connection is shown in Figure 4.6 (b). Figure 4.6 (d) and (e) shows a horizontal cross section of the vertical connection between the two short walls on the window and door side, respectively.
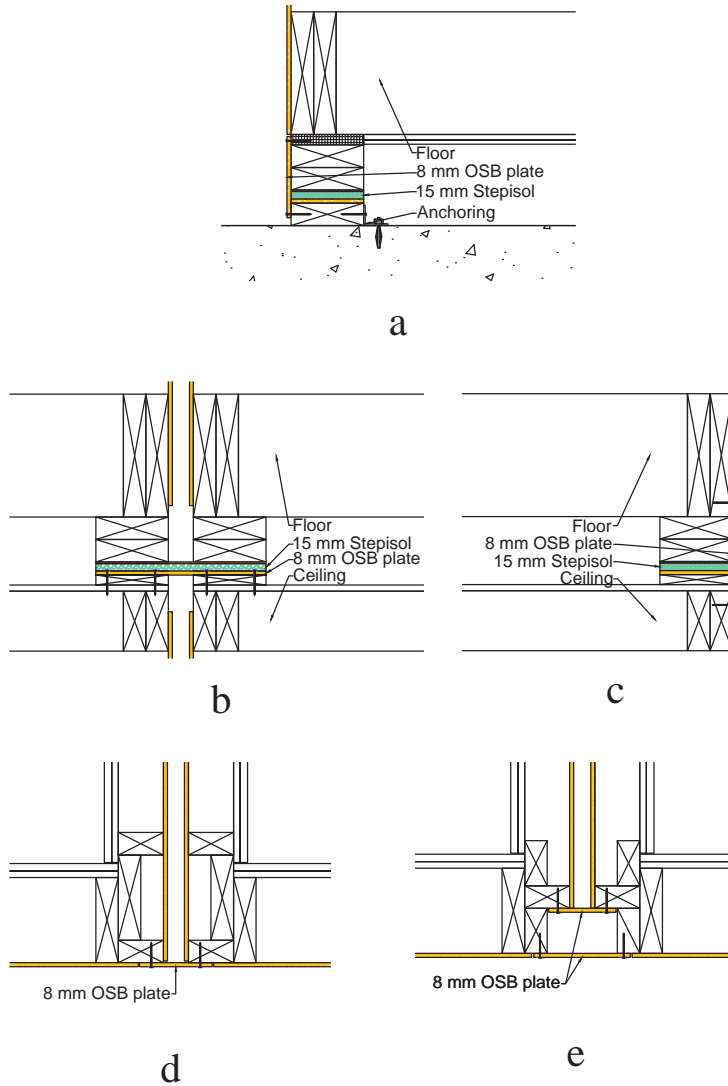
Figure 4.6: Foundation and Connection Cross Sections

The tests on single module setup was done at a different location than the two by two setup since there had been some trouble with electrical noise on the previous tests. It was therefor placed on top of five I-beams bolted to concrete blocks and propped up with bits of timber to make it horizontal. This made the testing easy, but was later found to be a mistake. Figure 4.4 illustrates the the support conditions which can also be seen in Figure 4.4. There was no Stepisol between the module and the foundation in this setup.
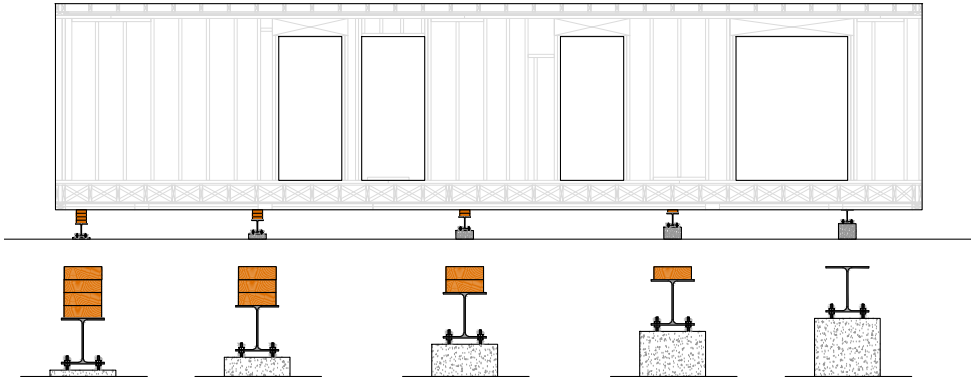
Figure 4.7: Single Module Foundations

Designation	Reference	Supplier
Modal Hammer	Heavy Duty type 8210	Brüll & Kjær
Piezoelectric accelerometer	8703A50M5	Kistler
Power supplier & signal conditioner	Type 5134	Kistler
NI dynamic module	NI 9234	NI Norway
NI Chassis	NI cDAQ-9174	NI Norway
Computer Recording Software	Record Impact Testing FRF data	LabVIEW 2010

Table 4.2: Equipment for Modal Analysis

4.3 Test Equipment

Two different test protocols were used, an *experimental modal analysis* (MA) protocol and a *system identification* (SID) protocol. The protocol require slightly different equipment and setups. The equipment used for each protocol is listed in Tables 4.2 and 4.3.

4.3.1 Modal Analysis

Figure 4.9 shows how the equipment were set up and connected before testing.

4.3.1.1 Modal Hammer

The hammer head weighs 5.44 kg and is instrumented with a piezoelectric load cell which registers the force of impact. The weight and the velocity of the hammer determines the excitation energy. The velocity is hard to control, but by choosing a heavy hammer the excitation energy will be large enough to excite large structures like buildings, bridges and ships.

The hammer is provided with four different tips of varying stiffness. The stiffens of the tip is chosen according to the frequencies of interest. If a stiff tip is chosen the impact will have a high peak force and short pulse duration. This will excite high frequencies. If a soft tip is chosen the peak force will be lower and the pulse duration longer. This will excite low frequencies. Figure 4.10 illustrates impulse shape and frequency response of the different tips [11]. Since the low frequencies are of most interest, the softest tip

Hammer

Accelerometer

NI Chassis and Dynamic Module

Power Supplier

Figure 4.8: MA Equipment
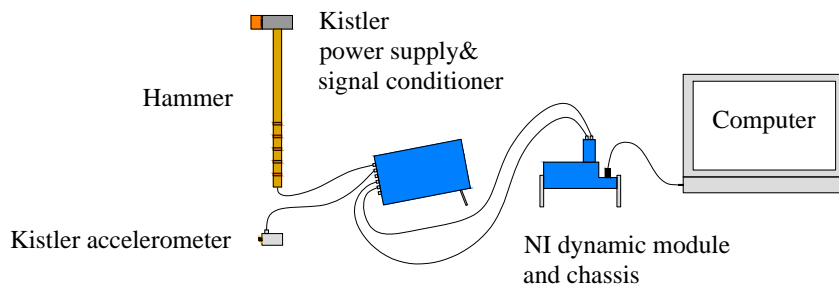
Figure 4.9: Modal Analysis Equipment Setup

was used.

4.3.1.2   Accelerometer (Kistler)

The Kistler accelerometer is a one dimensional piezoelectric accelerometer with a sensitivity of 97.3 mV/g. It has a Frequency range from 0.5 Hz to 10000 Hz and an acceleration range of ± 50 g. It is a non static accelerometer which means that it only registers changes in acceleration and measurements are not affected by gravity. Due to this, the accelerometer does not need to be calibrated against its orientation in the gravitational field. It is light weight accelerometer which is easily mounted to most structures by a threaded stud, cement or magnetic forces [35].
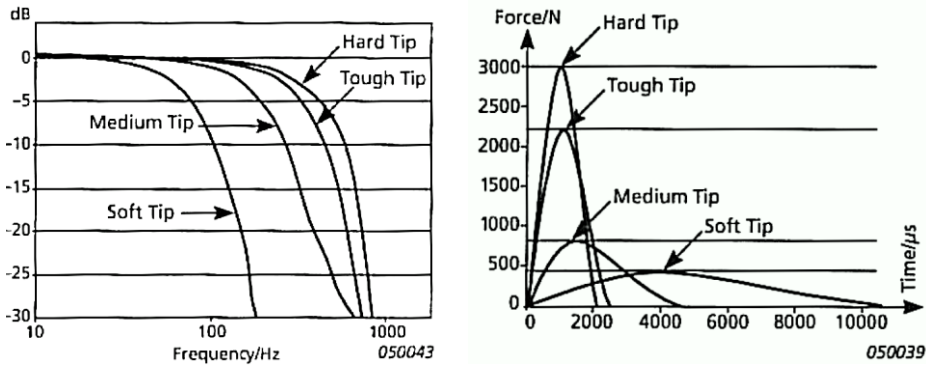
Figure 4.10: Hammer Tips [20]

4.3.1.3   NI Dynamic Module and NI Chassis

The NI[3] dynamic module is a four-channel C series dynamic signal acquisition module for accurate audio frequency measurements. It is used for integrated electronic piezoelectric and non-piezoelectric sensors with the NI C CompactRIO systems. It is a signal conditioner for accelerometers and microphones. The IN chassis is designed to be light weight, portable system, and can be combined with up to four NI C Series modules, which enables the user to gadder data from several type of systems, like load cells, accelerometers and microphones.The data may be imported to a computer via a USB cable [37].

4.3.1.4   Power Supply and Signal Conditioner

This is built to be a flexible and easy to use interface between voltage mode piezoelectric and measurement instruments. It is used as a signal conditioner that provides excitation power to the instruments. It can be used as a stand alone unit, or be connected to other unites [36].

4.3.2   System Identification

Figure 4.12 shows how the equipment were connected before testing. The hammer is not connected in this illustration, and was only used as an unknown excitation force. It can be connected and logged by connecting it via the Kistler power supply & signal conditioner to the Spider 8.

---

[3]National Instruments

Designation	Reference	Supplier
Modal Hammer	Heavy Duty type 8210	Brüll & Kjær
6 x Accelerometers	B12/500	HBM
Spider 8	Spider 8	HBM
Computer Recording Software	Catman Easy/AP 3.3	HBM

Table 4.3: Equipment for System Identification

Spider 8

Hammer

Accelerometer

Figure 4.11: SI Equipment

Figure 4.12: System Identification Setup

4.3.2.1   HBM Accelerometers

The HBM accelerometers B12/500 is a one dimensional stain gage based accelerometer which registers accelerations up to $1000m/s^2$ and has a working frequency up to 250 Hz. Since it is a strain gage accelerometer, it needs to be calibrated before use to make sure that when it is vertical it gives out 1 g and 0 g when it is horizontal. The accelerometer has a threaded stud at the end of it's cylinder shaped body, threw which it is attached to the test object [27].

4.3.2.2   Spider 8

Spider 8 is an electric measuring system for PCs, used for electric measurement of mechanical variables such as force, strain, pressure and acceleration. The main purpose of the Spider 8 is to digitalis electrical signals from the connected equipment to allow the measurements to be recorded in a computer. It has eight independent channels which can be connected to any suitable equipment at the same time. It is connected to a

computer via a USB-cable, threw which the unit is controlled by the computer interface [26].

4.4   Test Protocol

The practical difference in carrying out the MA and SID tests were small. The hammer was used to excite the structure and accelerometers registered the acceleration time history for both protocols. The main difference lies in how the data were treated after the time series has been recorded and in what order the impacts were registered. The setups of accelerometers were also different.

4.4.1   Modal Analysis Test Protocol

For the MA test, the impacts of the hammer were registered by the built in load cell and the accelerations registered by a single accelerometer. The structures were excited at several locations which corresponds to a preprogramed grid in the MA software, "LabView - Record Impact Testing FRF data". Each grid point[4] was excited three times in a row. The recorded data was than averaged to create one FRF for each impact point. To ensure that the vibrations in the modules had died out before the recording ended, the recording time was set to 3 seconds and a rectangular response window was applied.

The tests were carried out by two operators. One recording and monitoring the tests on the computer, and the other wielding the hammer. The impacts were recorded in the order given by the numbers in the figures in Section 4.5.2.

After the tests were finished the collected data was analyzed. Each analysis contained information from three impacts for all grid points. The output from the MA recording software was a FRF for each grid point, generated by applying a fast Fourier transformer (FFT). A curve fitting procedure was than applied to FRFs, in the analysis software "LabView - Modal Parameter Identification", to extract the modal parameters consisting of eigenfrequencies, damping ratios and the mode shapes.

4.4.2   System Identification Test Protocol

For the SID test, the excitations were also applied by the hammer, but the impact force was not recorded, nor was it required for the analysis. The structure could have been excited by any other force, but to be able to compare the two methods the hammer was used for both tests. Six tactically placed accelerometers measured the accelerations and a computer recorded the acceleration time histories (see Section 4.5.2 for accelerometer placement).

The acceleration time history from all or some accelerometers were then imported in to the SID software taht gives out the eigenfrequencies with corresponding damping ratios. The imported data may contain one or several impacts, as long as they are logged in the same time series. Each recorded time series included three impacts at the same location which could later be divided in to shorter parts or left as they were originally recorded, for the analysis part.

The SID test was carried out by recording two time series of three hits at each impact point. This gives six recorded impacts form each impact point. The order is given by the numbers in Figures 4.15 (a), 4.16 (a), 4.19 (a) and 4.20 (a), starting at 1. The time series were saved on the computer with names according to setup, location of impact

---

[4]Also referred to as *impact points*

and order of time series. E.g. M4L_1_2 read as: M4- four modules (two by two setup) L- impact on long side, 1- time series recorded for impact in location 1, 2 second time series at this location. The files can be found in the electronic Appendix.

4.5   Test Setup

4.5.1   Measurements

To get good measurements, it was important to hit the structural parts[5] of the modules with the hammer. If only the OSB plates were hit, the plate would flex or break and absorb most of the energy. By hitting the stiff structural parts the shock would be absorbed by the entire structure and the global modes excited. It was also important that the accelerometers were attached to the structural parts to register the global modes. If they were only attached to the OSB plates they might only register local modes of little interest.

Since the modules had no exterior cladding, it was easy to locate the studs and joists thew the OSB plates. This made it easier to excite the structure in the right spots and to make sure that accelerometers were connected to the structural frame. The accelerometers were attached to the structure threw 80 mm wooden screws with nuts welded on at the end, matching the threads on the accelerometers. The screws were screwed in to the studs or joists, threw the OSB plates and the accelerometers securely fastened. Figure 4.13 shows the screws, and how they were attached.

From the preceding lab tests and general assumptions, three fundamental mode were anticipated. Figure 4.14 illustrates the three modes, where I is a torsional mode, II is a transverse mode and III is a longitudinal mode. Based on this and the location of the structural elements in the modules, the location of impact points and accelerometers were determined. To excite the anticipated modes as much as possible, the impact points were located where the modes have their maximum deflection, i.e. the top of the modules. To get the mode shapes defined as a plane the modules were also excited lower down as illustrated in sections 4.5.2 and 4.5.2.2.

The accelerometers were attached to the opposite side of the modules as to where the hammer were used. This was to reduce the magnitude of possible local modes and not to interfere with the excitation process. This also enabled both the impacts and the accelerometers to be located in the maximum deflection points of the anticipated modes.

Since the modes are three-dimensional and it was only possible to measure one side of the modules at a time, the tests were first carried out on the short side, and then on the long side of the modules. This meant that the accelerometers had to be moved from the short side to the long side before the tests could be made again.

---

[5]Studs and joists

a   b

Figure 4.13: Screws for Attaching Accelerometers
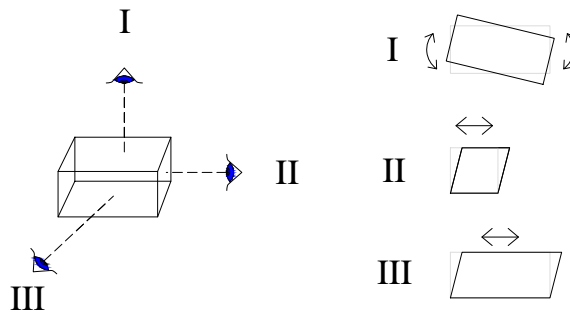
Figure 4.14: Anticipated Modes

4.5.2 Location of Impact Points and Accelerometers

4.5.2.1 Two by Two Setup

The original setup of impact points had to be slightly altered due to time issues, which was partially due to the scaffolding hawing to be moved between the impact points and problems with electrical noise. The modules were therefor excited as shown in Figures 4.15 and 4.16. Figure 4.15 (a) shows where the modules were excited at the long side for the SID test and Figure 4.15 (b) for the MA test. Figure 4.16 (a) shows where the modules were excited at the short side for the SID test and Figure 4.16 (b) for the MA test.
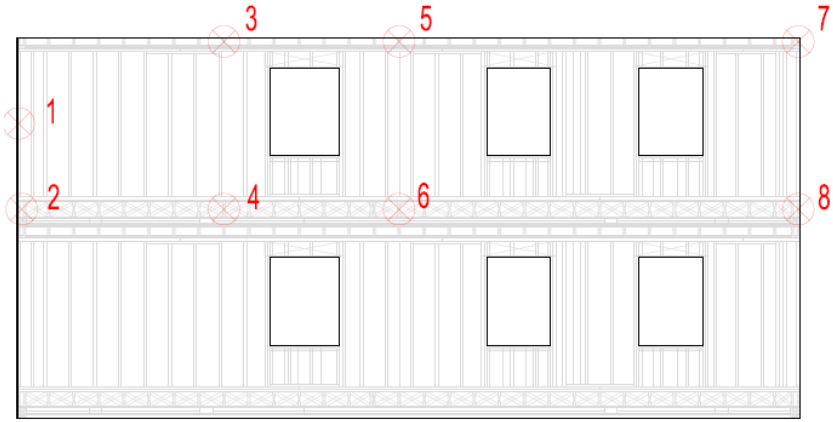
a
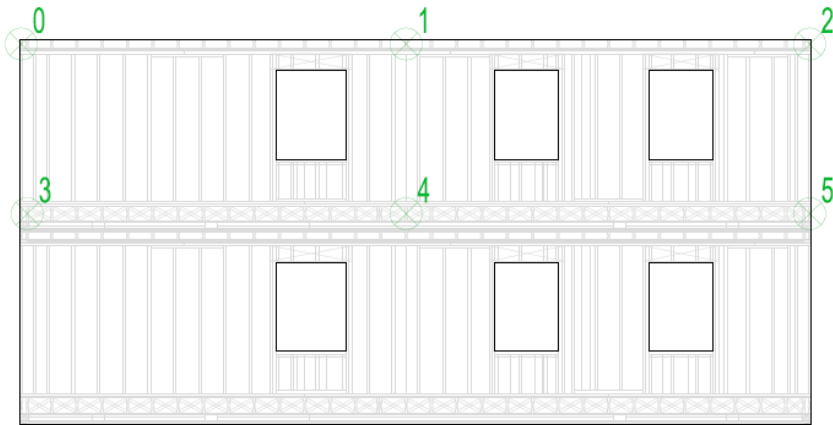
b

Figure 4.15: Two by Two Long Side, Excitation
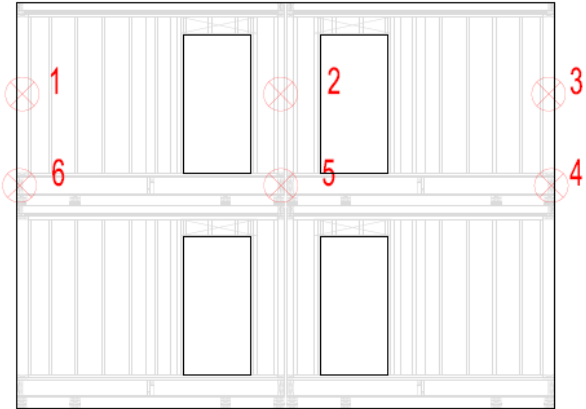
a
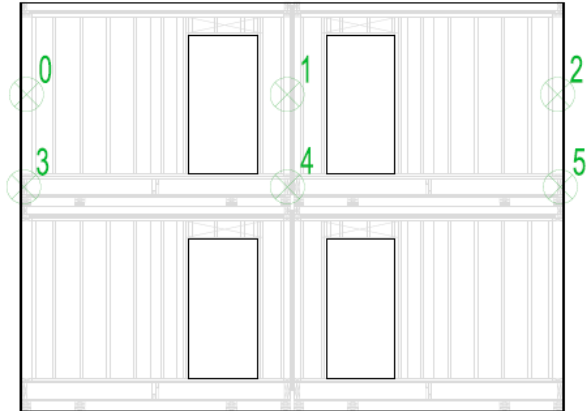
b

Figure 4.16: Two by Two Short Side, Excitation

For the SID test on the two by two setup, one more criteria was added to the choice of location for the accelerometers. Since the connection between the modules were an unknown element, the accelerometers were attached to different elements in the modules to detect any differences in response. In Figures 4.17 and 4.18 the blue, numbered marks represent the HBM accelerometers and the green "P" the Kistler accelerometer. Since the modal analysis test only involves one accelerometer, it was important that this was not located in a zero value of any modes. This is why it was placed some distance form the top of the modules, in case the top corner had zero value in an unanticipated mode.
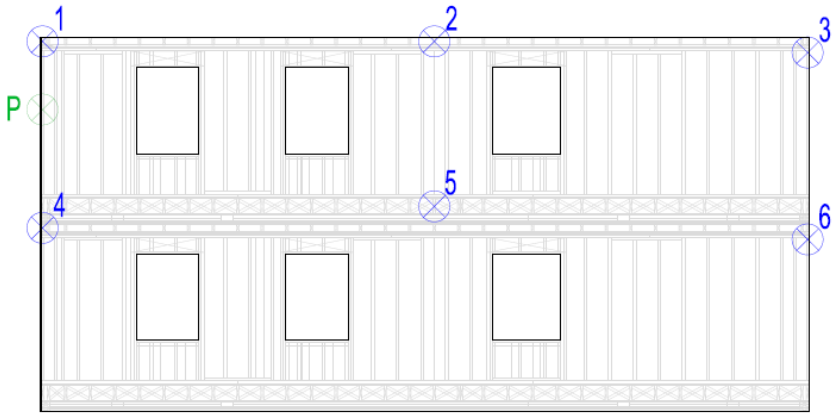
Figure 4.17: Two by Two Long Side, Accelerometers
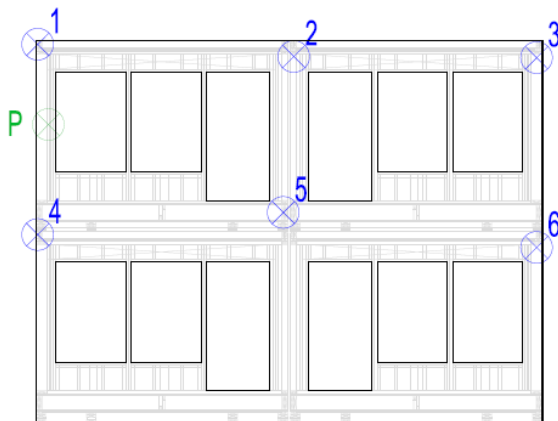
Figure 4.18: Two by Two Short Side, Accelerometers

4.5.2.2   Single Module Setup

For the single module setup, all tests could be carried out without the use of scaffolding. This saved a lot of time, and the tests were carried out as originally planed. Figure 4.19 (a) shows where the modules were excited at the long side for the system identification test and Figure 4.19 (b) for the modal analysis test. Figure 4.20 (a) shows where the modules were excited at the short side for the system identification test and Figure 4.20 (b) for the modal analysis test.

Since there were no connections to other modules in this setup, the location of the HBM accelerometers were chosen based of the anticipated modes and the location of structural elements. When the short side was tested, one HBM accelerometer was skipped, as its planed location would be between the windows. The weight of the windows would probably have caused the accelerometer to register a local mode and was therefor skipped. Figure 4.21 and 4.22 shows the location of the accelerometers on the long and short wall, respectively, where the blue numbered marks represent the HBM accelerometers and the green "P" the Kistler accelerometer.

During testing, something looking like a rigid body mode was noticed. This was investigated by changing the locations of excitation in the MA test to span the entire height of the short wall. Figure 4.23 illustrates the new grid.

a

b
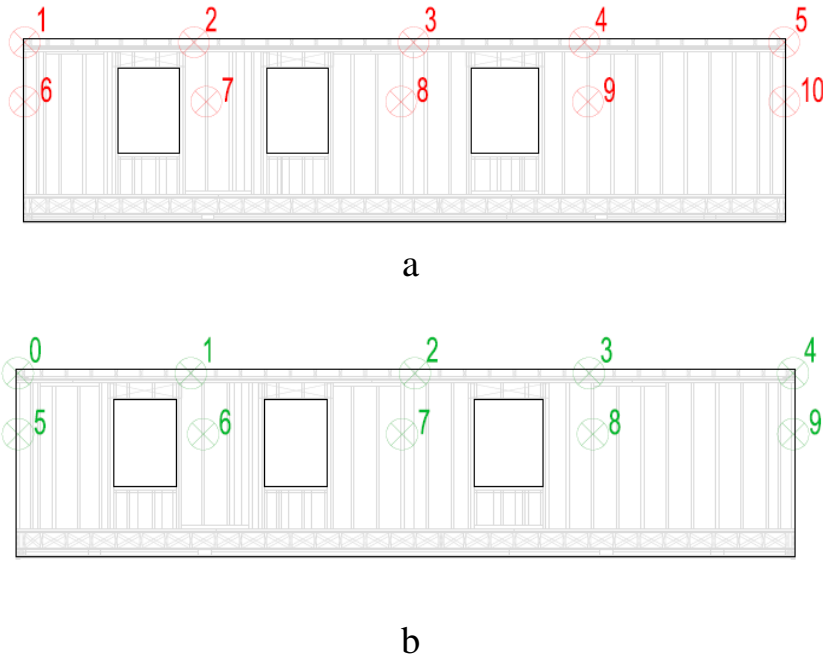
Figure 4.19: Single Long Side, Excitation

a   b
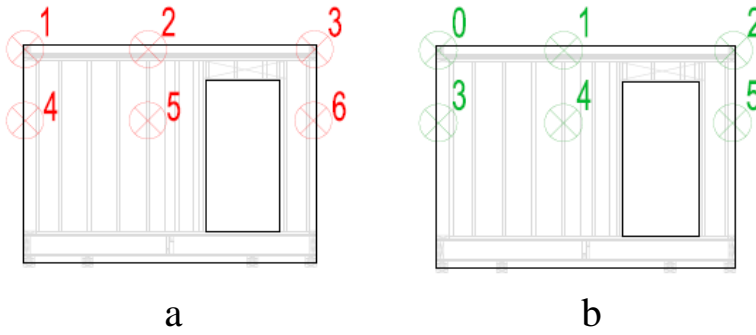
Figure 4.20: Single Short Side, Excitation
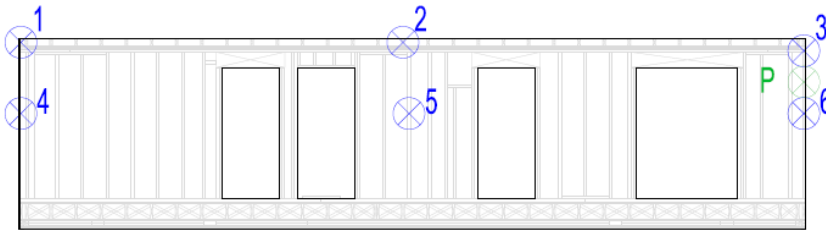
Figure 4.21: Single Long Side, Accelerometers
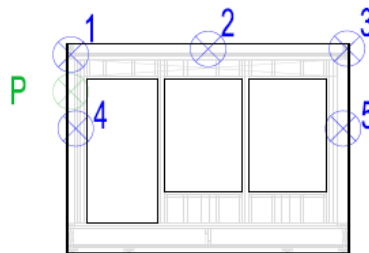
Figure 4.22: Single Short Side, Accelerometers
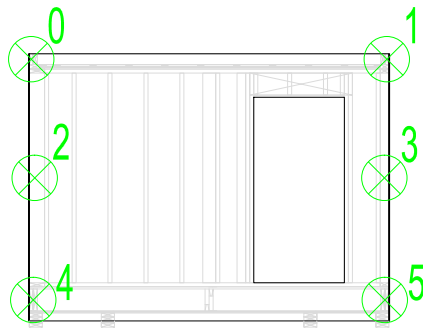
Figure 4.23: New Excitation Pattern For Single Module Setup

Chapter 5

Test Results for

After the tests were completed, the collected data was analyzed in two different programs. The time series from the system identification testes were analyzed in Matlab using a script provided by Ole Øyseth, NTNU. The frequency response functions from the modal analysis test were analyzed in a LabVEIW program called *Modal Parameter Identification*. Three modes of interest were detected in both tests, one torsional and two transverse modes. All below 20 Hz.

A short report of the findings in these tests were made when the analyses were completed [40].

5.1   Modal Analysis

The modal parameter identification software identifies the eigenfrequencies, damping ratios and mode shapes of the tested structure. The test results are given in Table 5.1. Due to limited time for testing, only one test was completed on each side for the two by two setup. For the single module setup, two tests were completed on each side. The FRF from the impacts on the short side of the two by two setup was jagged and the modes were very close. This makes the modal parameter extraction very unreliable. The results are only part of this table since this was the only MA test made on that side. The results form this test is regarded as a very rough estimate and little confidence is put the results.

Test Setup	Mode	Frequency [Hz]	Damping [%]
Two by Two	Transverse	5.5	3.17
Long Side	Torsional	10.7	3.14
Two by Two	Longitudinal	9	6
Short Side*	Torsional	10.7	2.8
	Transverse	7.4	3.3
Single	Transverse	7.2	3.4
Long Side	Torsional	10.2	3.3
	Torsional	10	3.5
	Longitudinal	7.5	2.3
Single	Longitudinal**	7.5	2.2
Short Side	Torsional	10.2	3.4
	Torsional**	10.2	3.5

* Low responses in this test resulted in a jagged FRF, and not so good results.
** Second set of impact points.

Table 5.1: Results, Modal Analysis

The estimated mode shapes from the two by two test setup matched the anticipated modes, and no other modes within 30 Hz were found. The following four figures shows the mode shapes for each excited side for each setup. The colors illustrates the maximum and minimum value of the mode at all times, where red is max and purple is min. This does not mean that they can not have the same direction, it only illustrates where the max and min values are at a certain time instant.

Each figure shows a plane and a side or top view of the mode, where the right hand side of sub-figures (a) and (c) are seen from the side, and (b) and (d) from the top. The side and top views show the modes at displacement +1 and -1 with the line in the middle being 0. The lines in the illustrated mode shapes are drawn between the impact points, which means that the mode shapes only represent the area within the impact points, not the entire wall.

In Figure 5.4 (a) and (b), the mode shows almost no deflection, only a rigid body mode. This was detected during the testing, and lead to the second pattern of impact points. In Figure 5.4 (c) and (d) (the second pattern) the bottom line of the mode shape represents the floor. Since there is a definite longitudinal movement in the floor it was concluded that, instead of the measuring the response of the module, the response
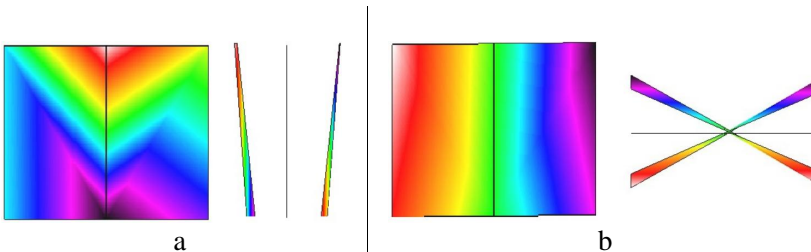

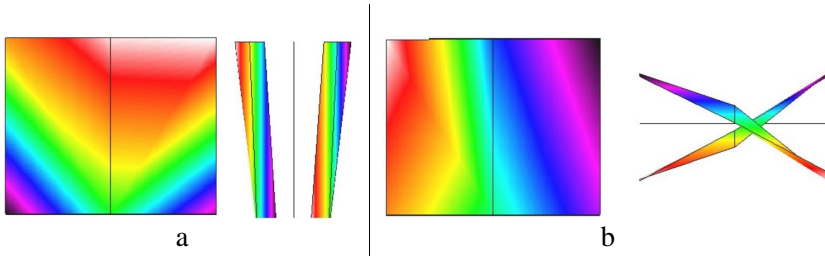Figure 5.1: Mode Shapes, Two by Two, Long Side

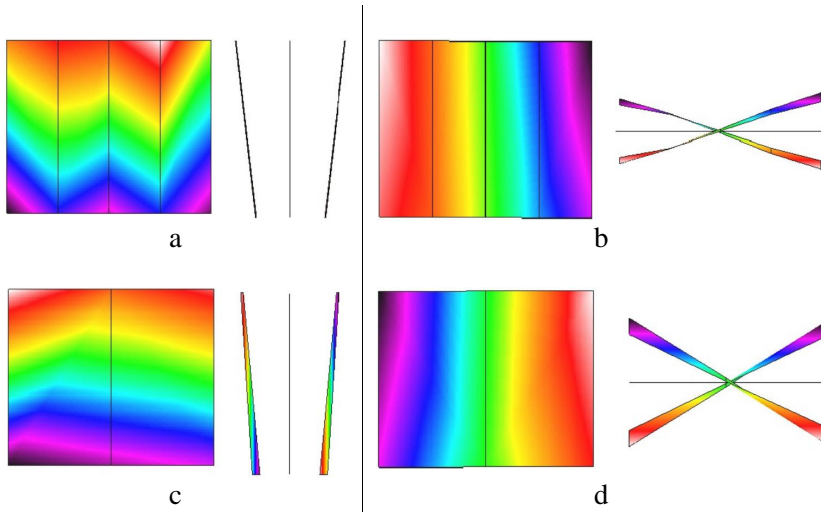Figure 5.2: Mode Shapes, Two by Two,Short Side
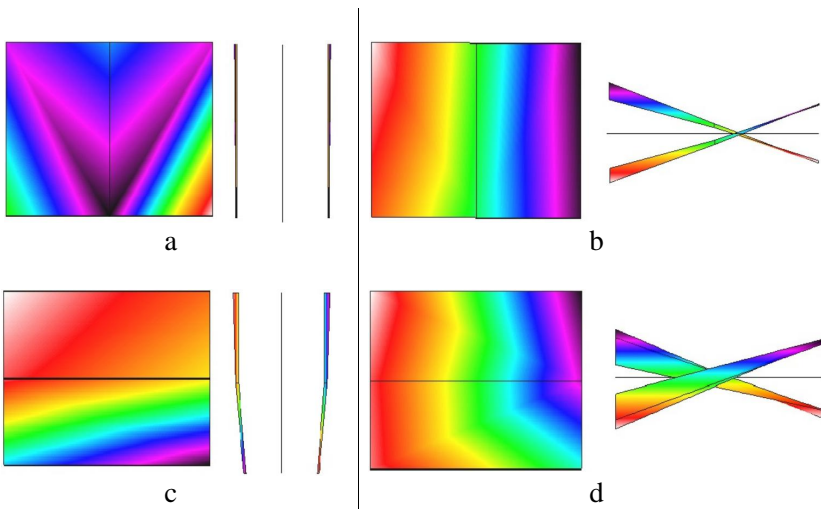

Figure 5.3: Mode Shapes, Single, Long Side

Figure 5.4: Mode Shapes, Single, Short Side

of the foundation was measured. Whether this is the case for the long side as well is more uncertain, but the nature of the foundations makes the test results very unreliable. Creating a numerical model of the foundations is also hard, due to the uncertainties regarding the timber blocks in the foundations.

5.2   System Identification

Due to the detected rigid body motion in the single module test setup, the results from this setup has been left out of this chapter. However the results were consistent and the SID method gave very stable readouts, proving that the methods works well for this kind of testing.

As described in Section 3.3 the quality of the analysis depends on choices made by the operator in the Matlab script. To optimize the analyzes each time series have been analyzed several times to find the optimal setup in Matlab, without compromising the reliability of the method.

5.2.1   Analyzed Time Series

To get good analyzes, the originally recorded time series including the response from three impacts, were dividing in to three new time series included one impact response each. These shorter time series were then analyzed one at a time. Only the best single impact times series form each original recording[1] was analyzed.

Due to a lot of electrical noise at the test location and low responses in the modules, the time series were strongly influenced by the noise. Therefor, the time series with the largest amplitudes and longest vibration durations, e.i. largest excitation energy, have been regarded as the best timeseries. Further, it is possible to chose which accelerometers to include in the analysis, in the Matlab script. This was utilized by first including all accelerometers in an analysis, and than reducing the number of accelerometers to only include the once that gave the best results in the first analysis, in a second analysis. Generally, the accelerometers mounted lower down on the modules recorded lower acceleration, and was therefor skipped in some of the second analyzes. The results in Figure 5.5 and Table 5.2 are based on both the first and second analysis. By doing this, all impact points are represented by four analyzes in the final results. The time series chosen for analysis, and the accelerometers included in each analysis can be found in the Digital Appendix **D.**

Some of the analysis also showed a frequency around 13.3 Hz for impacts on the long wall, this was however not present in all analyses and was not seen in the MA tests. It is therefor not part of the results presented here.

5.2.1.1   All Analyzes

Figure 5.5 shows a plot where all analysis are included. Damping ratios are plotted on the X-axis and frequencies on the Y-axis.

The plot shows good consistency regarding frequencies and damping ratios for the torsional modes. The frequencies are also consistent for the translational modes, but the damping ratios are more scattered. The average frequencies and damping ratios, with related standard deviations are listed in Table 5.2

The torsional mode, that is the same mode for impacts on the short and long side of the modules, show very close results in both frequency and damping. For the measure-

---

[1]Each recorded time series included three impacts, and two time series were recorded for each impact point. (totally six impacts at each impact point)
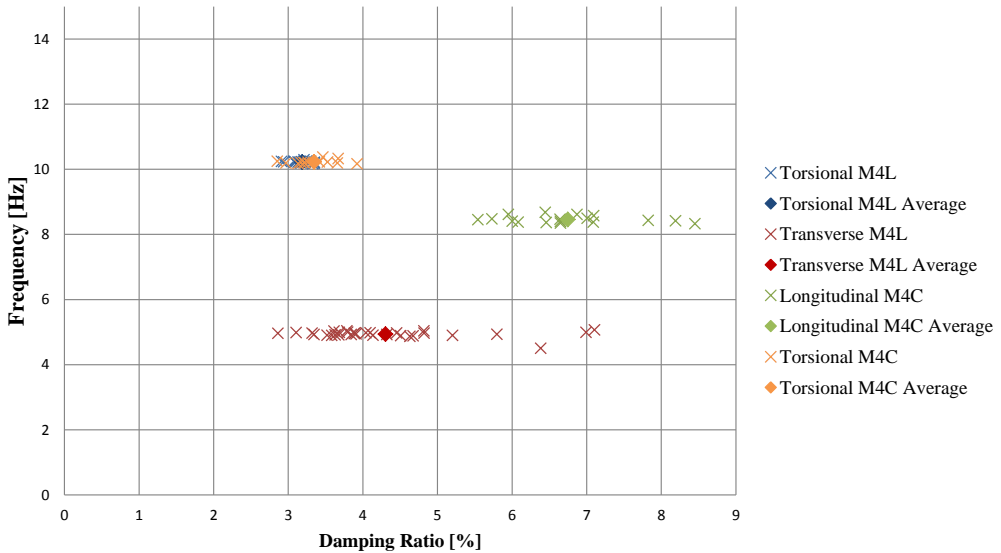
Figure 5.5: Frequencies and Damping Ratios, SID

Side	Mode	Frequency [Hz]	SD	Damping [%]	SD
Long Side	Transverse	4.94	0.094	4.30	1.03
	Torsional	10.22	0.027	3.18	0.117
Short Side	Longitudinal	8.46	0.101	6.75	0.797
	Torsional	10.23	0.057	3.34	0.289

SD - Standard Deviation

Table 5.2: Frequencies and Damping Ratios, SID

ments form the short wall, the standard deviation is a bit higher. This is probably due to the different impact locations. The impacts on the short wall has a shorter distance 90 degrees to the rotational center of the mode, which creates a smaller moment about the torsional axis compared to impacts on the long wall. This leads to lower response amplitudes, which leads to less consistent analysis and a more scattered result.

The standard deviation for the damping ratios for the translational modes are a lot higher than for the torsional. This may be due to lower response amplitudes.

5.2.1.2 Selected Analyzes

The criteria for selecting time series for the plot in Figure 5.5 may be good when all time series are good. However, for a global analysis with time series of varying quality, a different approach may be more appropriate. A second plot was made by only including the time series with the most consistent damping ratios versus model order, regardless of impact location. Figure 5.6 shows a typical example of two analysis, where only the green would have been chosen. Figure 5.7 shows a plot where some of the time series has been skipped due to inconsistent damping ratio versus increasing model order. It is clear that the spread has been narrowed for the damping in the transverse mode, but for
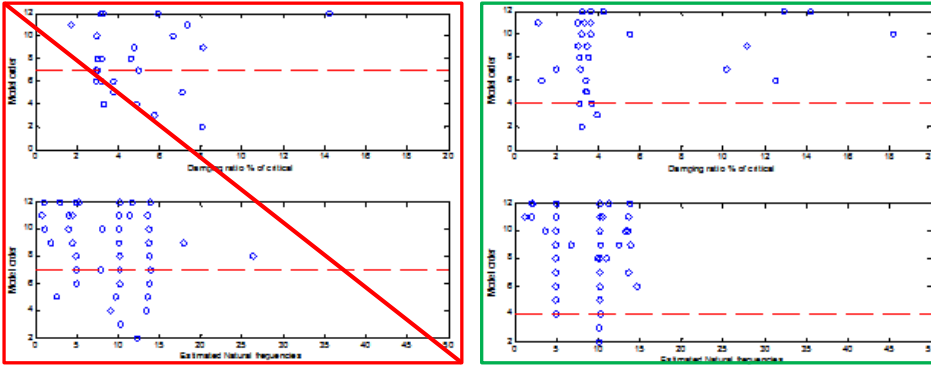
Figure 5.6: Selecting Time Series
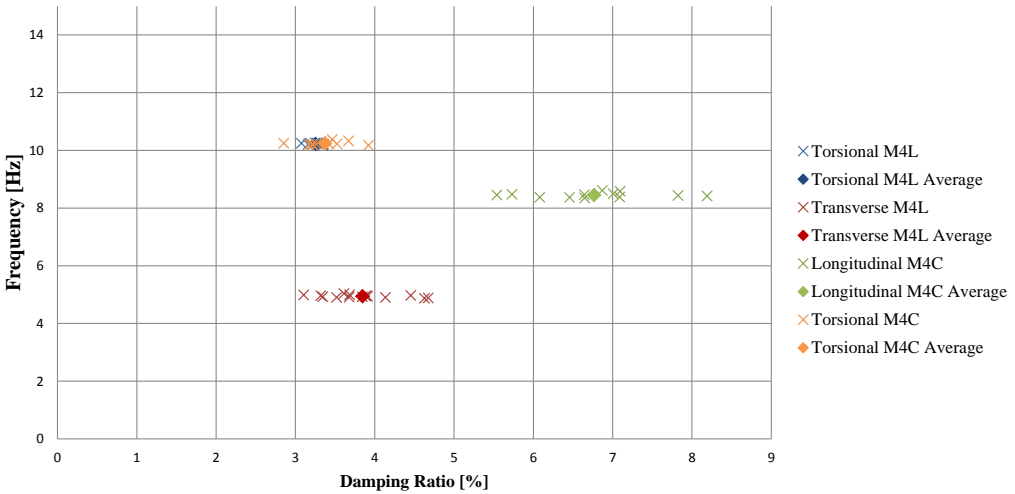
Figure 5.7: Selected Frequencies and Damping Ratios, SID

the longitudinal mode, the spread is more or less unchanged. There is no big change for the torsional mode. Table 5.3 shows the average modal parameters and corresponding standard deviations of the selected time series.

Side	Mode	Frequency [Hz]	SD	Damping [%]	SD
Long Side	Transverse	4.94	0.043	3.85	0.450
	Torsional	10.22	0.027	3.25	0.087
Short Side	Longitudinal	8.45	0.080	6.76	0.742
	Torsional	10.24	0.064	3.37	0.305

SD - Standard Deviation

Table 5.3: Selected Frequencies and Damping Ratios, SID

5.3   Comparing Results

When comparing the different sampling methods, was concluded that the second method gives more consistent results. The standard deviation of the damping has gone down considerably for the transverse mode, as shown in Table 5.4. The others remain fairly unchanged. This shows that the quality of the time series must be good for the SID method to give reliable results for damping. The frequency estimates are less affected by the quality of the time series.

When comparing the different test methods, it is obvious that the SID tests give frequencies that are roughly 0.5 Hz lower than the MA testes, and slightly higher damping ratios. The reason for these difference has not been looked in to in this thesis, but the results are quite close, and may be considered fair. Table 5.5 shows the differences between the two tests.

Since no mode shapes has been estimated for the SID tests, is has been assumed that the frequencies closest to one another for the SID and the MA tests represent the same modes. The confidence in this assumption is increased when looking at the time series from the different accelerometers in the SID test. Figure 5.8 shows the filtered time series form an impact on the opposite side of accelerometer 3 on the two by two module setup (see Figure 5.8 (e)). Figures (a), (b) and (c) shows time series from two accelerometers each, where the blue line represents the accelerometer directly above the accelerometer represented by the red line. Form (a), (b), and (c), it is clear that the accelerometers located lower down on the modules have lower amplitudes than the once higher up. The periods are the same for the accelerometers located high and low. This corresponds well with the estimated mode shapes from the MA test.

When comparing (b) to (a) and (c), it is obvious that accelerometers 2 and 5 mainly registers one mode with a period of roughly 5 Hz. While accelerometer 1, 3, 4, and 6 also registers a higher frequency. This means that accelerometers 2 and 5 are located in a zero value point of the higher mode, i.e. the torsional model.

Side	Mode	Set	Frequency [Hz]	SD	Damping [%]	SD
Long Side	Transverse	All	4.94	0.094	4.30	1.03
		Selected	4.94	0.043	3.85	0.450
		Difference	**0**	**-0.050**	**-0.45**	**-0.58**
		Difference [%]	**0**	**-58.8**	**-10.5**	**-56.3**
	Torsional	All	10.22	0.027	3.18	0.117
		Selected	10.22	0.027	3.25	0.087
		Difference	**0**	**-0.001**	**-0.07**	**0.03**
		Difference [%]	**0**	**-4.6**	**-2.2**	**34.5**
Short Side	Longitudinal	All	8.46	0.101	6.75	0.797
		Selected	8.45	0.080	6.76	0.742
		Difference	**-0.01**	**-0.021**	**0.01**	**-0.06**
		Difference [%]	**-0.1**	**-20.9**	**0.1**	**-6.9**
	Torsional	All	10.23	0.057	3.34	0.289
		Selected	10.24	0.064	3.37	0.305
		Difference	**0.01**	**0.007**	**0.03**	**0.016**
		Difference [%]	**0.1**	**11.9**	**0.9**	**5.5**

Table 5.4: Difference in Choice of Time Series

Side	Mode	Protocol	Frequency [Hz]	Damping [%]
Long Side	Transverse	MA	5.5	3.17
		SID	4.94	3.85
	Difference		**-0.56**	**0.68**
	Torsional	MA	10.7	3.14
		SID	10.22	3.25
	Difference		**-0.48**	**0.11**
Short Side	Longitudinal	MA	9	6
		SID	8.45	6.76
	Difference		**-0.55**	**0.76**
	Torsional	MA	10.7	2.8
		SID	10.24	3.37
	Difference		**-0.46**	**0.57**

Table 5.5: Difference Between the two Test Protocols

Figure 5.8 (d) shows the time series form accelerometer 1, 2 and 3 plotted together as red green and blue respectively. For the highest frequency of the red and blue lines, the red is roughly half a period behind the blue. This observation together with the one mentioned in the paragraph above, gives a typical torsional mode about the center of the modules. It can also be seen that the red and blue lines follows the green line as a "middle" trend, representing the transverse model.

There is little difference other than lower amplitude for the accelerometers attached to the first floor modules. This means that the modes of the modules engages the whole stack as a single structure.
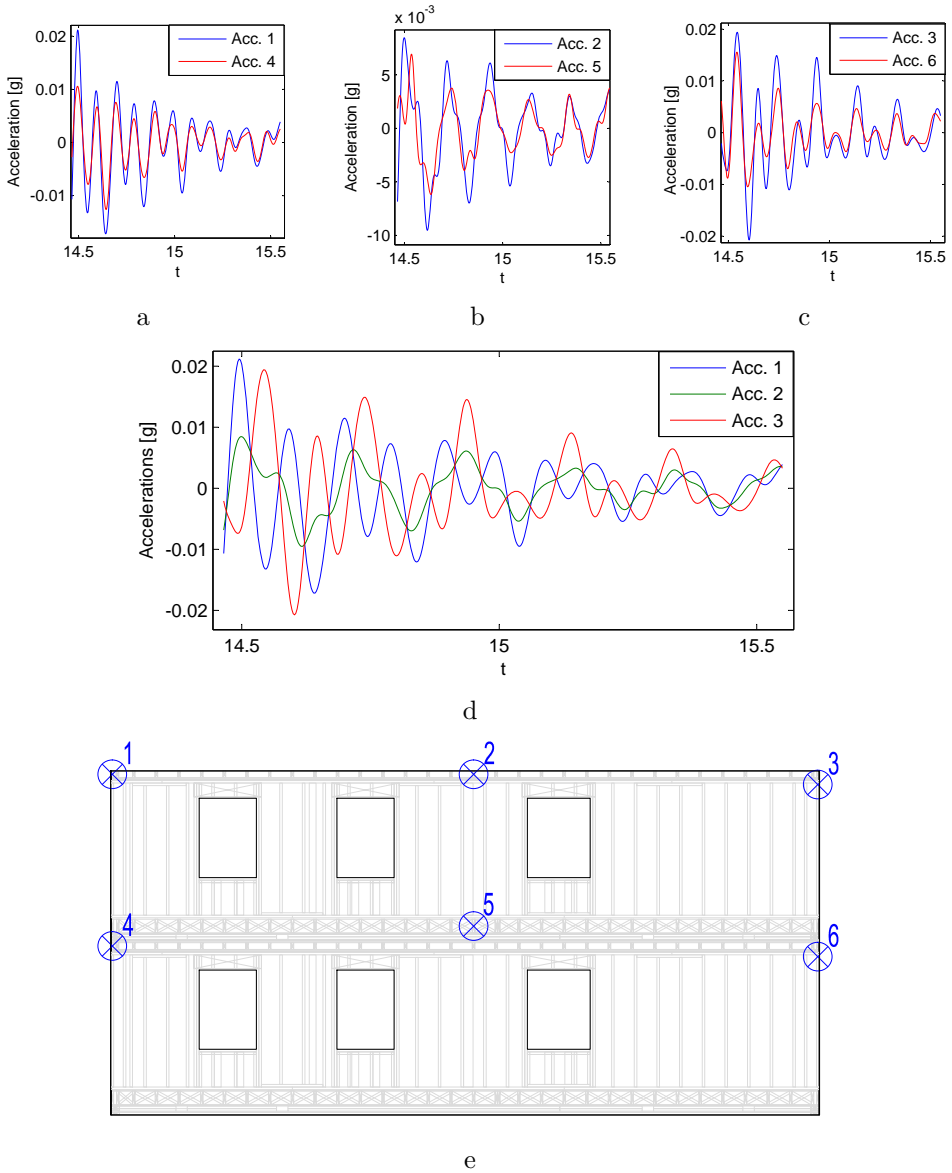
Figure 5.8: Time Series, SID, Mode Shapes

5.4   Sources of Error

There are many potential sources of errors involved in this kind of testing. These are listed below.

- Electrical noise at the test site represents a disturbance that can effect the results.

- The foundation of the two by two setup is less stable than the final foundation at a building site.

- The foundation for the single module setup compromised the entire setup.

- For the MA tests, it is very important that the hammer hits the structure straight on. If not, the correlation between the applied force and the response cause an error in the FRF.

- If the structure was exposed to other external forces than the hammer, this would cause errors in the relationship between applied force and response for the MA tests.

- The applied windows and recording time can affected the results of the MA tests.

- The curve fitting method used to extract the modal parameters can be inaccurate.

- The accelerometers used in the SID tests are over 20 years old, and can be inaccurate.

- Numerical errors in the SID algorithm may cause errors in the analysis.

- Human errors during test procedures and analysis procedures may affect the results.

Chapter 6

Simple Numerical Models

When the results from the tested modules were finished a simple numerical model model was made with the same dynamic properties as the tested modules. This model was used as a base for the VHT models. By altering the dimensions of first model to match the VHT modules the dynamic properties of the VHT modules could be estimated. The simple models of VHT modules were to be implemented in a larger model of the entire VHT building to see what effect the modules would have on the global response of the VHT building. This has been done by:

- Estimating the mass distribution in the modules.

- Establishing a simple plate model of the tested modules, with dynamic properties matching the test results.

- Scale the plate model to match the dimensions of the VHT modules.

- Estimate the dynamic properties of VHT plate models.

- Create shear frame models with the same dynamic properties and dimensions as the VHT plate models.

- Assemble the VHT shear frame models with the configuration they will have in the VHT building.

Abaqus/CAE 6.11-1 has been used for all the modeling and numerical analysis. All numerical analyses had been done the same way and include two steps. The first step is a static general step where gravitational forces are applied to the model. The second is a linear perturbation frequency analysis step using the Lanczos eigensolver. This gives the eigenfrequencise and mode shapes of the model. No damping had been applied to the models.

For the plate models, S4R elements has used with a mesh size of 0.25 m. The S4R element is a 4-node doubly curved shell element with reduced integration and finite membrane strain. In the shear frame models the same elements are used for the plates (floors and ceilings). For the beams and columns B31 elements have been used. These are simple 3D, 2-node elements [45].

6.1   Simple Plate Model

Due to the problems with the foundation in the single module tests, the simplified models are based on the two by two setup.

The estimated mass distribution is based on drawings of the tested modules provided by Kodumaja, with standardized mass density properties for the different materials. The mass distribution was estimated and then adjusted to match the measured mass of the modules. The adjustment was done by evenly distributing the mass of the internal nonstructural walls and the masses that were unaccounted for in the floors and ceilings. The calculations and estimated masses can be found in Appendix B.1.

To create a simple model of the tested modules, some assumptions had to be made about the properties of the modules. First it was assumed that the walls of the module had a plate like behavior. This implies that the main stiffness contribution form each wall, is parallel to the plate plane. By modeling the walls as plates the bending stiffness across the length of the wall becomes very high. This means that the stiffness of the walls is governed by the shear stiffness.

It has been assumed that the floors and ceilings are very stiff and they have their mass centers in the middle of the plate. The vertical distance between the floor and ceiling plates has therefor been sett equal to the distance between the mass centers of the plates (2.6555 m). The dimensions of the foundations and connections between the modules has been sett to match the over all height and with of the real modules. Figure **6.1** shows the simple plate model with parts and dimension.
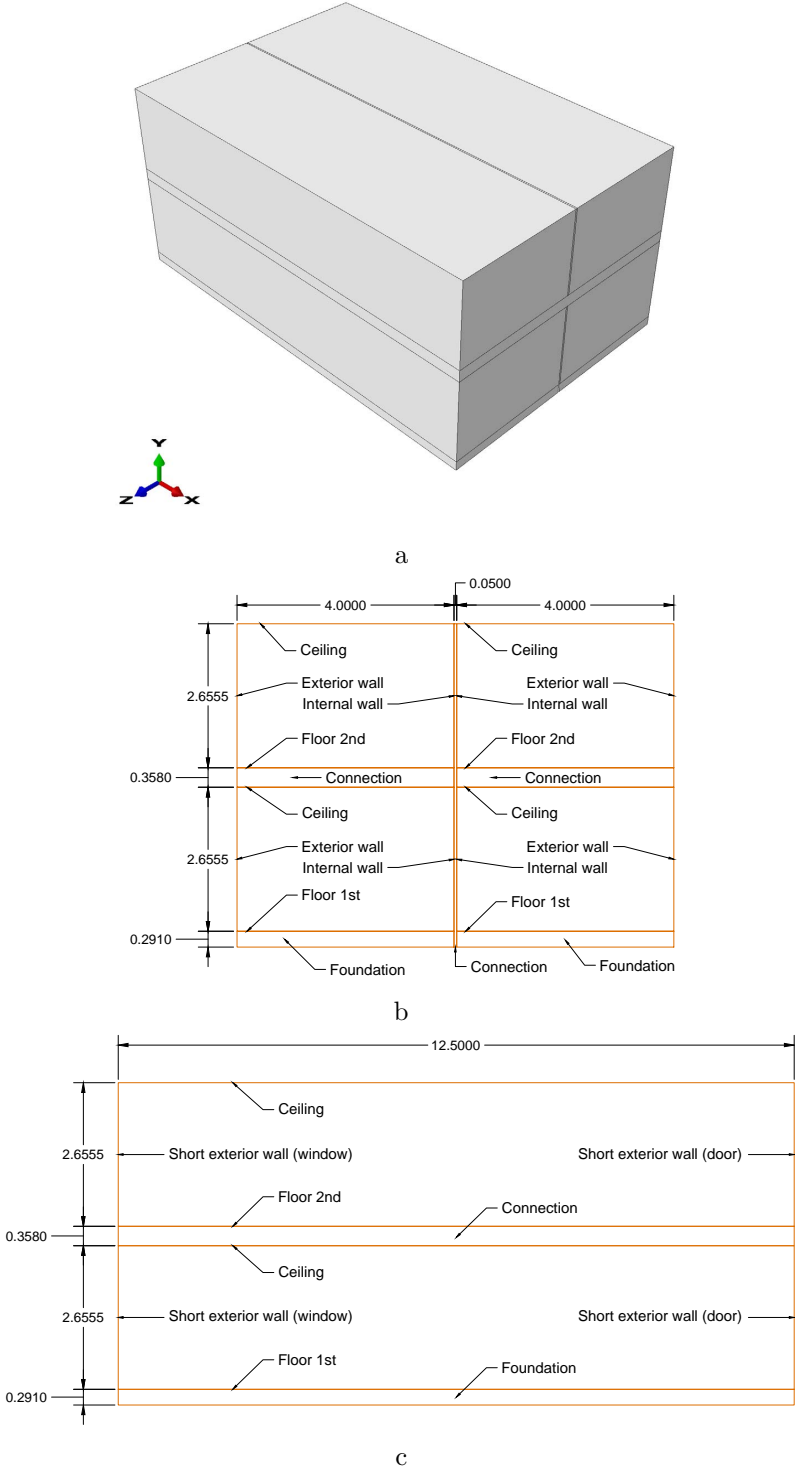
a

b

c

Figure 6.1: Simple Plate Model

By firs assuming that the connections between the modules and foundations are stiff due to the stiffness of floors and ceilings, the walls could be tuned to give the plate model dynamic properties matching the test results. This was bone by tuning the material stiffness of the long and short walls until the longitudinal and transverse eigenfrequencies matched the experimentally obtained frequencies. The properties of the parts involved in the plate model can be found in Appendix B.2

The thickness of the walls were sett to 0.17 m for the exterior walls and 0.09 m for the interior walls. The Young's modulus of the long and short walls were given different values, but for the short and long walls there was made no difference individually. This made the interior long wall less stiff than the exterior.

Table 6.1 shows the aimed frequencies and the obtained frequencies from the tuned model. The torsional mode has not been tuned, as it is dependent on the longitudinal and transverse stiffness. This has given a torsional frequency which is lower than the test results and shows that the plate model is only accurate for the tuned modes although the torsional mode is not far from the aimed frequency. This is typical when using tuned FE models. It is easy enough to get the results you want for a specific case, but hard to make a model that represents a structure accurately for all cases.

6.2   VHT Plate Models

Essentially three different types of modules will be used in the VHT building. Figure 6.2 shows a cross section of the VHT building with the different modules marked as I, II and III. For all three module types, one short wall faces out of the building and consists mainly of glass. The other faces the hallway inside the building and is continuous except for one door. Module type I is the once most similar to the tested modules, with one exterior long wall and one interior long wall. For type II all long walls are interior walls. Type III has the same long walls as II but the short walls are wider[1].

---

[1]Internal nonstructural walls are not considered in these models.
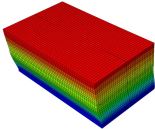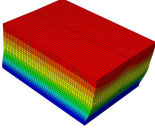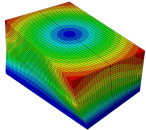
Mode	Aimed frequency [Hz]	Obtained frequency [Hz]	Mode shape
Transverse	5.25	5.36	
Longitudinal	8.65	8.66	
Torsional	10.4	9.25	

Table 6.1: Eigenfrequencies of Simple Plate Model

Figure 6.2: VHT, Cross Section[46]

Since the VHT modules will be built the same way as the tested modules, the properties of the walls, floors and ceilings has been assumed to be the same for both cases. By assuming this, the properties of the parts in the VHT plate models can be kept the same as for the first plate model. Thus, by only changing the geometry of the previous model and the long exterior walls to interior walls in module type II and III, the dynamic properties of the VHT modules can be estimated. The VHT plate models were analyzed the same way as the first plate model (two by two setup). The geometry of the VHT plate models is shown in Table 6.2 where I', II' and III' represents a two by two setup of module types I, II and III respectively. The dimensions of the modules were provided by Sweco. The mode shapes of the VHT plate model are the same as for the previous model, shown in Table 6.1 The results from the analyses are shown Table 6.3.

Model	Short Side	Long Side	3D
I' & II'			
III'			

Table 6.2: VHT Plate Models, Two by Two Setup, Geometry

Mode\Model	I'	II'	III'
Transverse	6.01	5.87	6.1
Longitudinal	8.21	7.62	6.83
Torsional	10.05	9.51	9.04

Table 6.3: Eigenfrequencies of VHT Plate Models

6.3   VHT Shear Frame Models

The purpose of the simplified models was that they were to be implemented in a model of the entire case building, to see what effect they have on the dynamic behavior of the building and whether or not they constitute a potential problem or could increase the damping in the building. Since running a dynamic FEM analysis of a large building, like the case building, takes a lot of computational time and creates large amounts of output data if the modeled structure involves a lot of elements. And since the case building involves 68 modules, the number of elements involved in each module had to be kept as low as possible. This made the plate models inefficient due to the high number of elements in the models. The plate models were therefor only used to estimate the dynamic properties of the three different kinds of modules involved in the building.

To reduce the number of elements in the modules and at the same time keep the dynamic properties, a simpler model was needed. This could be achieved by removing the wall, foundation and connection plates and represent them with a different system that could give the same dynamic properties. The floor and ceiling plates were kept to represent the mass of the modules.

Two different designs were considered for the simpler models. The first was a *shear frame* model and the second was a *truss frame* model. The two designs are shown in Figure 6.3 where a is the shear frame and b is the truss frame. The shear frame model was chosen because the behavior and deformed shape is more similar to plate behavior
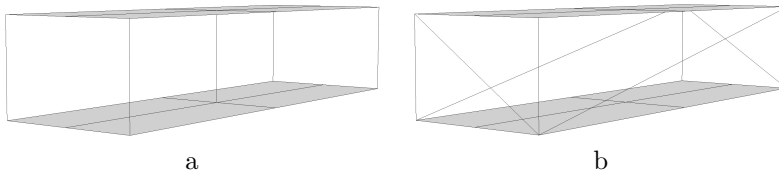
Figure 6.3: Shear Frame and Truss Frame Models

than the truss model. The truss model can also be tuned to give the same response as the plate model, but, for the reasons mentioned above, the shear frame was preferred.

The principle of the truss frame was based on using truss elements which can only take axial forces, and tune the long and short diagonal elements to get the desired models and frequencies. The shear frame model is based on four columns which are clamped[2] to floor and ceiling. This only allows bending in the normal directions of the columns. Box profiles were used in the corner columns, so the stiffness could be adjusted in both directions. The column in the center of the module was there to adjust the torsional stiffness of the model. The bending stiffness of the center column was sett close to zero, so the translational stiffness contribution was neglectable.

The weight of the VHT modules has not been calculated since no accurate drawings other than the cross sectional drawings shown in Figure 6.2 were available at the time of modeling. To find a representative mass for the models, the tested modules were used as a base. First it was assumed that all modules of the same type had the same mass. This is not an accurate assumption, but the additional weight from the extra timber due to smaller center distance between the studs in the lower modules is small. It was also assumed that the wind plates on the bottom floor will not be necessary for the VHT modules, since the modules will be placed inside the exterior cladding of the VHT building it self.

The weight of the modules has been estimated by adding half the mass of each wall to the floor and the other half to the ceiling of the tested modules. This gives two 12.5 m x 4 m plates of different masses that represents the floor and ceiling of the module. These plates contain the total mass the module with a representative mass distribution. The plates were then scaled geometrically to fit the VHT modules whilst the mass$/m^2$ was kept unchanged. This gave a rough estimate of the masses of the VHT modules. The weight difference of interior and exterior walls has not been taken into account in this estimation.

The two by two setup were used for the shear frames, to make the comparison to the plate models as simple as possible. All parts except for the five columns between the floors and ceilings of each model was kept quite stiff, as for the plate models. The two by two setup of the VHT share frame models are shown in Table 6.4, where I*, II* and III* consists of module types I, II and III respectively. The modules were tuned by altering the box profiles in the corner columns till the desired modes and frequencies were fount. All corner columns of each model has the same properties. The tuned mode shapes and eigenfrequencies are shown in Table 6.5 Since the torsional stiffness depends on the tuned translational stiffness of the modules, the torsional mode ended up being stiffer than for the plate models. The center columns was therefor superfluous, and could have been removed from the model. The masses and final properties of the parts in the shear frame models can be found in Appendix B.3

---

[2]Rotational and translational degrees of freedom = 0, relative to adjacent elements.
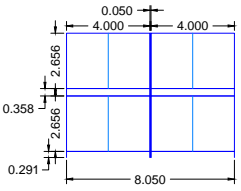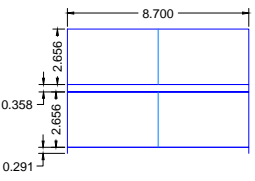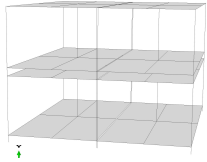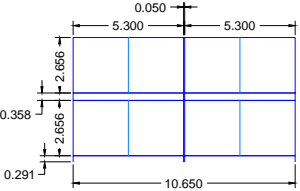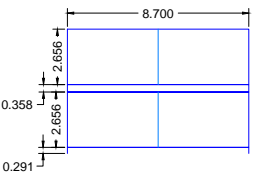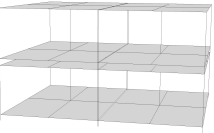
Model	Short Side	Long Side	3D
I* & II*			
III*			

Table 6.4: VHT Shear Frame Models, Geometry
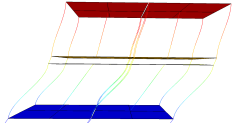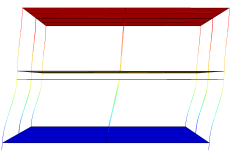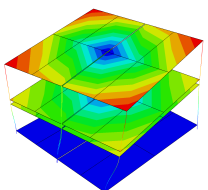
Mode\Model	I*	II*	III*	Mode shape
Transverse	5.98	5.85	6.01	
Longitudinal	8.25	7.60	6.84	
Torsional	12.06	13.02	10.37	

Table 6.5: Eigenfrequencies and Mode Shapes of VHT Shear frame models

6.4 VHT Final Configuration

Configuration	Transverse [Hz]	Longitudinal [Hz]	Torsional [Hz]
5x4	2.64	3.35	3.89
2x4	2.62	3.58	4.74
2x3	3.53	4.80	6.33

Table 6.6: VHT Configurations, Eigenfrequencies

a 5x4   b 2x4   c 2x3
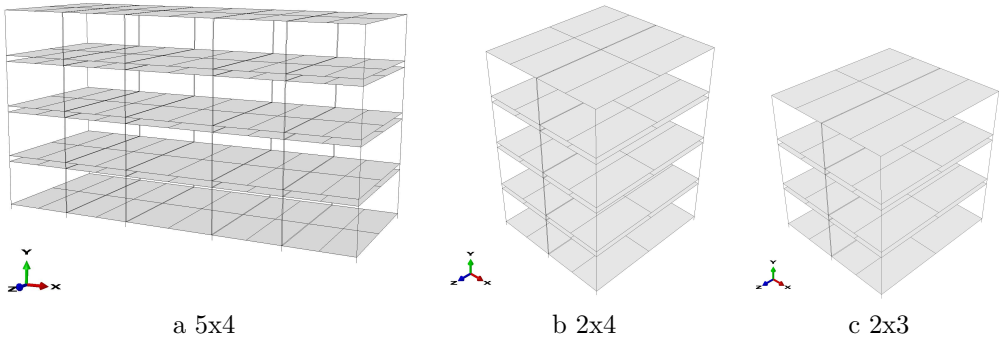
Figure 6.4: VHT Modules Configurations

After the models had been calibrated, they could be assembled and made ready for implementation in the model of the VHT building made by Ingunn Utne. Three different configurations were made for the building. These are shown in Figure 6.4.

The three first fundamental modes of the different configurations are the same as for the two by two setup. The eigenfrequencies of the different configurations are shown in Table 6.6. Further reading about the effect of the modules in the VHT building can be found in [48].

Chapter 7

Detailed Numerical Models

A detailed numerical model of the tested modules was made in the FEM software Abaqus/CAE 6.11-1 to get a better understanding of the modules dynamic behavior. The model was made to be as similar as possible to the the tested modules. It is however important to remember that it still *only a numerical model*. The properties of any numerical model depends entirely on the choices made by the creator. The number of choices to make in a large model is many and increases drastically with the complexity of the model. Small errors made along the way can therefore accumulate to give a model that are not at all representative of the modeled structure.

The approach in this thesis has been to first make the complete model of a module and than look at the separate parts individually afterwords. This way, the contribution of each part can be identified and the behavior of the complete model explained. With this approach the small errors may be reduced, or at least identified to explain the deviation between the numerical model and the real structure.

The models made in this chapter are complex and a lot of simplifications has been made. Thus, a detailed description of the modeling proses is presented in the next section.

7.1   Complete Model - Modeling Process

To make a numerical model that gives the results you want is not hard since you control all the input. It is therefor important not to make a model with an aimed result if the model is to be representative for a general case. Thus, the material parameters in this model has been gathered from different Eurocodes and papers. Detailed drawings and material lists has been provided by Kodumaja. A list of materials and the applied material properties can be found in Appendix B.4. The drawings are not presented in this thesis due to confidentiality. Further descriptions of the modules are given in Chapter 4.

The complete model has been built in two steps. The first is a frame including all the timber, Stepisol and horizontal plates, modeled as one part. The second is all the vertical plates. The vertical plates are separate parts which have been tied to the frame individually to make the complete model. Figure ?? shows the complete model (a), the frame (b) and the plates (c).
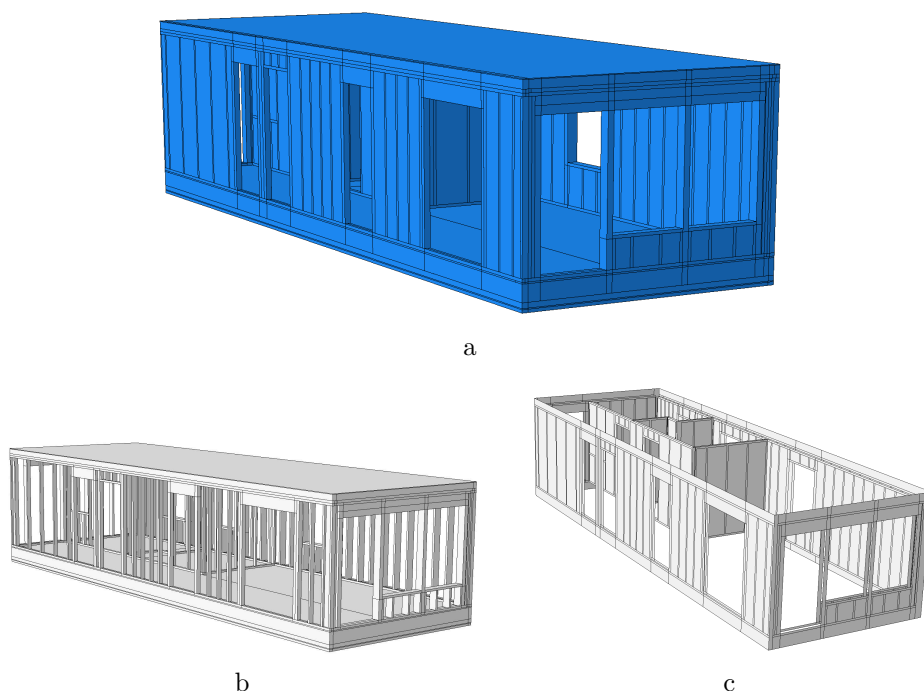
a

b   c

Figure 7.1: Detailed Model, Frame and Plates

7.1.1   Model Frame

The frame can be seen as the skeleton of the model, designed to carry all the vertical load. The frame has no cross bracing, which makes it sensitive to horizontal forces before the plates are attached. All elements in the frame are C3D8R elements which are 8-node linear brick elements with reduced integration. An automatic mesh of 0.04 m was applied to the frame[45].

The horizontal plates were part of the frame partially to maintain the correct height of the module and partially because it made the modeling easier. This is however not a good way of modeling plates. The size of the mesh and choice of elements meant that the horizontal plates would not have genuine plate behavior since they were only represented with one element across the thickness of the plate. It has been assumed that the compromised plate behavior has little effect on the dynamic properties of the model that are of interest in this thesis. Since the plates are horizontal, the bending stiffness across the thickness of the plates does not effect the horizontal stiffness of the model much.

Since the frame is built as one part, all the connections within the frame are rigid. This makes the modeling easier, but gives a stiffer model than the real structure. This is however a necessary simplification due to the amount of time it would take to model each connection individually. In the real module the connections between the timber members are made with nail guns, which makes a quite stiff connection. These connections will have a non linear stiffness when subjected to large excitations, but remain quite stiff and linear for small excitations like the once in the tests preformed in this survey. The simplification made here is considered too stiff, but acceptable.

A 15 mm high continuous layer of Stepisol is part the frame below the floor. This
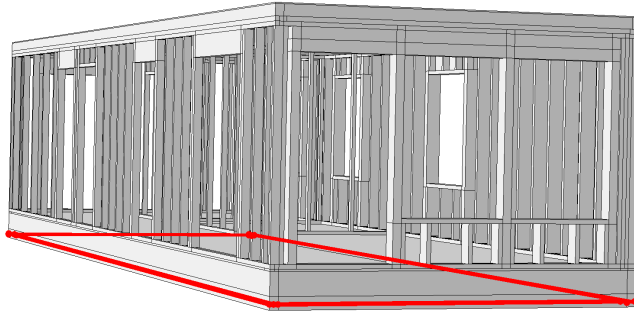
Figure 7.2: Stepisol Layer

a   b
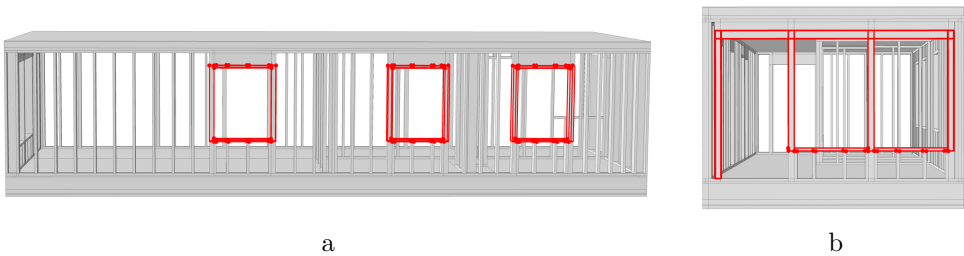
Figure 7.3: Added Mass of Windows

is shown in Figure 7.2. The Stepisol layer has been given a finer mesh (0.0015 m) than the rest of the model, since it is only 15 mm thick and it is important that it behaves correctly.

The doors and windows have not been modeled because their properties are unknown. Doors have been completely kept out of the model since it has been assumed that they are light and contribute only marginally to the stiffness of the walls. The wight of the windows have been added to the timber frame surrounding the hole where the windows would have been placed, as shown in Figure 7.3. The stiffness contribution of the windows is hard to anticipate since they are made up of lots different materials, are hinged and can be opened. Since glass is a stiff material it attracts a lot of forces if it is used as a load bearing component. Glass is also brittle and expensive, which is the reason why glass is only used as a load bearing component in very special constructions. The stiffness of the windows has therefor been left out of this model.

The materials and material orientations within the part has been assigned so that each member has the correct material and material orientation. The orientation of the different members are shown in Table 7.1.

The model was restrained from movement in x-, y- and z-direction along the bottom frame as shown in Figure 7.4. When compared to the foundations of the tested modules, this is also a too stiff representation. It is however more similar to the foundation the module will have in its finished stat.

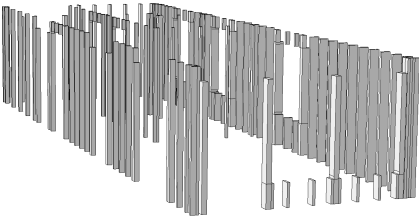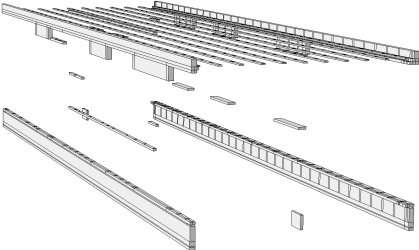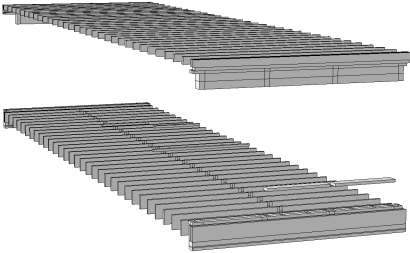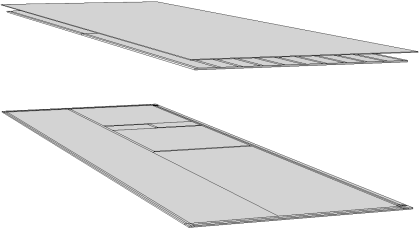| Orientation	Members
Vertical	
Horizontal X	
Horizontal Y	
Horizontal Plates	

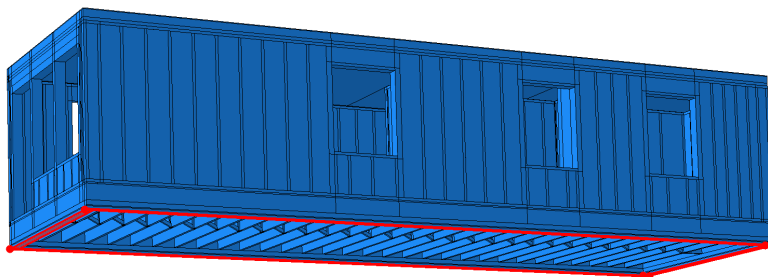Table 7.1: Frame Members, Orientation

Figure 7.4: Boundary Conditions

7.1.2 Vertical Plates

The vertical plates consist of 8 mm OSB plates on the outside and 28 mm plaster-board plates on the inside of the module. The plasterboard in the real modules consisted of two layers, one of 13 mm (class A) and one of 15 mm (class F). In the model, these have been merged to one 28 mm plate of their combined average mass density. All vertical plates have been modeled with S4R elements which are 4-node doubly curved shell elements with reduced integration and finite membrane strain. An automatic mesh of 0.04 m was applied to the plates as well.

It was hard to find any good information about the stiffness properties of plasterboard. A reason for this may be that plasterboard is rarely used as a load bearing material. It is brittle and its effective stiffness depends largely on how it is attached to the rest of the structure. The parameters used in this thesis was found in [50]. NS-EN 520 suggests a test setup for testing plasterboard plats [2]. This has not been looked into in this thesis.

The plates were modeled as continuous plates tied to the module frame using tie-constrains along most of the contact surface between the plates and the frame. Both these simplifications gives a too stiff representation of the module, but was necessary due to limited modeling time. In the real modules several plates of roughly 2.4 m x 1.2 m were used. The plasterboard plates are attached with screws and the OSB-plates with nails. In [29], it is suggested that nails and screws should be modeled as springs with a given stiffness. This is probably a more correct way of modeling the connections, but is very time consuming for large models. Figure 7.5 shows an example of how the plates were tied to the frame. The highlighted area is where the parts were tied together.
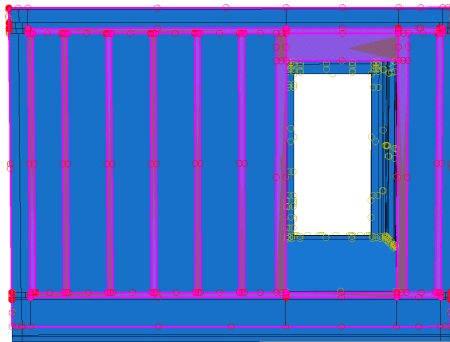
Figure 7.5: Plate - Frame Connection

7.2 Results for the Complete Model

The dynamic properties of the complete single module were found by running a two step analysis. The first was a static general step, which applied gravitational forces. The second was a linear perturbation frequency analysis using the Lanczos eigensolver to determine the eigenfrequencies and mode shapes of the model. The eigenfrequencies and mode shapes are shown in Table 7.2.

The eigenfrequency are within the expected range, though slightly low. When comparing the mode shapes of the model and the test results, it is clear that the short wall with the windows is less stiff in the model than in the tested structure. In the tested
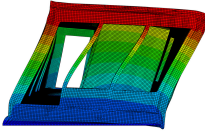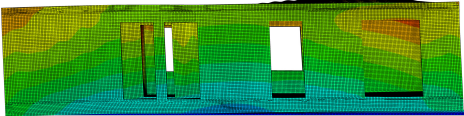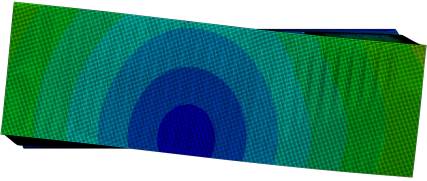
Mode	Frequency [Hz]	Mode shape
Transverse	6.13	
Longitudinal	10.16	
Torsional	9.71	

Table 7.2: Complete Module Model, Frequencies and Mode Shapes
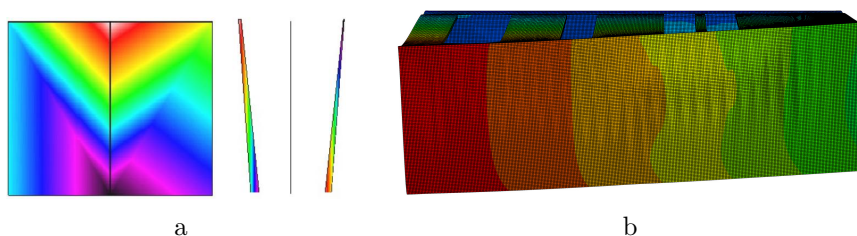
Figure 7.6: Compared Mode Shapes

modules, there is little difference between the displacement in the two short walls, while
the difference in the model is substantial. Figure 7.6 shows the transverse mode of the
tested structure together with the transverse mode of the model.

By further studying the mode shapes the it became clear that the layer of Stepisol
played an important role for the dynamic behavior of the model. The material parame-
ters of the Stepisol had been estimated from a statical load displacement curve, and the
material had been given the same parameters in all directions. The stiffness estimation
of the Stepisol can be found in Appendix C.1. Since the material seemed to have a large
influence on the dynamic behavior of the model, the material was given a second look.
By looking at the structure of the material, it was suspected that it has an orthotropic
material behavior. Figure 7.7 shows a picture of the material where it can be seen that
the particles in the material have been pressed together across the thickness of the stripe.
The material was therefor tested in the lab, to find more accurate material properties. A
numerical model was also made, to verify the lab results. The tests and the test results
are described in Chapter 8.

The material properties estimated in the lab tests and numerical modeling were
implemented in the large model, and the analysis run again. This gave the frequencies

| Flat | Vertical Side |
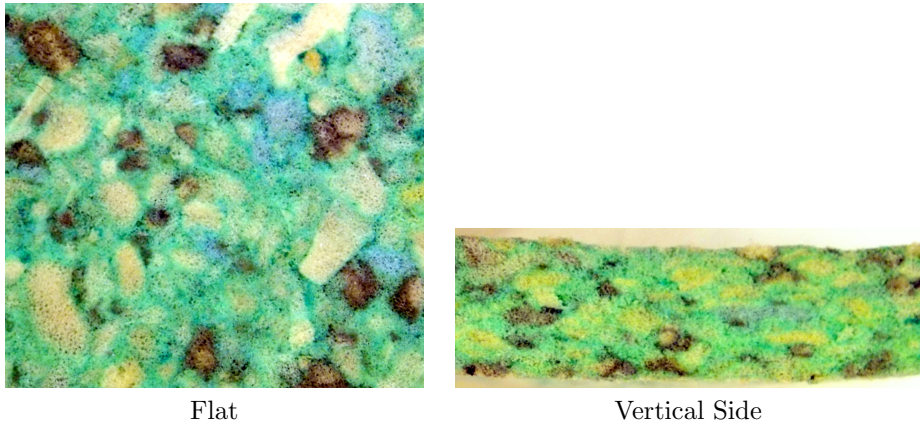
Figure 7.7: Stepisol Material
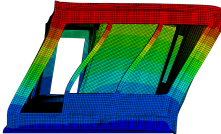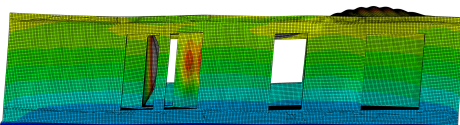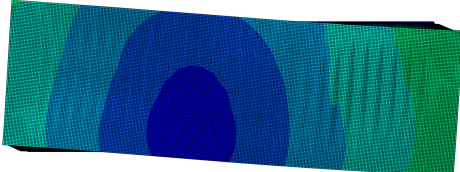
Mode	Frequency [Hz]	Mode shape
Transverse	6.82	
Longitudinal	12.86	
Torsional	10.92	

Table 7.3: Complete Module Model, Frequencies and Mode Shapes with new material properties.

and mode shapes shown in Table 7.3. The mode shapes remained pretty much unchanged but the frequencies were increased. When studied closely, it can be seen that the Stepisol layer has changed the longitudinal mode slightly. Figure 7.8 shows the Setpisol layer for the original and the changed model, where a is the original and b is the changed model. The Stepisol in the longitudinal mode has gone from a typical rocking mode in a, to a more shear dominated mode in b. This may account for the larger increase in frequency for the longitudinal mode compared to the other modes.

a

b
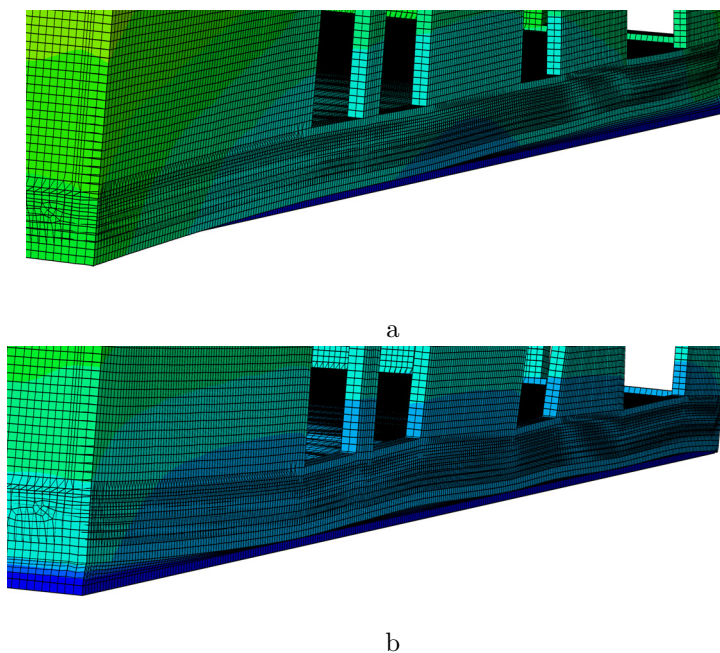
Figure 7.8: Change in Mode Shape, Stepisol

7.3   The Effect of Stepisol and Windows

To get a better understanding of the effect of the Stapisol layer between the modules and between the modules and the foundation, two models of two long walls stacked on top of each other was made. To look at the effect of the Stepisol layer, two tests were made. One dynamic frequency analysis and one static displacement analysis. The deformed shapes, eigenfrequencies and displacements were analyzed to see how the stiffness of the walls and the Stepisol layer affect the behavior of the modules.

In addition to the effect of the Stepisol, the effect of windows were tested. This was done by making one model with two windows and another with no windows. By comparing the two models the effect of the windows were found. The models were built the same way as the exterior walls of the compete model, with the same material properties and the same construction method. The walls were 12.5 meters long and 2.5 meters tall. The plate materials in the foors and ceilings were skipped and some of the dimensions were changed to make the modeling easier. The parts representing the floors and ceilings were given the mass of half the the floor and ceiling of the complete model. This meant that the total mass of the each module wall with floor and ceiling would be roughly equal to the mass of half a module. This was done due to the assumption that the stiffness contribution of each wall is mainly in the wall plane, meaning that the short walls contribute with very little stiffness in the longitudinal direction of the module that was tested here. The models are shown in Figure 7.9, where the Stepisol layer is marked as red.

In addition to the Stepisol layer, the modules were connected by an 8 mm OSB plate, as shown in Figure 7.10. To determine the effect of the OSB plate, the models were tested with and without the plates. The plates were tested with and without corrected material properties according to Eurocode 5, where the stiffness was reduced according to how

a

b
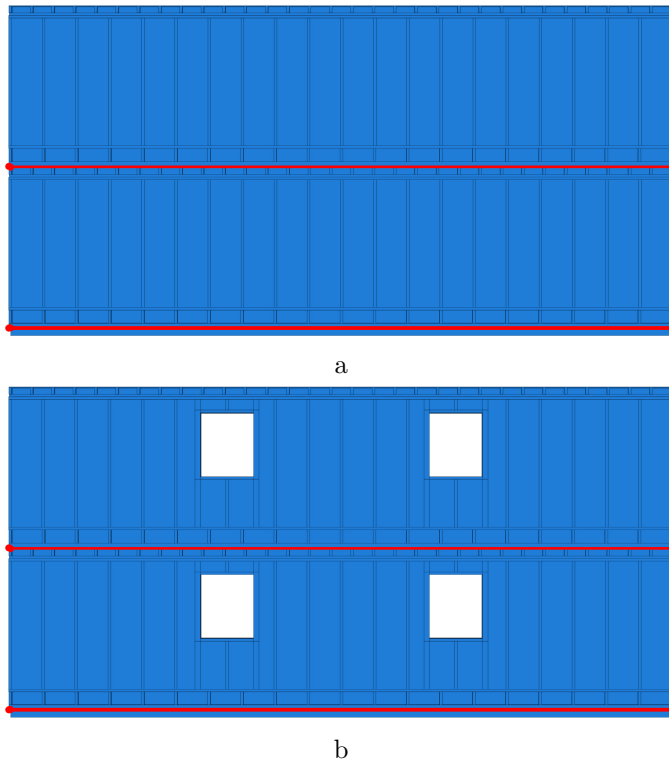
Figure 7.9: Stepisol Test Models

thy were connected to the modules. (The calculations for this can be found in Appendix B.5.1). A fourth test was made where the material properties of the Stepisol layer were changed to normal C24 timber material properties. This was done to compare the testes with a model without the Stepisol layer. Figure 7.10 shows the connection between the modules, and the modules and the foundation.

a   b
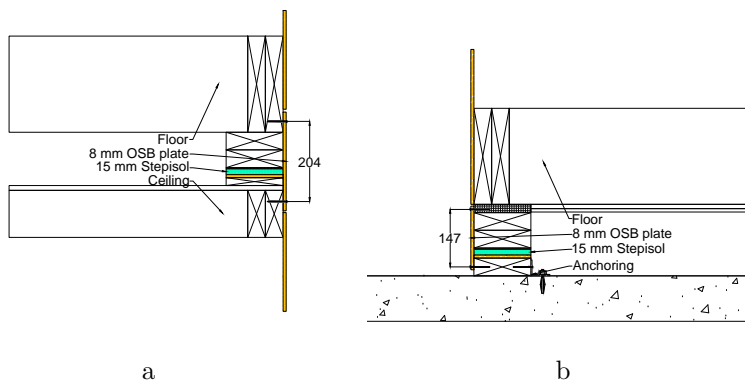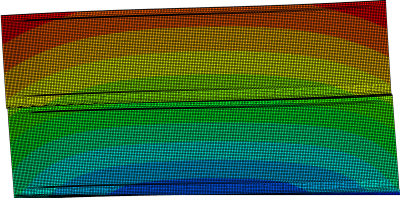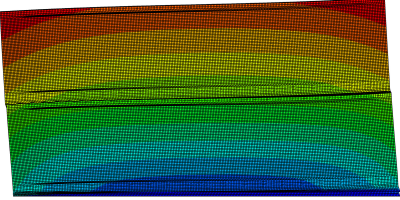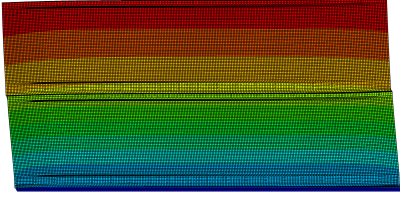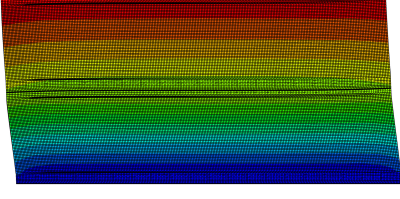
Figure 7.10: Module Connections

7.3.1   Dynamic Analyses

The dynamic analyses were done the same way as the complete model, with a static step applying the gravitational forces and an eigenfrequency analysis in the second step. The boundary conditions were sett so that the bottom of the models could not move in the x-, y- and z-direction, and the whole model restrained form moving out of the wall plane. This way the longitudinal stiffness could be tested without other modes interfering the analysis. The results form the tests are shown in Table 7.4 and 7.5 for models without and with windows respectively.

Model	Frequency [Hz]	Mode Shape
S	6.53	
S,CO	6.94	
S,O	8.27	
-	10.40	
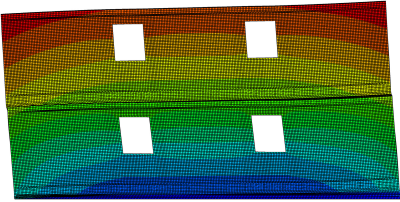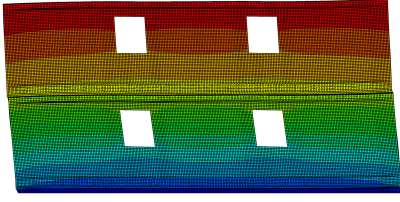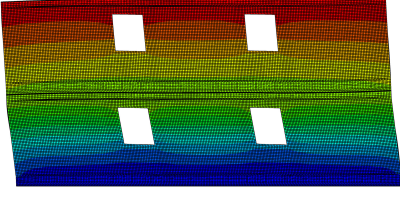
S = With Stepisol
O = With OSB plates
CO = With OSB plates with corrected stiffness

Table 7.4: Dynamic Test, Model without Windows

The dynamic testes show that the Stepisol have two important effects on the dynamic behavior of the modules. First, is makes the modules a lot softer. Second, it changes the mode shape from a more or less straight shear mode to a mode including rocking. The OSB plate reduces the effect of the Stepisol, but with corrected stiffness of the OSB

Model	Frequency [Hz]	Mode Shape
S	6.27	
S,CO	6.65	
S,O	7.87	
-	9.723	

S = With Stepisol
O = With OSB plates
CO = With OSB plates with corrected stiffness

Table 7.5: Dynamic Test, Model with Windows

plates, the effect is small. Whether the reduction in stiffness is to large or not has not been looked into since questioning the Eurocode is not the scope of this thesis. However, the results shows that the modules can gain much stiffness by altering the stiffness of the connection between the modules. This may lead to a reduced soundproofing effect, but acoustics is not the scope of this thesis and has not been looked into here.

7.3.2 Static Displacement Analyses

The static displacement analysis was set up the same way as the dynamic test regarding the boundary conditions. This was also a two step analysis with the same first step as for the dynamic analyses. The second step was a static general step where a traction load of totally 1 kN was applied along the top of the upper module ceiling as shown in Figure 7.11. The displacement was measured at four points along the vertical center
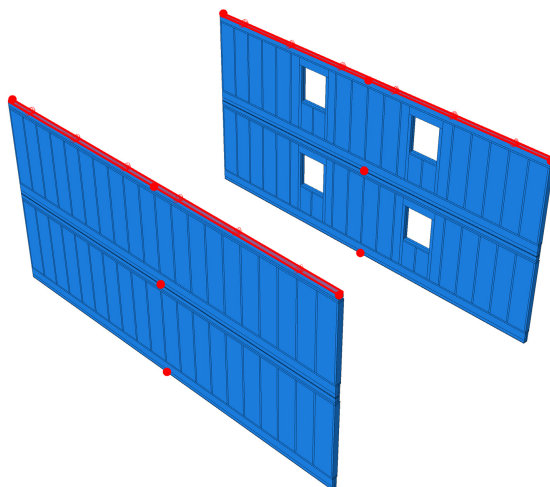
Figure 7.11: Stepisol Tests, Static Displacement Test Setup

line of the models, marked as red dots in Figure 7.11. The points were located on both sides of the Stepisol layers, and at the top of the upper wall. The vertical displacement was measured on the upper corners of the models to estimate the rotation of the walls. The results are shown in Table 7.6 and 7.7 for the models without and with windows, respectively.

Setup		Stepisol	Lower Wall	Upper Wall	Total
S	Displ. [mm]	0.039	0.065	0.078	0.182
	% of Total Displ.	21.6	35.5	42.9	100
S,CO	Displ. [mm]	0.033	0.060	0.071	0.164
	% of Total Displ.	20.3	36.4	43.3	100
S,C	Displ. [mm]	0.027	0.043	0.047	0.117
	% of Total Displ.	23.2	36.4	40.4	100
-	Displ. [mm]	0.0005	0.040	0.044	0.084
	% of Total Displ.	0.63	47.7	51.6	100

Table 7.6: Horizontal Displacements, without Windows

The total rotation of the walls are listed in Table 7.8. The results were then plotted in Figures 7.12 a and b, for the walls with no windows and for the walls with windows, respectively. The y-axis represents the height of the measurement points and the x-axis the horizontal displacements.

Setup		Stepisol	Lower Wall	Upper Wall	Total
S	Displ. [mm]	0.041	0.057	0.08	0.179
	% of Total Displ.	23.0	31.8	42.1	100
S,CO	Displ. [mm]	0.034	0.052	0.070	0.157
	% of Total Displ.	22.1	33.4	44.4	100
S,C	Displ. [mm]	0.028	0.037	0.042	0.107
	% of Total Displ.	26.2	34.7	39.0	100
-	Displ. [mm]	0.0003	0.036	0.038	0.075
	% of Total Displ.	0.43	48.2	51.4	100

Table 7.7: Horizontal Displacements, with Windows

Setup	No Windows [deg]	Windows [deg]
S	0.00079	0.00082
S,CO	0.00066	0.00069
S,O	0.00021	0.00023
-	0.00014	0.00016

Table 7.8: Total Rotation at the Top of the Models
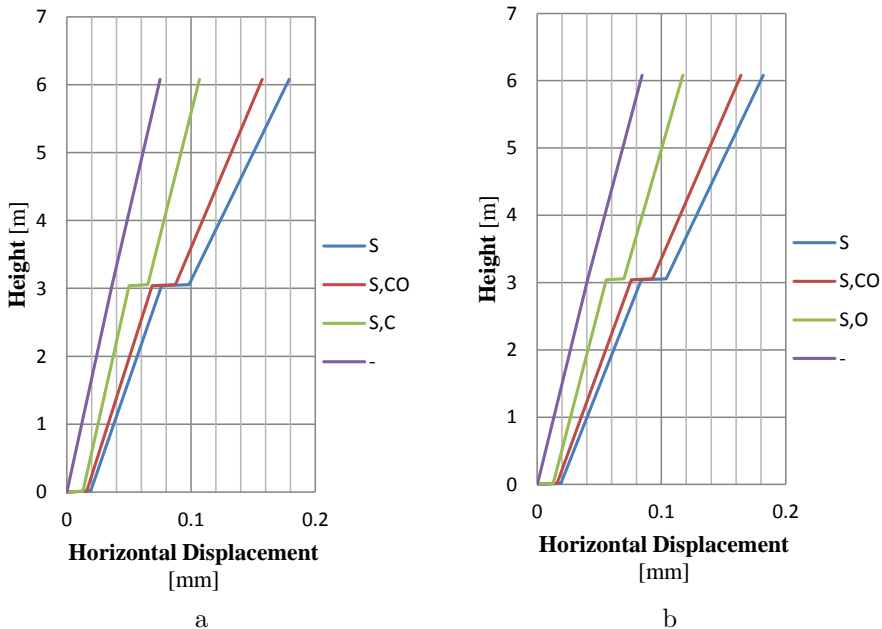
S = With Stepisol
O = With OSB plates
CO = With OSB plates with corrected stiffness

Figure 7.12: Stepisol Tests, Horizontal Displacements

The plot illustrates the deformed shape of each setup, in respect to each other.

The results show the same effects as for the dynamic test, where the Stepisol layer decreases the stiffness of the system in two ways. First, the horizontal deformation of

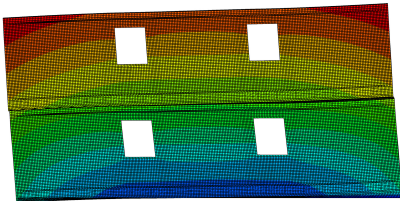the Stepisol layers is considerable. Second, the rotation of the model is affected by the connection between the models. The inclination of the lines in Figure 7.12 shows that although the rotation is small, it contributes much to the total deflection in a high stack of modules. If there had been no rotation, the inclination of the lines representing the wall elements should have been the same for all four setups.

For the setup with the uncorrected OSB plates, the horizontal displacement of the Stepisol makes up a larger part of the total horizontal displacement than for the corrected setup. This is because the stiffness of the nails is so much lower than the stiffness of the plate in stress or strain that they dominate the stiffness of the connection. The difference in shear stiffness and tension/compression stiffness is therefor reduced for the corrected setup. This means that rotation contributes more to the total horizontal displacement than the shear displacement for the corrected setup than for the uncorrected.

If it is of interest to build higher stacks of modules where the lack of dynamic stiffness can be a problem. Altering the connections between the modules and between the modules and the foundation much stiffness could be gained, especially by increasing the vertical/rotational stiffness of the connections.

Comparing the results of the numerical tests to the tests preformed on the real models shows that the models are fairy close to the test results, but not quite stiff enough. Since there were no accelerometers recording the vertical accelerations of the tested modules, it was hard to estimate any rocking motion to compare with what was found in the numerical tests.

7.3.3   Effect of Windows

The only difference between the two models was the windows. The windows were modeled as shown in Figure 7.13. Like for the complete model, there was no stiffness added for the windows, only added mass to the timber frame surrounding the hole. The

a   b
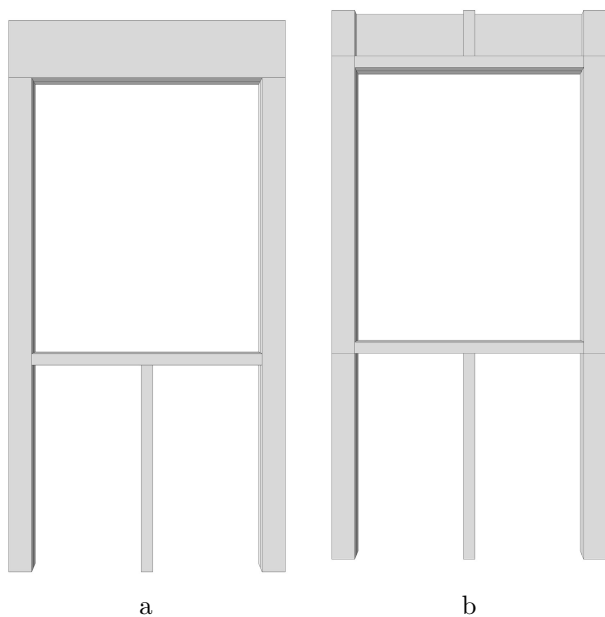
Figure 7.13: Modeled Windows, Front and Back

total added mass to the model, compared to the model with no windows was 160 kg. The added mass was therefor to small to account for the change in frequency.

Comparing the results from the static displacement test shows clearly that the stiffness is reduced for the wall with windows. The difference is best expressed by the stiffest setups, where the connections were made with timber instead of Stepisol. Here the walls account for all the stiffness without any interference form the connections. The difference in displacement for these walls were 0.0094 mm, which is 12.6 % more displacement for the walls with windows.

Since little is known about the stiffness contribution from the windows, these tests only reveal the difference for the modeled walls, and can therefor give a wrong picture of the stiffness reduction in the walls. This is obvious when looking at the transverse mode shape of the complete model, where the lack of stiffness contribution form the windows have given a too soft response.

7.4 Modifying the Length of Module Walls

7.4.1 Detailed Models

If a general model shall be made, it is important to see what happens when the length of a wall changed. To test this, three walls of different lengths were modeled and tested. The length of the walls was 12.5 m, 8.7 m and 6.25 m. The walls were modeled the same way as the exterior walls of the complete module, but with no windows. The studs were 50 mm × 170 mm and had a height of 2.4 m. The sill and top plates have the same cross section as the studs which makes the total height of the walls 2.5 m. The center distance between the studs were sett to 0.6 m.

The boundary conditions were sett so that the walls could not move out of the plane along the height of the walls. The sill plate was restrained form movement in all directions om the bottom side. Figure 7.14 shows the boundary conditions of the shortest wall.
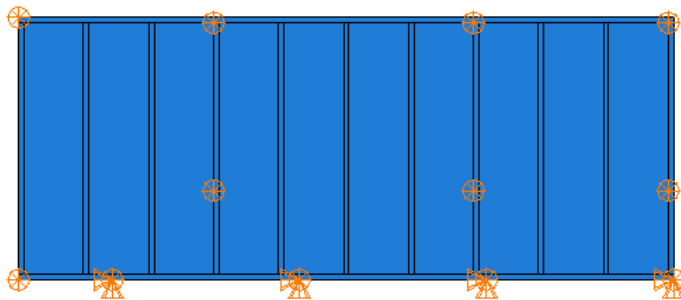
Figure 7.14: Modified Length of Walls , Boundary Conditions

The walls were tested by running a frequency analysis. Table 7.9 shows the walls with corresponding lengths, eigenfrequencies and mode shapes.

The result show that there is only a small drop in the eigenfrequencies for decreasing length. This shows that the stiffness to weight ratio is almost the same for all the tested lengths and that scaling the walls by assuming plate behavior is a realistic approach.

A static displacement test was set up to confirm the results. The test was made by applying traction forces along the top plate. The applied force was 500 N/m^2 which is
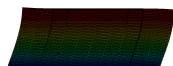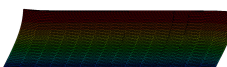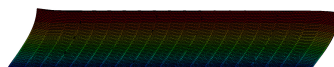
Length [m]	Model	Frequency [Hz]	Mode shape
6.25		40.07	
8.7		40.58	
12.5		40.89	

Table 7.9: Frequencies and Mode Shapes for Different Wall Lengths

equivalent to 85 N/m along the length of the walls. The boundary conditions were kept the same as for the previous test. Figure 7.15 shows the test setup. The results form
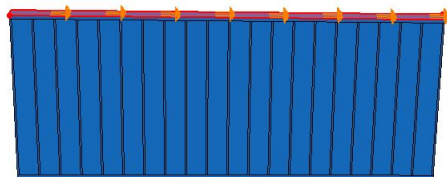
Figure 7.15: Static Test for Different Wall Lengths

the static test is shown in Table 7.10, where the displacement Δx is measured in the middle of the top plate.

The results are very close, which means that stiffness per meter is also very close for all three models. The deformed shapes show that the response is dominated by the shear strength of the walls. The curves at the ends of the walls are due to bending. The curved area of the shortest wall dominates a larger part of the response which means it is slightly less stiff than the other two. For even shorter walls, bending will dominate more and more, and the stiffness per meter decrease further.
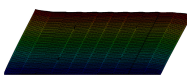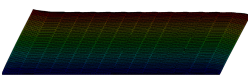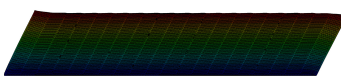
Length [m]	Load [N]	Displacement Δx [mm]	Deformed shape
6.25	521.3	0.00375	
8.7	739.5	0.00370	
12.5	1062.5	0.00366	

Table 7.10: Static Test for Different Wall Lengths
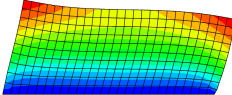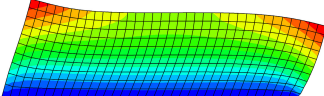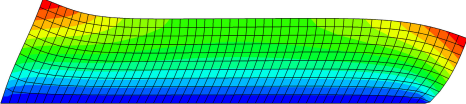
Length [m]	Frequency [Hz]	Mode shape
6.25	38.34	
8.7	39.85	
12.5	40.95	

Table 7.11: Plate Models Frequency Test

7.4.2 Plate Models

To see how well this this matches models with continuous plates of the same dimensions, the same tests were made on three simple plate models. The stiffness of the plate models were calculated by using a formula for vertical concrete plates [14]. The calculations can be found in Appendix B.6. The calculated Young's modulus for the three walls were, as expected, very close to each other. The Young's modulus was sett to 101 MPa, which was calculated for the 8.7 m long model. The mass density was sett to 206.7 kg/m^3, which was calculated from the total weight of the wall models. The mesh size was sett to 0.25 m.

The boundary conditions were the same as for the two previous tests. The results from the eigenfrequency test and the static displacement test are shown in Table 7.11 and 7.12, respectively. The deformed shapes show that the vertical movements in plate models are far larger than for the detailed models. This can be explained by the vertical stiffness of the studs. The studs do not contribute much to the horizontal stiffness, but since the fibers of the timber go in the vertical direction, it contributes much to the vertical stiffness.

The plate models are more sensitive to bending than the detailed models. This can be seen in the deformed shapes and the larger variation in eigenfrequency and displacement for the two tests. Scaling a wall by representing it as a plate will therefor give a slightly different stiffness than the real scaled wall. However, the difference is *very small*, and by down scaling a wall the result will be conservative[1].

---

[1]In most cases lower frequencies are considered more dangerous.
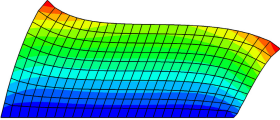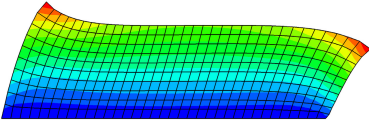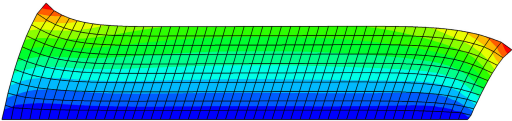
Length [m]	Load [N]	Displacement Δx [mm]	Deformed shape
6.25	521.3	0.00395	
8.7	739.5	0.00351	
12.5	1062.5	0.00327	

Table 7.12: Plate Models Static Displacement Test

7.4.3   Shear Frame and Truss Frame Models

Two more model setups were made to see how the simplifications made in Chapter 6 can be calculated instead of iterated and how well the simplifications represent the real model[2]. The shear frame and truss frame models were tested the same way as the previous models. The stiffness calculations can be found in Appendix B.6.

The mass of the walls are represented by the top beams of the models, which has a total mass of half the total mass of the detailed models. The other half would be represented by a floor beam which is not part of these models for obvious reasons. The top beam has a cross sectional area of 1 m^2 and a mass density of 43.93 kg/m^3.

The results form the testes are shown in Tables 7.13 and 7.14, for the shear frame and the truss frame models respectively. The results form the static displacement tests show that the stiffness can be calculated quite accurately for both models and that the shear frame model is slightly more accurate than the truss frame. The dynamic tests show that the mass distribution for this specific test setup is not quite accurate. The difference would have been reduces if the mass of ceiling had been part of the model.

---

[2]The real model referred to here is still a numerical model
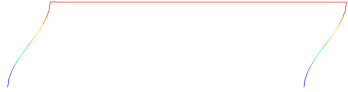
Length [m]	Frequency [Hz]	Displacement Δx [mm]	Mode shape
6.25	35.64	0.00386	
8.7	36.19	0.00374	
12.5	36.34	0.00371	

Table 7.13: Shear Frames Frequency and Static Displacement Tests
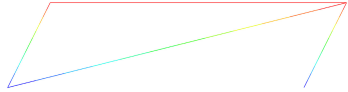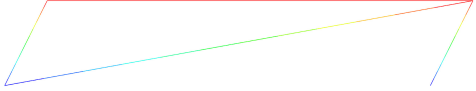
Length [m]	Frequency [Hz]	Displacement Δx [mm]	Mode shape
6.25	34.50	0.00412	
8.7	35.67	0.00385	
12.5	36.22	0.00374	

Table 7.14: Truss Frames Frequency and Static Displacement Tests

7.4.4   Comparing Results

The best way of scaling a wall by calculation and modeling has been found by comparing the results form all the tested models. It has been assumed that the detailed models represent real walls best and that the simple models with the least deviation form these are the the best simplified models. Table 7.15 shows the results from all models with calculated deviation form the detailed models. From the compared results, the models matching the stiffness of the detailed models best are the shear frame models. The plate models are closest in the dynamic tests.

A good way of scaling and modeling a wall like these would be to determine the

Length	Model	Frequency	Difference	Displacement	Difference
[m]		[Hz]	[Hz]	[mm]	[%]
6.25	Detailed	40.07	-	0.00375	-
	Plate	38.34	-1.73	0.00395	5.33
	Shear	35.64	-4.43	0.00374	-0.27
	Truss	34.50	-5.57	0.00412	9.87
8.7	Detailed	40.58	-	0.00370	-
	Plate	39.85	-0.73	0.00351	-5.14
	Shear	36.19	-4.39	0.00374	1.08
	Truss	35.67	-4.91	0.00385	4.05
12.5	Detailed	40.89	-	0.00366	-
	Plate	40.95	0.06	0.00327	-10.66
	Shear	36.34	-4.55	0.00371	1.37
	Truss	36.22	-4.67	0.00374	2.19

Table 7.15: Compared Results

stiffness of one wall, assuming that the stiffness per meter is constant, like shown for these walls, and multiplying the stiffness per meter by the length of the new wall. The new wall can then be modeled as a shear frame with a stiffness calculated as shown in Appendix B.6.

Chapter 8

Dynamic Testing of Stepisol

8.1 Background

Stepisol is a product used for acoustic purposes in buildings. It is made of a flexible polyurethane foam, with 90% reclaimed granulated plastic and 10% new materials. Its main area of application is soundproofing of floors, and comes in two different stiffness and density classes. Kodumaja use the green Stepisol with a mass density of 195 kg/m^3, in strips of 145 mm x 15 mm[13] horizontally between the stacked modules and between the modules and the foundation. It is applied as a continuous layer on the base fame of the modules, so that all the vertical forces from the modules above are carried trough this layer. Figure 8.1 shows how it is attached to the foundation on which the test modules were placed. As Stepisol is commonly used to reduce sound vibrations in the vertical direction, the material properties are well documented in the transverse direction. However, in a situation where the material is subjected to dynamic shear forces, the material properties are not as well documented. The material is as mentioned earlier used as a sound reducing agent, and its effect as a structural element is therefor not as well documented. Therefor, a test setup was made to determine the dynamic shear stiffness and dynamic transverse[1] stiffness of the material.

---

[1] Transverse - vertical stiffness

Figure 8.1: Stepisol Coverd Base Frame
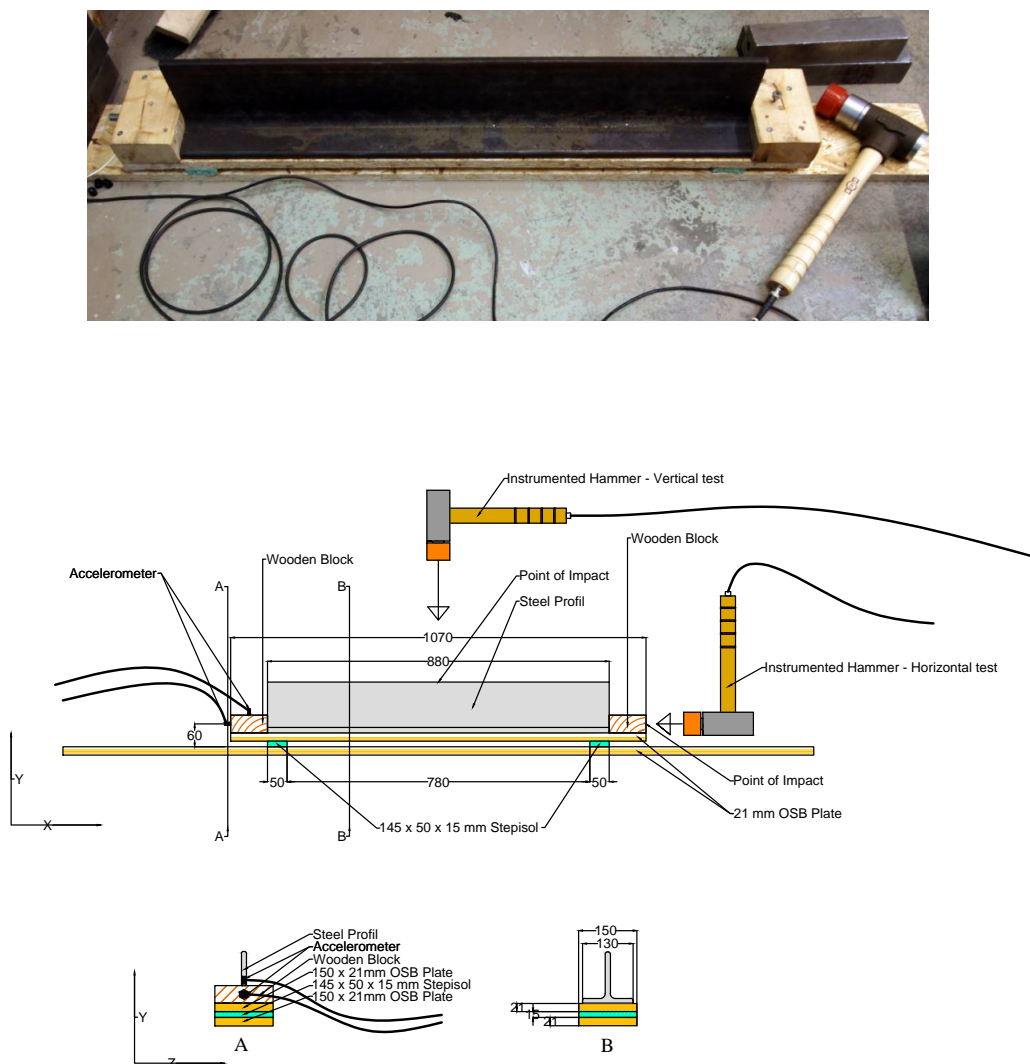
Figure 8.2: Stepisol Test Setup

8.2 Test Setup and Protocol

To make the tests as quick and simple as possible, the modal analysis equipment form the module testes was used in this setup as well, but with a smaller modal hammer (1.36 kg) of the same brand (see Section 4.3.1.1) [11]. Figure 8.2 shows the test setup. For the shear test , the wooden block to the right in Figure 8.2 was hit by the hammer to excited the upper OSB-plate and steel profile in the x-direction. The accelerometer on the opposite block recorded the accelerations. The lower OSB-plate was fixed to a rigid surface, to isolate the movement of the upper. The two plates were monitored closely to detect any relative translation before and after impact. If any translation was detected the data was discarded. The vertical test was done the same way, only with impacts in the middle, on top of the steel profile, with the accelerometer mounted vertically. Both

testes are driving point testes, which means the mode shapes are not identified. In order to get more reliable estimates, each test was carried out with three impacts that were averaged in the output FRF. A rowing hammer test was also carried out, to verify that the first vertical mode was correct. Three impact points were used. One at each end of the steel profile and one in the middle.

The steel profile was used mainly as weight, but it was a also to ensure an evenly distributed load on the pads, and no local bending modes in the vertical test. A relatively long profile was chosen to avoid horizontal rocking modes. The weight of the profile was chosen to resemble the load for a single building module. The total mass of the system above the Stepisol pads was 29.51 kg, which represents a load of 19.96 kPa on the Stepisol pads. Assuming evenly distributed load, the load from a single first floor module is 19.5 kPa.

To establish a static stiffness, the effective height of the Stepisol pads were measured before and after the load was applied.

8.3   Calculations

Since there is no slip between the components and the system, it can be modeled as a damped single degree of freedom systems as shown in Figure 8.3. Where the Stepisol pads are represented by the stiffness, k and the damping coefficient, c, while the weight of the steel profile, upper OSB-plate, accelerometer and the wooden blocks are represented by the mass, m. With assumed linear stiffness and small damping, the circular eigenfrequency of the system is given by:

$$\omega_n = \sqrt{\frac{k}{m}} \tag{8.1}$$

The mass is known and the frequency can be read from the test results, which means that the stiffness k can be calculated. Since the frequency output from the test is given in Hertz[2] and ω_n in rad/sec the frequency is multiplied by 2π to obtain the stiffness k ($\omega_n = Hz \times 2\pi$). Now the stiffness, k can be calculated by:

$$k = (frequency[Hz] \times 2\pi)^2 m \tag{8.2}$$

To obtain the material properties, the system stiffness k is divided by the height h of the Stepisol pads which is represented by the length of the spring in Figure 8.3. The stiffness is then calculated form Equation 8.3. Where A is the combined horizontal area of the Stepisol pads. It has been assumed that the modes are perfectly one dimensional in the vertical and the horizontal direction.

$$Stiffness = \frac{kh}{A} \tag{8.3}$$

The static stiffness is estimated from Equation 8.4 where linear stiffens has been assumed.

$$E = \frac{\sigma}{\epsilon} \tag{8.4}$$

---

[2]Hertz is given by cycles/sec, $\frac{1}{T}$.
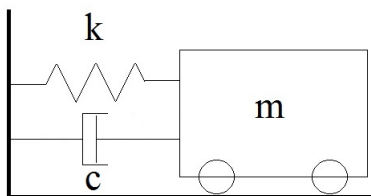
Figure 8.3: Damped Single Degree of Freedom System

Modulus	Frequency [Hz]	SD	Damping [%]	SD	Stiffness [kPa]	SD
E	20.57	0.437	6.36	0.453	464	19.8
G	16.92	0.281	7.18	0.696	314	10.4

SD - Standard Deviation

Table 8.1: Test Results, Stepisol

8.4   Results

8.4.1   Static Test

The static deflection was measured to 1,35 mm which gives:

$$\epsilon = \frac{1.35}{15} = 9\% \tag{8.5}$$

This gives a static stiffness of:

$$E \quad = \quad \frac{\sigma}{\epsilon} \tag{8.6a}$$

$$= \quad \frac{19.96 kPa}{0.09} \tag{8.6b}$$

$$E \quad = \quad 221.77 kPa \tag{8.6c}$$

Compared to the stiffens estimated from [13], which can be found in Appendix C.1, this is a plausible result.

8.4.2   Dynamic Tests

The results from the dynamic tests are shown in Figure 8.4, where damping is plotted on the x-axis and frequencies on the y-axis. Both the frequencies and the damping vary in some degree, but the variation is not to big, especially regarding the frequencies. The average results are given in Table 8.1 together with the calculated material stiffnesses and corresponding standard deviations.

The mode shapes found in the roving hammer test confirmed that the first vertical mode was a pure translation mode. It also showed that the second mode (a rocking mode) had a frequency of roughly 33.5 Hz.

Tests show relatively high damping values. Thus it can be assumed that the Stepisol contributes to increase the overall damping in the modules.

From these tests, it is obvious that there is a profound difference between static and dynamic stiffness, and that the static stiffness should not be used to model the material in a dynamic test.
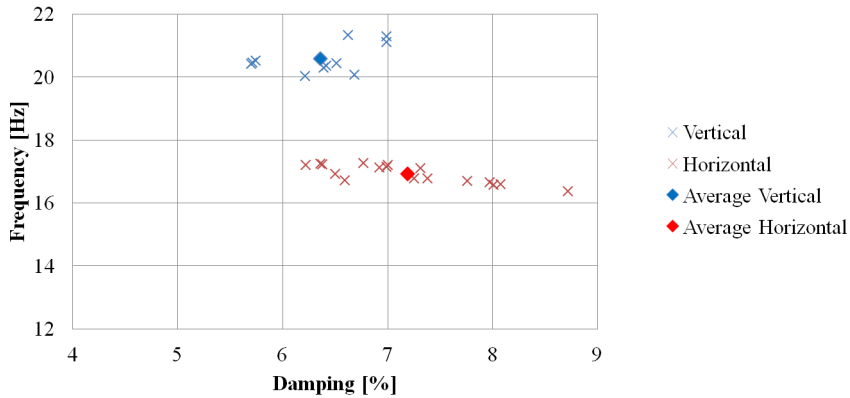
Figure 8.4: Test Results, Stepisol

The difference in static and dynamic stiffness is probably due to the porosity of the material. The air pressure within the pours is not given enough time to be equalized, which makes the material stiffer. Due to this effect, Stepisol can have a frequency dependent stiffness that decreases with lower frequencies. This has however not been tested in this survey.

8.5   Numerical Analyses of Stepisol

A numerical test was set up in Abaqus/CAE 6.11-1 to see how well the calculated stiffness values corresponded with a numerical model. To use the calculated values from the lab test without verifying the results in a numerical test could give a wrong impression of the stiffness values. Keeping in mind that the mathematical model used to estimate the stiffness values is a simplification of the real situation. The setup is shown in Figure 8.5 where the Stepisol is represented by the pads, and the upper system by the T- shaped profile. In this setup the geometry and weight of the steel profile was set to match the properties of the system above the Stpeisol pads from the lab test. The height of the pads was reduced slightly, so that the compressed height in the numerical model would be the same as for the lab tests. This was done due to the difference in static and dynamic stiffness, so that only the dynamic stiffness could be included in the numerical model. Calculations for the height reduction can be found in Appendix C.2. The Young's modulus of the profile was sett to 210 GPa, as for normal construction steel, whilst the Stepisol pads were given orthotropic material properties with values matching the results
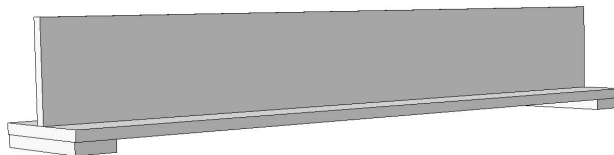
Figure 8.5: Numerical Test of Stepisol

E_1 [kPa]	E_2 [kPa]	E_3 [kPa]	ν_{12}	ν_{13}	ν_{23}	G_{12} [kPa]	G_{13} [kPa]	G_{23} [kPa]
464	464	464	0.01	0.01	0.01	314	314	314

Table 8.2: Material Properties, Stepisol

	E [kPa]	G [kPa]	Frequency Mode 1[Hz]	Frequency Mode 2 [Hz]
Lab	464	314	15.35	20.1
Numerical	490	387.5	16.89	20.65

Table 8.3: Numerical Test Results, Stepisol

form the lab tests. However, since only the shear stiffness and transverse stiffness were known, the material was given the same properties in all directions as shown in Table 8.2. The Poisson's ratios was sett to 0.01 since the material is very porous.

The analysis was run in two steps, first a static step that applied gravity, then a linear perturbation step with a frequency analysis. The results of the first analysis showed that the estimates from the lab matched the numerical model quite well, but that the FE model was a bit too soft. The material properties were tuned and further analyses run to match the frequencies form the lab tests as closely as possible. This was done by adjusting the E and G modulus of the Stepisol. Both the E and G had to be increased to match the frequencies form the lab, as shown in Table 8.3. The third mode, which was not thoroughly tested in the lab, had a frequency of 32.6 Hz in the first analysis, and 33.5 Hz in the final, matching the lab tests very well without having been calibrated. This increases the confidence of the numerically obtained stiffness values.

The mode shapes are shown in Figure 8.6 where a is the horizontal mode (shear) and b is the vertical mode. When the mode shapes were studied closely, it was found that the first mode (shear) was not a clean shear mode. There was also some vertical movement that is not accounted for in the calculated values form the lab test. This effect is due to the height of the steel profile, which creates a small moment of inertia about the Stepisol pads.

Since the numerically obtained stiffness values match the measured frequencies best, these were the values used in the further modeling in this thesis.
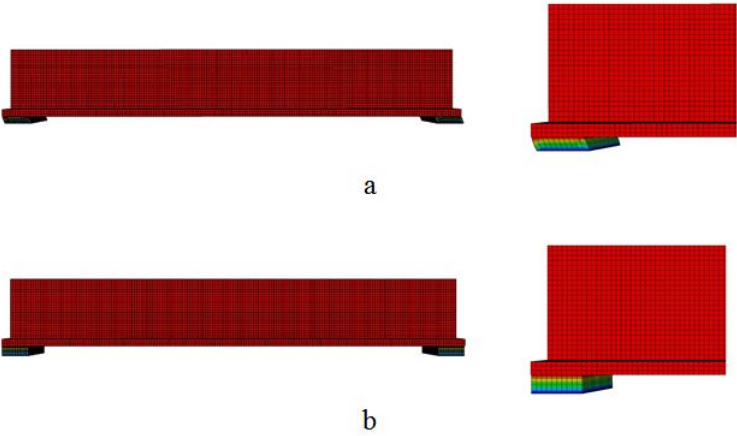
Figure 8.6: Numerical Modes, Stepisol

Chapter 9

Conclusions and Further Work

9.1 Conclusions

The dynamic tests preformed on the building modules are only regarded partially successful. This is due to the unfortunate foundation of the single module setup and problems related to low excitations and large amounts of noise for the two by two setup. The limited time for testing gave fewer measurements than what was desired of the MA tests.

Using the hammer to excite the stacked modules in the longitudinal direction gave low response due to high stiffness and mass. This made it hard to get good and stable results form the analyses. Applied in the transverse direction and for the single module setup, the hammer worked well.

When the analyses were finished the results from the two methods showed good correlation. The frequencies found in the SID tests were very consistent, but the damping ratios were more scattered, especially for the translational modes in the two by two setup. Only one analysis on each side of the two by tow setup was made with the MA test which makes stability assessments impossible. Although larger excitation forces would bee preferred, an over all evaluation of the test methods deems both methods suitable for evaluating dynamic properties of building modules.

The further conclusions presented here only applies to the tests carried out on the two by two setup. No relevant conclusion has been made for the test results of the single module setup due to the unfortunate foundations.

The results form both tests showed three modes of interest, two translational and one torsional mode. All modes were symmetrical about the center of the modules and had frequencies below 11 Hz. The modes and frequencies were widely influenced by the layers of Stepisol and the connections between the modules, and between the modules and the foundation. The Stepisol makes the stacked modules a lot less stiff and causes a rocking motion in addition to the shear deformations in the modes.

The equivalent viscous damping of the tested building modules should be set to 3%. This value is slightly more than one standard deviation lower than the mean value for all relevant test results. From the lab tests of the Stepisol it was found that Stepisol has a relatively high damping. Thus it is concluded that the Stepisol contributes much to the total damping of the modules.

Stepisol has been identified as the element that effects the dynamic properties of modules the most and that changing the connections between the modules will affect the dynamic properties of the system severely.

The numerical models showed that the stiffness of windows can not be neglected for walls with large areas of glass. The effect is however less noticeable for walls with fewer windows.

The stiffness of the the modules without the Stepisol layer is dominated by the shear stiffness of the walls, since the bending stiffness in the wall plane is very high. The upshot of this is that the stiffness of walls built the same way but with different length can easily be calculated if the stiffness of one wall is known.

Predicting the stiffness of different sized modules by assuming plate behavior in the walls gives a plausible result. Thus, the shear frame models made for the large model of the VHT building is a fair representation of the real modules, and should be given a damping ratio of 3% in further analyses.

9.2   Further Work

Suggestions for further work:

- Further dynamic testing of building modules

- Evaluation of the effects of plasterboard

- Evaluation of the stiffness contribution form large windows/glass areas

- Evaluation and implementation of damping in numerical models

- Further evaluation of the structural dynamic effects of sound reducing layers and connections between modules

First of all, further dynamic testing of building modules are wanted to establish a better bases for numerical modeling. In situ test of building modules would give more relevant results than the tests made in this thesis since the foundations would be properly made. Using different excitation methods for the SID tests would probably help stabilizing the measured damping ratios. Tests on both stacked and single modules would be beneficial.

Plaster boards are widely used in building modules and contributes much to the stiffness of the structure when subjected to relatively low forces. Plasterboard is however brittle and could break in ultimate limit state (ULS) situations. Removing the stiffness of the plaster boards would make the modules a lot less stiff and the modules may have problems coping with ULS situations like earthquakes.

Since many modules have walls made of large glass areas, an evaluation of the stiffness contribution form glazed walls would give better numerical prediction models for building modules.

The damping of the modules has only been measured globally in this thesis. It is therefor hard to say what parts contribute to the damping of the modules. Further evaluation of this subject could give better prediction models for damping in building modules. Implementing damping in the numerical models would make the models more complete.

The sound reducing agent Stepisol was used between the modules that were tested in this thesis. Other materials are available which may change the dynamic properties of stacked modules. Further surveys of this subject could improve the design and increase the damping of building modules. Altering the connections between the modules could also increase the maximum height of stacked modules in purely module based buildings.

References

[1] Engineering wood. http://en.wikipedia.org/wiki/Engineered-wood Accessed 15.01.2013.

[2] Norsk standard ns-en 520:2004+a1:2009 gipsplater. definisjoner, krav og prøvingsmetoder.

[3] Ns-en 12369-1 trebaserte plater, karakteristiske verdier for dimensjonering a trekonstruksjoner del 1: Osb-plater, sponplater og trefiberplater.

[4] Ns-en 388:2009 - structural timber - strength classes.

[5] Rena bru - kjøllseterbrua, verdens sterkeste trebru. http://www.sweco.no/no/Norway/Markedsomraader/Infrastruktur/Bruer/Rena-bru/ Accessed 16.01.2013.

[6] Tre og miljø. http://www.treteknisk.no/fullstory.aspx ? m = 1453 Accessed 13.01.2013.

[7] The fundamentals of modal testing, application note 243 -3, 2000. http://cp.literature.agilent.com/litweb/pdf/5954-7957E.pdf Accsessed 1.12.2012.

[8] Befolkningsstatistikk. befolkning og areal i tettsteder, 1. januar 2012, 9 2012. http://www.ssb.no/vis/emner/02/01/10/beftett/main.html Accessed 10.01.2013.

[9] Murray grove - the worlds tallest modern timber residential building, 2012. http://www.waughthistleton.com/project.php?name=murray&img=1 Accessed 16.01.2013.

[10] Specific modulus, 2012. http://en.wikipedia.org/wiki/Specific-modulus Accessed 13.01.2013.

[11] Specifications, heavy duty type 8210, 11 2012. http://www.bksv.com/Products/transducers/vibration/impact-hammers/8210.aspx?tab=specifications Accessed 22/11/2012.

[12] World's tallest timber building "tops uot" in merbourne, 11 2012. http://www.timberdesignandtechnology.com/worlds-tallest-timber-building-tops-out-in-melbourne/ Accessed 16.01.2013.

[13] Emballageteknik AB. Stepisol, ljuddampande underlag for moderna golv. Information Sheet, 2012.

[14] J. Hopp & S. Alexander. *Betongelementboken Bind B, Avstiving og kraftoverføring, 3. opplag.* Betongelementforeningen, 2005.

[15] Dr. Randall J. Allemang. Experimental modal analysis. http://www.sdrl.uc.edu/academic-course-info/academic-course-info/docs/ucme663/v3-1.pdf. Accessed 10.12.2012.

[16] R. Brincker & P. Andersen. Understanding stochastic subspace identification. In *Proceedingds of the 24th International Modal Analysis Conference (IMAC)*, 2006.

[17] Reidulf Ramstad Architects. http://www.barents.no/barentshuset.156868.no.html Accessed 12.01.2013.

[18] Peter Avitabile. Modal space in our own little world. http://macl.caeds.eng.uml.edu/umlspace/mspace.html, 1998 - 2009. Accessed 9.12.2012.

[19] A. Q. Nyrud & T. Bringslimark. Opplevelsen av trematerialer i innemiljø. *Fokus på tre*, 54:–, 2012.

[20] Brüll & Kjær. *Product Data, Heavy Dyuty Impact Hammers Type 8207, 8208 and 8210*, 5 2012.

[21] Bybrann.no. http://www.bybrann.no Accessed 12.01.2013.

[22] Byggforskserien. Byggevarer og materialer, byggningsglass, byggedetaljer a571.951. Technical report, SINTEF, Høsten 1993.

[23] Byggforskserien. Gipsplater, typer og egenskaper, byggdetaljer 571.047. Technical report, SINTEF, Sending 1 2005.

[24] A. K. Chopra. *Dynamics of Structures, Theory and Applications to Earthquake Engineering, third edition.* Pearson Education Inc., 1995.

[25] D.J. Ewins. *Modal Testing: Theory and Preactice.* Research Studies Press Ltd., 1995.

[26] HBM. *Operating Manual, PC measurement electronics, Spider8.*

[27] HBM. *Hottinger Baldwin Messtechnik, Mounting instructions, Accelerometer Transducer B12*, 2 2000.

[28] G. Hemery. Climate change, timber quality and carbon, 3 2011. http://gabrielhemery.com/2011/03/11/climate-change-timber-quality-and-carbon/ Accessed 16.01.2013.

[29] Adby Kermani Jan Weckendorf, Binsheng Zhang. Prediction of modal frequencies, modal shapes and static point load deflectiond of i-joist timber flooring systems using finiteelement method. In *WCTE, World Conference on Timber Enginairing*, 2010.

[30] Olsson A. Jarnerö K., Brandt A. Vibration properties of a timber floor assesed in laboratory and during building construction. In *Inter Noise 2010 Noise and Sustainability*, 2010.

[31] A. Jørstad. Dynamic testing of building module model. Labtests and Numerical Modeling, 7 2012.

[32] L. H. Kaasa. Design of an experimental setup for measurements of aerodynamic properties of bridge decks. Master's thesis, NTNU (Norwerian University of Sience and technology, 2012.

[33] Anders Olsson Kirsi Jarnerö, Anders Brandt. In situ testing of timber floor vibration properties. In *WCTE, World Conference on Timber Enginairing*, 2010.

[34] Anders Olsson Kirsi Salmela. Dynamic properties of a sawn timber floor element with high transverse bending stiffness. *Journal of Building Acoustics*, 13:294–310, 2006.

[35] Kistler Instrument Corporation. *Kistler Instruction Manual K-Shear Accelerometers*, 11 2006.

[36] Kistler Instruments Corporation. *Piezotron Coupler, 4-Channel PiezoSmart (TEDS) Power Suply/Signal Conditioner*, 2008.

[37] Nathalie Labonnote. *Experimental Evaluations and Prediction of Material Damping in Timber Structures*. PhD thesis, NTNU-Trondheim Norwgian University of Science and Technology Faculty of Engineering Science and Technology Department of Structural Engineering, June 2012.

[38] G. Glasø & H. Landrø. «tre og brann». *Fokus på tre*, Nr 37:–, 2005.

[39] R. M. Larssen. *Estimation of Structural Parameters From Response Measurements on Submerged Floating Tunnels*. PhD thesis, NTNU (Norwegian University of Sience and Technology), 1996.

[40] A. Jørstad & K. A. Malo. Measurements of structural damping in prefabricated residential modules fabricated by kodumaja, estonia. Technical report, Norwegian University of Science and Technology, Department of Structural Engineering, 2012.

[41] LMDG Ltd & BTY Group mgb ARCHITECTURE + DESIGN, Equilibrium Consulting. The case for "tall wood" buildings, 2 2012. http://wecbc.smallboxcms.com/database/rte/files/TallAccessed 12.01.2013.

[42] K. De Cock & B. De Moor. Subspace identification methos. http://www.esat.kuleuven.ac.be/sista-cosic-docarch/ Accessed 12.12. 2012.

[43] P. Van Overschee & B. De More. *Subspace Identification for Linear Systems*. Kluwer Academic Publishers, 1996.

[44] M. E. Plesha & R. J. Witt R. D. Cook, D. S. Malkus. *Concepts and Applications of FiniteElement Analysis*. John Wiley & Sons, INC, 2002.

[45] Simulia. *Abaqus 6.11 Documentation*, 2012.

[46] BOB & Artec SWECO. Vht - drawings. Technical report, VHT Plantegning, 2012.

[47] & W.-S. Chang. T. Reynolds, R. Harris. Dynamic response of tall timber buildings to wind load, 2012. http://reynoldstom.files.wordpress.com/ 2012/ 04/ thomas-reynolds-full-paper1.pdf Accessed 12.12.2012.

[48] Ingunn Utne. Numerical models for dynamic properties of a 14 storey timber build-
     ing. Master's thesis, NTNU - Norwegian University of Science and Technology,
     2012.

[49] P. Verboven. *Frequency-domain System Identification For Modal Analysis*. PhD
     thesis, Vrije Universiteit Brussel - Faculteit Toegepaste Wetenschappen Pleinlaan,
     2002.

[50] Telu YK and Mahendram M. Behaviour and design of cold-formed steel wall frames
     lined with plasterboard on both sides. *Journal of Engineering Structures*, 26/5:565
     – 579, 2004.

Appendix A

Test Results - Dynamic Testing of Building Modules

A.1   System Identification Analyses Results

The analyzed time series with their respective results are listed in Table A.1 and A.2. The time series marked as bold was chosen for the selected time series plot.

Time Series	Longitudinal Mode		Torsional Mode	
	Frequency [Hz]	**Damping Ratio** [%]	**Frequency** [Hz]	**Damping Ratio** [%]
M4C_1_1_1	**8.6146**	**6.8707**	**10.2079**	**3.1722**
M4C_1_2_1	**8.3646**	**6.458**	**10.2312**	**3.417**
M4C_1_2_1	**8.4633**	**6.6438**	**10.2234**	**3.5249**
M4C_2_2_2	8.4028	6.6477	-	-
M4C_2_2_2	8.6154	5.9499	-	-
M4C_3_1_2	**8.376**	**6.0823**	**10.1709**	**3.922**
M4C_3_1_2	**8.4169**	**8.1919**	**10.3292**	**3.6701**
M4C_3_2_3	8.4051	6.0021	10.1926	3.659
M4C_3_2_3	**8.3778**	**7.0897**	**10.3771**	**3.4639**
M4C_4_1_2	**8.4538**	**5.5405**	**10.1972**	**3.2239**
M4C_4_1_2	**8.4327**	**7.8245**	**10.219**	**3.2644**
M4C_4_2_2	8.3286	8.4509	10.1955	2.9686
M4C_4_2_2	**8.3487**	**6.6492**	**10.2078**	**3.2101**
M4C_5_1_3	**8.5802**	**7.0944**	-	-
M4C_5_2_3	**8.4934**	**7.0076**	-	-
M4C_6_1_3	8.6776	6.4447	10.1764	3.1327
M4C_6_2_3	**8.4795**	**5.7307**	**10.2445**	**2.8546**

Table A.1: Results From Impacts on Short Side

Time Series	Transverse Mode		Torsional Mode	
	Frequency [Hz]	Damping Ratio [%]	Frequency [Hz]	Damping Ratio [%]
M4L_1_1_3	**4.902**	**4.1349**	**10.198**	**3.3514**
M4L_1_1_3	**4.8843**	**4.6739**	**10.2323**	**3.1745**
M4L_1_2_2	5.0368	4.818	10.2224	3.1327
M4L_1_2_2	4.9324	5.7964	10.2382	2.9108
M4L_2_1_2	**4.8697**	**4.6288**	**10.2595**	**3.2495**
M4L_2_1_2	**4.9256**	**3.3457**	**10.2415**	**3.283**
M4L_2_2_1	**4.9283**	**3.8451**	**10.2454**	**3.0754**
M4L_2_2_1	**4.9861**	**3.1049**	**10.2522**	**3.2726**
M4L_3_1_2	4.9941	6.9902	10.2421	3.0837
M4L_3_1_2	4.9621	2.8604	10.2175	3.1769
M4L_3_2_3	4.8917	4.5071	10.1921	3.1739
M4L_3_2_3	5.0368	3.7844	10.2198	3.1506
M4L_4_1_2	**4.9013**	**3.5198**	**10.2068**	**3.1592**
M4L_4_2_2	4.9257	4.3199	10.2112	3.0935
M4L_4_2_2	4.9157	3.6275	10.244	3.2999
M4L_5_1_1	**4.9656**	**3.3191**	-	-
M4L_5_1_1	**4.9534**	**3.8861**	-	-
M4L_5_2_3	4.9793	4.097	-	-
M4L_5_2_3	4.9818	4.0406	-	-
M4L_6_1_2	**4.9138**	**3.6784**	-	-
M4L_6_1_2	**5.0336**	**3.6121**	-	-
M4L_6_2_3	4.9678	4.8194	-	-
M4L_6_2_3	4.8967	5.2021	-	-
M4L_7_1_2	**4.9711**	**4.4537**	**10.18**	**3.3443**
M4L_7_1_2	**4.9938**	**3.6848**	**10.2141**	**3.209**
M4L_7_2_3	**4.9639**	**3.8924**	**10.1703**	**3.3266**
M4L_7_2_3	**4.9456**	**3.9098**	**10.2157**	**3.3508**
M4L_8_1_1	4.8974	3.5825	10.2268	2.9392
M4L_8_1_1	4.5046	6.3827	10.2956	3.2125
M4L_8_2_2	5.0685	7.1033	10.2118	3.1806
M4L_8_2_2	5.0001	3.7964	10.2171	3.0922

Table A.2: Results From Impacts on Long Side

The formulas used to calculating the standard deviation was:

$$\sigma \;=\; \sqrt{\frac{1}{N} \sum_{i=1}^{N} (x_i - \mu)^2} \tag{A.1}$$

$$\mu \;=\; \frac{1}{N} \sum_{i=1}^{N} x_i \tag{A.2}$$

Where σ =the standard deviation, $\mu =$ the mean value, N =number of samples and x_i = sampling value number i.

Appendix B

Numerical Modeling and Model Properties

B.1 Calculated Mass Distribution of Tested Modules

The mass distribution in the tested modules were not known, so a simple weight estimation was made. The masses of the used for the different materials is listed in the table below.

The mass of the windows has been estimated by assuming a total glass thickness of 10 mm in each window, and multiplying this by the window are. The mass density of glass is sett to $2500\text{kg}/m^3$ [22].

By calculating the volume of each material in each element of the module, the mass distribution has been estimated. 1

The mass that is unaccounted for, has been distributed in the floors and ceilings. The reestimated masses of floors, ceilings and modules is written in red.

B.2 Properties of Plate Models

The thicknesses and material properties of the parts used in the tuned plate models are listed in Table B.3.

B.3 Properties of Shear Frame Models

The properties of the tuned shear frame modules are listed in Table B.4 The mass of each shear frame models is listed in Table B.5

B.4 Material Properties for Detailed Models

The material properties used in the detailed models are listed in Table B.6.

B.4.1 Added mass of glass

The extra mass of glass has been added to the timber surrounding the windows. The calculations have been done by assuming a glass thickness of 10 mm in the whole window

	Timber (C24)	OSB plates (8 mm)	PB (Class A)	PB (Class F)	PB (Class EH)	PaB (22 mm)	PaB (12 mm)
kg/m^3	420	550	720	833.3	790	650	550
Source	[4]	[3]	[23]	[23]	[23]	[3]	[3]

PaB - Particleboard
PB - Plasterboard

Table B.1: Mass Properties

Element	Floor	Mass [kg]	First Floor Module	Second Floor Module
Floor 1	1	2405 (2872)	2405 (2872)	
Floor 2	2	1950 (2417)		1950 (2417)
Ceiling	1 & 2	2015 (2482)	2015 (2482)	2015 (2482)
Interior Wall 1	1	815	815	
Interior Wall 2	2	800		800
Long Exterior Wall	1 & 2	1463	1463	1463
Internal Walls	1 & 2	921	921	921
Short Wall (Windows)	1 & 2	550	550	550
Short Walls (Door)	1 & 2	393	393	393
Total Estimated Mass [kg]			**8562 (9536)**	**8092 (9066)**
Measured Mass [kg]			~9500	~9100

Table B.2: Mass Distribution

Part	t	ρ	E	ν
	[m]	[kg/m^3]	[MPa]	
Long Interior Wall	0.095	259.3	97	0.3
Long Exterior Wall	0.17	253.4	97	0.3
Short Exterior Wall (door)	0.17	217.4	94	0.3
Short Exterior Wall (window)	0.17	303.8	94	0.3
Ceiling	0.3	197.8	90000	0.3
Floor 1st	0.352	193.7	90000	0.3
Floor 2nd	0.3	193.7	90000	0.3
Links	0.05	1	21000	0.3
Foundation	0.05	1	21000	0.3

Table B.3: Simple Plate Model, Properties

Part	ρ [kg/m^3]	E [MPa]	ν	a	b	t
Corner Columns (I*)	1	210000	0.3	0.153	0.245	0.0117
Corner Columns (II*)	1	210000	0.3	0.155	0.231	0.0116
Corner Columns (III*)	1	21000	0.3	0.185	0.2274	0.0115
Center Column (All)	1	21000	0.3	-	-	-
Horizontal Connections	1	21000	0.3	0.1	0.1	0.01
Vertical Connections	1	21000	0.3	0.1	0.1	0.01
Foundations	1	21000	0.3	0.1	0.1	0.01
Floors	300	21000	0.3	-	-	0.3
Roof	305	21000	0.3	-	-	0.3

Table B.4: Properties of Shear Frame Models

opening, and adding this as a distributed mass in the surrounding timber.

$$\frac{A_{glass} \times 10mm \times \rho_{glass}}{V_{timber}} = \rho_{extr} \tag{B.1}$$

$$\rho_{timber} + \rho_{extr} = \rho_{tot}$$
$$\rho_{glass} = \text{Mass density of glass}$$
$$\rho_{extr} = \text{Added mass tensity}$$
$$\rho_{timber} = \text{Mass density of timber}$$
$$\rho_{tot} = \text{Mass density of the timber surrounding the window}$$
$$V_{timber} = \text{Volume of timber surrounding the window}$$
$$A_{glass} = \text{Area of glass}$$

This was done for the windows on the long and short side. ρ_{tot} for the long side was calculated to $\rho_{tot,L}$=1000 kg/m^3 and $\rho_{tot,S} = 1110$ kg/$m^3$for the short side. The sides

Model	Mass/Module [kg]
I*	6316
II*	6316
III*	8368

Table B.5: Mass of Shear Frame Models

Material	ρ [kg/m³]	E_1 [GPa]	E_2 [GPa]	E_3 [GPa]	ν_{12}	ν_{13}	ν_{23}	G_{12} [GPa]	G_{13} [GPa]	G_{23} [GPa]	Source
Timber C24	420	11	0.37	0.37	0.39	0.49	0.3	0.69	0.69	0.026	[4]
OSB plate 8mm		3.8	3.8	3	0.3	0.3	0.3	0.05	1.08	1.08	[3]
Plasterboard (Class A)	720	0.2	0.2	0.14	0.3	0.3	0.3	0.18	0.18	0.18	[50][23]
Plasterboard (Class F)	833	0.2	0.2	0.14	0.3	0.3	0.3	0.18	0.18	0.18	[50][23]
Stepisol I	195	0.0002	0.0002	0.0002	0.001	0.001	0.001	0.0002	0.0002	0.0002	[13]
Stepisol II	195	490	490	490	0.001	0.001	0.001	387.5	387.5	387.5	Lab tests

Material	ρ [kg/m³]	E [GPa]	ν	G_{13} [GPa]		Source
Particleboard 22 mm	550	1.6	0.3	-	-	[3]
Particleboard 12 mm	650	1.7	0.3	-	-	[3]
Construction Glass	2500	-	-	-	-	[22]

Table B.6: Detailed Model, Material Properties

were calculated separately due to different sized windows and volume of surrounding timber.

B.5 Calculation for Numerical Tests of the Effect of Stepisol

B.5.1 Stiffness of Timber Plates

The stiffness calculations were done according to NS-EN 1995-1-1 Section 7.1 " Glidning i forbindelser"

It has been assumed that the diameter of the nails $d = 2.5mm$ and that the nails have a center distance of c/c = 30 cm, the stiffness of the plates can be calculated by:

$$K_{p,c} = \frac{EA}{L} \tag{B.2}$$

And the shear stiffness by:

$$K_{p,s} = \frac{GA}{L} \tag{B.3}$$

where L =height of the plate, A = cross sectional area of the plate, E = 3800 MPa and G = 50 MPa [3].

Stiffness of nails according to Table 7.1 NS-EN 1995-1-1:

$$K_{ser} = \rho_m^{1.5} d^{0.8}/30 \tag{B.4}$$

Where K_{ser} =the stiffness of the connector given in N/mm, d =Diameter of the connector (nail) and $\rho_m = \sqrt{\rho_{m,1}\rho_{m,2}}$ = square root of the multiplied material density of the two connected parts[4, 3].

$$
\begin{aligned}
\rho_m &= \sqrt{420 \times 550} = 481 \\
K_{ser} &= 481^{1.5} 2.5^{0.8}/30 = 731.9 N/mm
\end{aligned}
\tag{B.5}
$$

The height of the plates connected to the foundation was L_f =147 mm and the height of the plates connecting the modules L_m =204 mm. The stiffness per meter was therefor given as:

$$
\begin{aligned}
K_{p,c,f} &= \frac{3800 \times 8000}{147} = 206803 N/mm \\
K_{p,s,f} &= \frac{50 \times 8000}{147} = 2721 N/mm \\
K_{p,c,m} &= \frac{3800 \times 8000}{204} = 149020 N/mm \\
K_{p,c,m} &= \frac{50 \times 8000}{204} = 1961 N/mm
\end{aligned}
$$

Where subscript p denotes plate, s =shear, c = compression/tension, f =foundation and m = modules. The stiffness of the nails per meter is calculated by:

$$K_{ser,tot} = \frac{K_{ser}}{c/c} = \frac{731.9}{0.3} = 2440 N/mm \tag{B.6}$$

K	Stiffness [N/mm]
$K_{c,f,tot}$	1212.8
$K_{s,f,tot}$	842.4
$K_{c,m,tot}$	1210.1
$K_{s,m,tot}$	752.1

Table B.7: Calculated Stiffness

Connection	E [MPa]	G [MPa]
Foundation	39.42	27.38
Models	39.33	24.44

Table B.8: Material Properties Connection Plates

Since the connection between the plates and nails is a serial connection the total stiffness is found by:

$$\frac{1}{K_{tot}} = \sum_{n}^{1} \frac{1}{K_i} \tag{B.7}$$

$$K_{i,tot} = \frac{1}{K_{p,i}} + \frac{2}{K_{ser,tot}} \tag{B.8}$$

The material parameters for the mode was then calculated by rearranging Equations B.2 and B.3, and using the modeled height of the plates. L-model = 260 mm. The calculated material parameters are listed in Table B.8.

B.5.2 Rotation

Total rotation measured at the top of the walls was calculated form vertical displacement of the top corners of the models. The formula used to calculate the angles is shown below:

$$\theta = \tan^{-1}\left(\frac{\bar{u}}{l/2}\right) \tag{B.9}$$

Where θ =rotated angle, $\bar{u}$ =averaged vertical displacement of the absolute value of displacement measured at the two corners and l =total length of the wall = 6.25 m.

B.6 Length Variation, Calculated Values for Plate, Shear Frame and Truss Frame Models

B.6.1 Plate Models

Calculations of the Young's modulus for simple plate walls has been done as shown below. The formulas were found in [14]. The stiffness of a wall can be described as:

$$\frac{1}{K_i} = \frac{1}{K_{si}} + \frac{1}{K_{bi}} \tag{B.10}$$

Length [m]	Displacement Δx_i [mm]	Load F_i[N]	Stiffness K_i [MN/m]	Area $A_i [m^2]$	Young's Modulus E_i [MPa]
6.25	0.00375	521.3	13.9	1.06	98.1
8.7	0.00370	739.5	20.0	1.48	101
12.5	0.00366	1062.5	29.0	2.13	102

Table B.9: Young's Modulus for Plate Walls

Where K_i is the total stiffness of the plate and K_{si} and K_{bi} are shear and bending stiffness, respectively. K_{si} and K_{bi} are defined as:

$$K_{si} = \frac{k_s A_i E_i}{l_i} \tag{B.11}$$

$$K_{bi} = \frac{k_b I_i E_i}{l_i^3} \tag{B.12}$$

Where k_s and k_b are load dependent constants, $A_i=$ cross sectional area of the plate, $I_i = $ 2nd moment of area of the horizontal cross section of the plate, $l_i=$ height of the plate (wall) and $E_i = $ the Young's modulus of the plate.

For long plates, like the wall plates that are modeled here, K_{bi} becomes much larger than K_{si}. Due to Equation B.10, K_{bi} does not effect the total stiffness of the system. Equation B.10 can therefor be written as:

$$K_i = \frac{k_s A_i E_i}{l_i} \tag{B.13}$$

Since K_i can be found from the static test, E_i can be calculated by:

$$K_i = \frac{F_i}{\Delta x_i} \tag{B.14}$$

$$E_i = \frac{K_i l_i}{k_s A_i} \tag{B.15}$$

The Young's modulus for the different walls are listed in Table B.9, where $k_{si} = \frac{1}{3}$.

B.6.2 Shear Frame Models

The stiffness of the shear frame models are based on the displacement of the detailed models. The stiffness of the beam on top of the columns is much higher than the stiffness of the columns and can be regarded as rigid. This means that the shear stiffness of the frame can be expressed as:

$$K = \frac{24EI}{L^3} \tag{B.16}$$

Where $L = $ height of the wall and $K = \frac{F}{\Delta x}$ form the detailed modules, $E = 210$ GPa and $I = $Second moment of area of the columns. By rearranging Equation B.16 I can be found:

$$I = \frac{KL^3}{24E} \tag{B.17}$$

To make the calculations simple, a quadratic cross section was chosen and calculated by:

Length [m]	Displacement Δx [mm]	Load F [N]	Stiffness K [MN/m]	2nd M of $\mathbf{A}$ I $[m^4]$	Cross Section h [m]
6.25	0.00375	521.3	13.9	4.309E-5	0.151
8.7	0.00370	739.5	20.0	6.196E-05	0.165
12.5	0.00366	1062.5	29.0	9.000E-05	0.181

Table B.10: Shear Frame Calculations

Length [m]	Displacement Δx [mm]	Load F [N]	Stiffness K [MN/m]	Angle α	Cross Section A $[m^2]$
6.25	0.00375	521.3	13.9	21.8014	4.7988E-04
8.7	0.00370	739.5	20.0	16.0323	8.9638E-04
12.5	0.00366	1062.5	29.0	11.3099	1.7961E-03

Table B.11: Truss Frame Calculations

$$I = \frac{bh^3}{12} \tag{B.18}$$

$$b = h \tag{B.19}$$

$$h = \sqrt[4]{12I} \tag{B.20}$$

The calculated values are shown in Table B.10

B.6.3   Truss Frame Model

The calculations for the truss frame is based on the same stiffness as the other models. The stiffness of the diagonal stay is what gives the model its stiffness. The cross section of the stays can be calculated as:

$$K = \frac{EA}{L} \cos^2 \alpha \tag{B.21}$$

Where L =length of the wall, E =Young's modulus = 210 GPa, A =cross sectional area of the diagonal stays and α =the angel between the diagonal stay and the horizontal line. A can thus be found by:

$$A = \frac{KL}{E \cos^2 \alpha} \tag{B.22}$$

The calculated values for the truss frame models are shown in Table B.11

Appendix C

Appendix C

C.1   Static Stiffness Estimation of Stepisol form Load-displacement Curve

The static stiffness of Stepislo has been calculated from load-displacement curves produced by "Svensk Emballagteknik AB". The curves are shown in Figure C.1
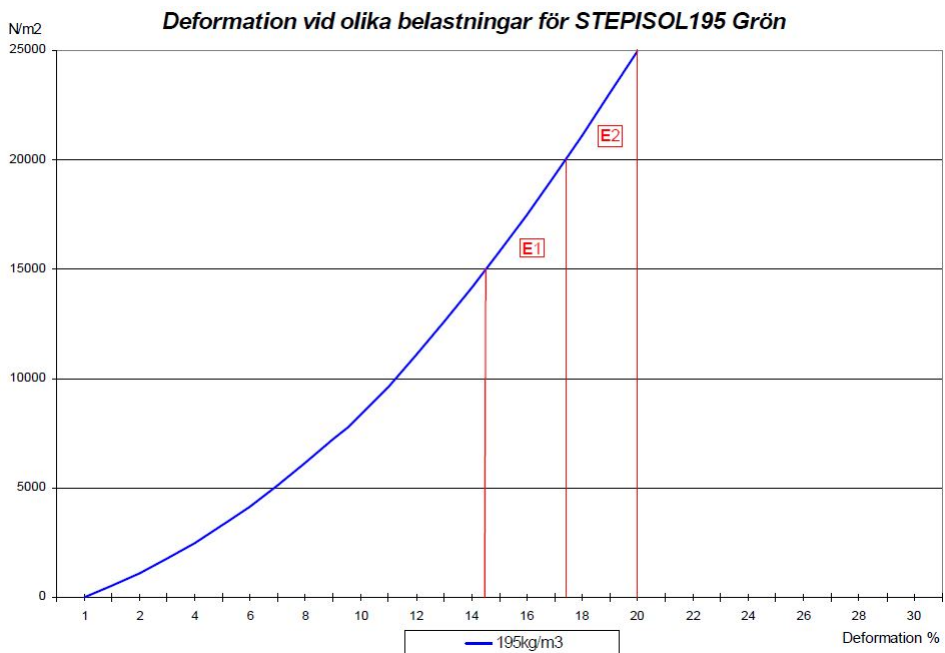
Figure C.1: Stepisol, Load-Displacement curve[13]

$$E \quad = \quad \frac{\triangle \sigma}{\triangle \epsilon} \tag{C.1}$$

$$E_1 \quad = \quad \frac{5000 \text{ N/m}^2}{0.029} \tag{C.2}$$

$$= \quad 172.4 \ kPa \tag{C.3}$$

$$E_2 \quad = \quad \frac{5000 \text{ N/m}^2}{0.026} \tag{C.4}$$

$$= \quad 192.3 \ kPa \tag{C.5}$$

C.2 Height Reduction of Stepisol In Numerical Model

Calculation of base height of Stepisol pads, pre loading (h_0), assuming compression in numerical static step.

Stiffness estimated from lab tests E = 464 kPa

Compressed height $h_t = 13.65$ mm

$$\epsilon = \frac{\sigma}{E} = \frac{19.96 kPa}{464 kPa} = 4.3\% \tag{C.6}$$

$$h_t = h_0 - h_0 \epsilon \tag{C.7}$$

$$h_o = \frac{h_t}{(1 - \epsilon)} = \frac{13.65 mm}{(1 - 0.043)} = 14.26 mm \tag{C.8}$$

C.3 Results from Lab Tests of Stepisol

The results from the lab tests are listed in Tables C.1 and C.2.

The formulas used to calculating the standard deviation was:

$$\sigma \quad = \quad \sqrt{\frac{1}{N} \sum_{i=1}^{N} (x_i - \mu)^2} \tag{C.9}$$

$$\mu \quad = \quad \frac{1}{N} \sum_{i=1}^{N} x_i \tag{C.10}$$

Where σ =the standard deviation, μ = the mean value, N =number of samples and x_i = sampling value number i.

	Frequency [Hz]	Damping Ratio [%]
1	16.724	6.59
2	16.578	8.006
3	16.373	8.715
4	16.59	8.077
5	16.692	7.756
6	16.777	7.25
7	16.668	7.972
8	16.773	7.381
9	16.916	6.501
10	17.14	6.99
11	17.205	6.22
12	17.238	6.375
13	17.133	6.918
14	17.104	7.308
15	17.244	6.356
16	17.262	6.77
17	17.213	7.00

Table C.1: Horizontal Dynamic Shear Tests of Stepisol

	Frequency [Hz]	Damping Ratio [%]
1	21.33	6.62
2	21.29	6.99
3	21.1	6.99
4	20.514	5.74
5	20.456	5.709
6	20.413	5.7
7	20.034	6.212
8	20.356	6.416
9	20.435	6.512
10	20.288	6.386
11	20.072	6.684

Table C.2: Vertical Dynamic Tests of Stepisol

Appendix D

Digital Appendix

The digital appendix contains:

Matlab files - Used for system identification

Test results - The test results shows detailed analysis information from the system identification analyses and modal analyses.